DEVELOPMENT OF A CONTINUOUS EQUAL CHANNEL ANGULAR EXTRUSION (ECAE) PROCESS

A Thesis

by

RAHUL RAJENDRA MURUDKAR

Submitted to the Office of Graduate Studies of
Texas A&M University
in partial fulfillment of the requirements for the degree of

MASTER OF SCIENCE

August 2009

Major Subject: Mechanical Engineering

DEVELOPMENT OF A CONTINUOUS EQUAL CHANNEL ANGULAR EXTRUSION (ECAE) PROCESS

A Thesis

by

RAHUL RAJENDRA MURUDKAR

Submitted to the Office of Graduate Studies of
Texas A&M University
in partial fulfillment of the requirements for the degree of

MASTER OF SCIENCE

Approved by:

Co-Chairs of Committee,	Jyhwen Wang
	Karl Hartwig
Committee Member,	Amine Benzerga
Head of Department,	Dennis L. O'Neal

August 2009

Major Subject: Mechanical Engineering

ABSTRACT

Development of a Continuous Equal Channel Angular Extrusion (ECAE) Process.

(August 2009)

Rahul Rajendra Murudkar,

B.E., University of Mumbai, India

Co-Chairs of Advisory Committee: Dr. Jyhwen Wang
Dr. K. T. Hartwig

Equal Channel Angular Extrusion (ECAE) has great potential for developing ultra-fine grain structure consisting of homogeneous and equiaxed grains dominated by high angle grain boundaries. In addition, the ECAE-processed specimens retain their original cross-section, providing capabilities of multi-passing. However, the process is discontinuous as the length of the billet is limited due to potential buckling of the extruding ram. This problem provides an opportunity of making the process continuous.

The objectives of this study were to examine the feasibility of a process obtained by combining ECAE and Equal Channel Angular Drawing (ECAD), evaluate the potential of the combined process for continuous processing of sheet metal, and to analyze the mechanical response of sheet metal subjected to the ECAE and ECAD techniques using numerical study. Numerical analyses of ECAE and ECAD were performed using the commercial FE analysis package ABAQUS/explicit. Experimental data and analytical models available in literature were used to validate the numerical results. Parametric studies on the effects of drawing angle, and sheet thickness to die radius ratio (t/r), on reduction in thickness, strain uniformity and resulting microstructure are presented.

Numerical results indicate that ECAD through a closed channel should be preferred over conventional drawing (open channel) operation as reduction in thickness is decreased by 2-3% after a single pass. In the experimental study, it was observed that during ECAD, the reduction in thickness increases by 2.5-3.5% per pass. Also, a higher reduction is observed in route C compared to route A. Use of sharper die corners (higher *t/r* ratios) and smaller channel intersection angles tend to increase this thickness reduction, and results in an increase in hardness i.e., results in strengthening. ECAD most likely results in a non-uniform microstructure with low fraction of high angle grain boundaries. In addition, for a given pass, the average hardness of the ECAD-processed samples is approximately half that of ECAE-processed samples. This suggests that ECAD alone may not be commercially viable. However, a significant improvement in minimizing reduction in thickness is achieved by providing a little gap between the sheet metal and support plates.

From the numerical analyses, the proposed continuous process appears to be effective in retaining continuity of the drawing operation, minimizing the percent reduction in thickness and imparting higher plastic strains. It is believed that an experimental study of the process will reveal some more promising information.

ACKNOWLEDGEMENTS

First of all, I wish to thank my advisor Dr. Jyhwen Wang. I am greatly honored for having had an opportunity to work with him. He constantly inspired and motivated me to achieve my academic goals. I warmly thank my co-advisor Dr. Karl T. Hartwig, for providing me guidance and immense support. Whenever I had questions in my research, he was always there to patiently explain things to me and has always motivated me to try out new ideas. I extend my gratitude to Dr. Amine Benzerga for serving on my thesis committee. I am highly privileged to have worked with him.

Special thanks to Mr. Robert Barber, not only for his invaluable help during experiments, but also for teaching me the intricacies of design and manufacturing. His persistent guidance throughout the research is deeply appreciated. I am greatly indebted to David Foley, Shreyas Balchandran, Dough, Shawn (Huang) YuHsuan, Udaya Sunku, and my colleagues in the research group. I thank all my friends and roommates for encouragement and friendship over the years.

And most importantly, I wish to thank my parents Rajendra and Ruchita Murudkar for their love, support and inspiration. Without them, it would have been impossible for me to achieve this goal. I am greatly thankful for all the sacrifices they have made over the years to give me the best possible.

TABLE OF CONTENTS

Page

CHAPTER Page

CHAPTER Page

LIST OF FIGURES

FIGURE Page

FIGURE Page

FIGURE Page

FIGURE Page

FIGURE Page

FIGURE Page

LIST OF TABLES

CHAPTER I

INTRODUCTION

1.1. Motivation

Over past few decades, severe plastic deformation (SPD) techniques have attained wide attention for production of bulk ultrafine-grained (UFG) materials. UFG materials are polycrystalline materials with an average grain size of the order of 100 nanometers to 1 micrometer. For bulk UFG materials there is an additional sought condition of being fairly uniform, homogeneous with equiaxed grains, and with the majority of the grain boundaries having high angles of misorientation.

Conventional heavy deformation techniques such as drawing and cold rolling are also accompanied with significant refinement in the microstructure. However, in general, the resulting substructure is of a cellular type with cells elongated in the direction of drawing or rolling, and containing high fraction of low angle grain boundaries (LAGB). On the contrary, the material processed by SPD techniques contains a granular type of ultrafine grains, containing mainly high angle grain boundaries (HAGBs). This also has favorable influence on the recrystallization kinetics and thus thermal stability. In addition, often these SPD techniques are carried out at ambient temperatures, which make them attractive. The most successful method to date, developed in late 1970's is Equal Channel Angular Extrusion/ Pressing (ECAE/ ECAP). The process has great potential for developing ultra-fine grain structure consisting of homogeneous and

---

This thesis follows the style of Material Science and Engineering A.

equiaxed grains with grain boundaries dominated by high angles of misorientation. The processed specimens retain their original cross-section. Also important is the ability to control the resulting microstructure by choosing specific routes, i.e. the billet orientation between successive passes. However, a shortcoming of the process is that the length of the billet is limited due to potential buckling of the extruding ram. This limitation makes the process discontinuous. Hence, there is an opportunity to retain the advantages to ECAE process by making it continuous. In recent years there are some methods which try to improve on ECAE, such as Equal Channel Angular Drawing (ECAD), Continuous Confines Strip Shearing (C2S2), Conshearing, and Accumulative Roll Bonding (ARB). These methods are based on the principle of conventional rolling. In this study, an effort is made to combine two of these processes: ECAE and ECAD. It is proposed that this method has the potential of producing a shear deformation which is very similar to ECAE while retaining the continuous nature of drawing process.

1.2. Strengthening process

In general strengthening involves two major factors which contribute as a result of the plastic deformation: grain refinement and formation of equiaxed grains.

The improved properties of ultrafine or nano-crystalline grained structures are mainly due to the large number of grain boundaries as compared to the coarsely grained materials. In these materials, a large fraction of atoms are in the grain boundary region. The percentage of atoms at the grain boundaries is a function of grain diameter. These grain boundaries which are a discontinuity in crystal orientation, act as obstacles to dislocation movement. Dislocations are a source of internal stress; they represent the

absence of one or more planes of atoms in the crystal structure. Dislocations have a tendency to move along crystallographic planes during plastic deformation and often cross each other's path. With the decrease in the grain size, it becomes difficult for dislocations to travel further and they have a higher tendency of interacting with each other. Depending on the applied stress and resulting strain, the dislocation density can rise, and may be distributed randomly or in regular patterns. This results in an increase in the material flow stress during deformation in case of polycrystalline materials. The expression that governs the relationship between yield stress (σ_y) and the grain size (diameter d) is given by the Hall-Petch equation:

$$\sigma_y = \sigma_0 + \frac{k_y}{\sqrt{d}} \tag{1}$$

where, σ_0 is the friction stress, i.e. the overall resistance of the crystal lattice to the dislocation motion and k_y represents the locking parameter which is the relative hardening contribution from grain boundaries.

According to Hughes et al. [1], boundaries that consist of randomly stored dislocations are termed incidential dislocation boundaries (IDBs), while boundaries with a regular arrangement of dislocations are called geometrically necessary boundaries (GNBs). These IDBs divide grains into subgrains, while GNBs separate different grains and hence provide the space for the differences in lattice orientation which occurs during deformation. It is seen that if the resulting strains are very high, then GNBs are more preferred and hence subgrains are very few in severely deformed materials. Even in the case of strains as low as two, the geometrically necessary grain boundaries have a very

large misorientation and can even exceed 15° resulting in high angle boundaries. On the other hand, IDBs can yield boundaries with only 2-3° of misorientation at strains as high as 5-10. Thus SPD techniques offer a huge advantage with regards to improvement in the mechanical strength of the materials.

1.3. Severe plastic deformation and methods

There are some necessary conditions for a SPD process [2]. First it is important that the resulting ultrafine grain structure has high-angle grain boundaries. This is because they are prime sources which lead to significant improvement in the mechanical properties. Secondly, to ensure the stability of the properties imparted to the processed material, the process should result into a uniform and homogeneous microstructure. Another unique feature of the SPD technique is that high strain is imposed without significant change in the overall dimensions of the specimen. The principles of various SPD techniques [3] are summarized in the following sections:

1.3.1. High Pressure Torsion (HPT)

The HPT technique is illustrated in the Fig. 1, where the specimen in the form of a thin disk (typically with a diameter of 10 to 20 mm and thickness of 0.2 to 0.5 mm) is subjected to torsional straining under high hydrostatic pressure (a few GPa). One of the anvils is fixed while the other rotates. The friction between the anvils and specimen causes the shear strain in the sample. The simultaneously applied compressive stress prevents the sample from breaking under the high strain. The equivalent strain in processed samples is given by the equation,

$$\varepsilon = \frac{n\pi d}{\sqrt{3}.t} \tag{2}$$

where, ε is the equivalent strain, t is the thickness, and d is the diameter of the specimen. Also, n denotes the total number of passes.

Though the success of the HPT process lies in the advantage that parameters such as equivalent strain, applied pressure and strain rate can be independently controlled, the specimen size is restricted by the geometry of the cavities and hence only small size specimens can be processed. The process needs further investigation for processing larger samples.

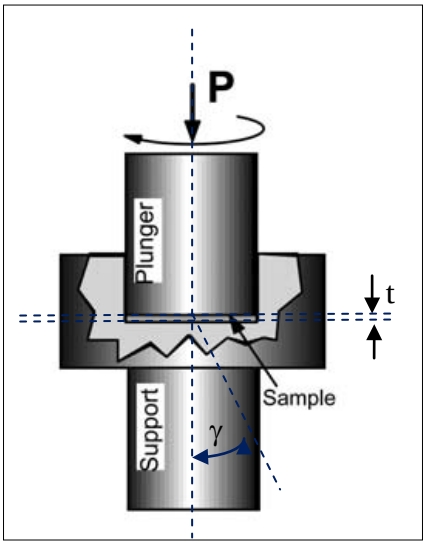

Fig. 1. Illustration of high pressure torsion [3].

1.3.2. Accumulative Roll Bonding (ARB)

ARB can be thought of an extension of conventional rolling wherein as shown in Fig. 2 a sheet is rolled and reduced to one-half of its initial thickness. The rolled sheet is

then cut into two equal halves which are then stacked together and rolled again. To achieve good bonding between sheets during the rolling operation the two halves are degreased and wire-brushed before placing them in contact. With a repeated series of these cutting, stacking and roll-bonding operations, a large strain is accumulated in the sheet, which is given by (in general):

$$\varepsilon = \frac{2n}{\sqrt{3}}.\ln\left(\frac{T}{t}\right) \tag{3}$$

where, T/t is the thickness reduction ratio and n denotes the total number of passes.

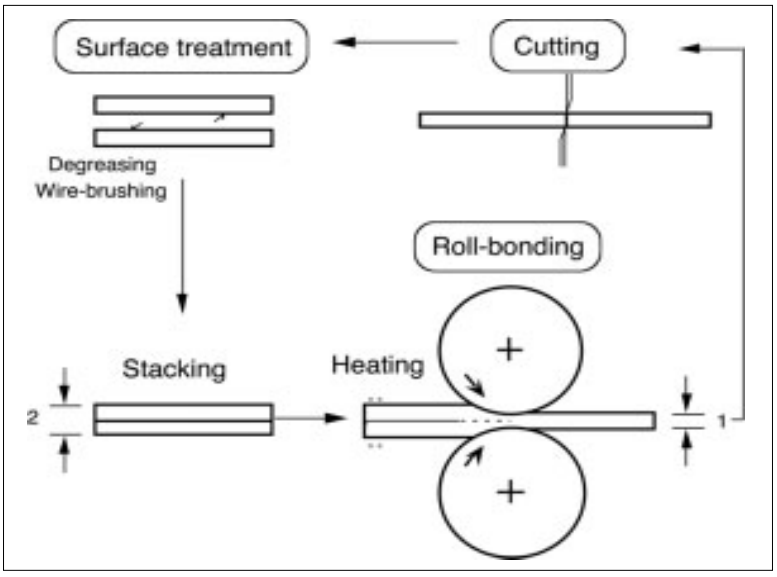

Fig. 2. Illustration of accumulative roll bonding [3].

As for good bonding conditions, the process often needs to be carried out at high temperature. Edge cracking problems some time occur. In addition, it is seen that similar

to conventional rolling, the resulting microstructure is elongated in the direction of rolling and is not a three-dimensionally equiaxed microstructure.

1.3.3. Repetitive Corrugation and Straightening (RCS)

As shown in Fig. 3 RCS is a two stage process: in first stage the specimen in the form of a sheet is initially deformed into a corrugated shape; in the next stage, it is straightened between two rollers. The cumulative strain induced in the specimen is due to both alternate bending-unbending and shear, and is given by the expression (4);

$$\varepsilon = \frac{4n}{\sqrt{3}}.\ln\left(\frac{r+t}{r+0.5t}\right) \tag{4}$$

where, n is the number of passes, r is the corrugated radius of curvature, and t is the initial thickness of specimen.

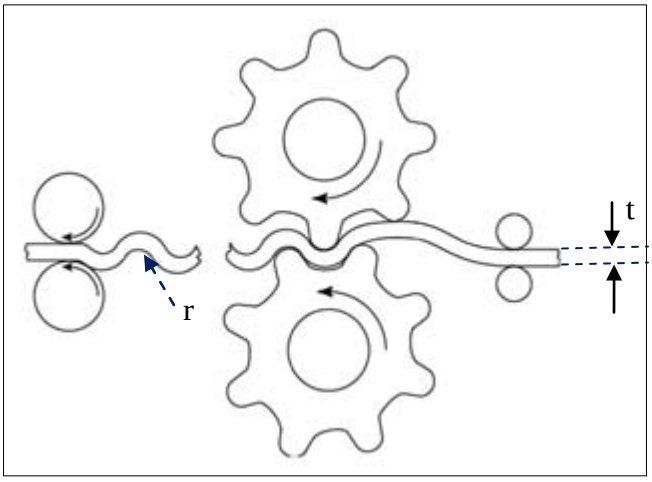

Fig. 3. Illustration of repetitive corrugation and straightening [3].

The greatest advantage of this method is that by redesigning the roller assembly, the current rolling process can be easily modified to RCS. However, though with an increase in passes this process shows great potential for producing nanostructured material. Similar to conventional rolling, it cannot assure equiaxed subgrains, and the numbers of passes are restricted by an unavoidable reduction in the sheet thickness.

1.3.4. Twist extrusion

As illustrated in Fig. 4 in twist extrusion the metallic billet is pushed through an extrusion die. The shape and area of the extrusion channel remains the same however, it is twisted through a specific angle around the extrusion axis. The shape of the cross-section (except circular) is unchanged and hence repetitive multi-pass extrusion is possible attaining high plastic strains.

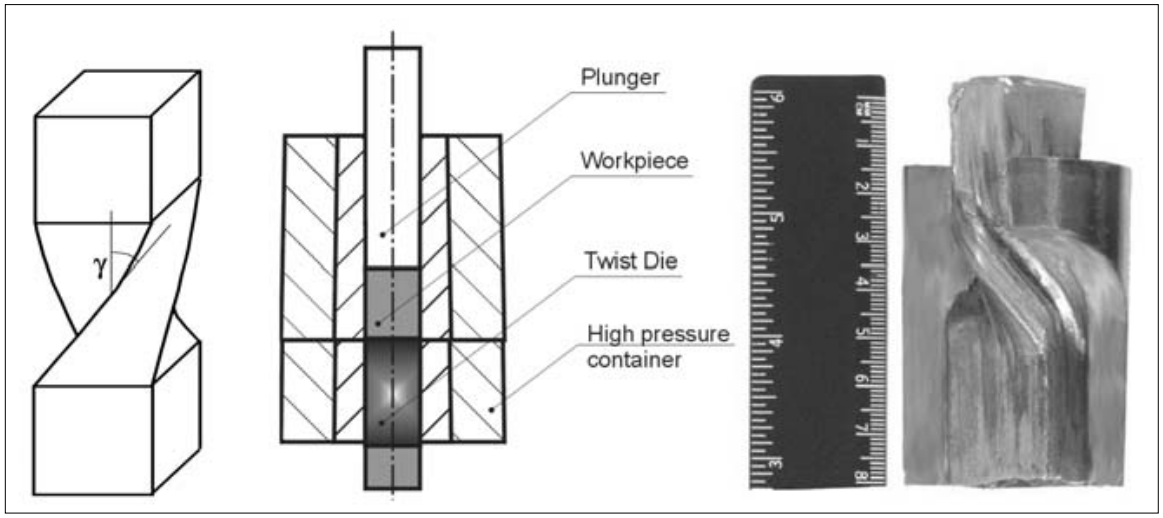

Fig. 4. Illustration of the twist extrusion process (b) specimen installation scheme for twist extrusion (C) processed copper workpiece [3].

It is observed [4] that the plastic strain is not uniform across the cross-section but increases with an increase in distance from the extrusion axis. As a result, a more fine grain structure and thereby higher strength is found at distant regions as compared to the core of the billet. This heterogeneity in microstructure lessens with increasing passes.

1.3.5. Conshearing

Conshearing (Fig. 5) is another continuous pure shear deformation process based on the principle of rolling. As the material is guided through the equal channel dies by passing over a large central roll and assisted using satellite roll, and a guide shoes; it undergoes pure shear deformation and improves the mechanical properties. Once again, as the material dimensions are unchanged multipassing can be performed.

However, Conshearing has some limitations, as it does not yield UFG microstructure. In addition, it is difficult to make a channel angle of 90º, which imparts the maximum plastic strain as the plate/ billet passes through the dies.

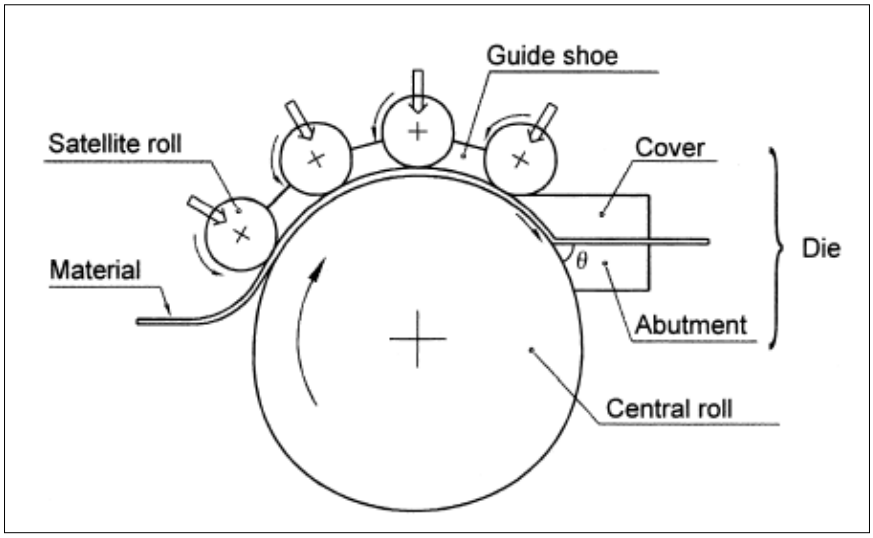

Fig. 5. Illustration of conshearing process [5].

1.4. Equal Channel Angular Extrusion/ Pressing (ECAE/ ECAP)

In the 1970's, V. M. Segal [6] developed equal channel angular extrusion (ECAE), the most popular plastic deformation method with the potential of producing very high true strains and UFG microstructures. As the principle was to develop the ultrafine grain by extreme shear deformation without a change in work piece cross-sectional area, multi-pass processing was feasible. This led to the possibility of producing specimens with grain size ranging between a few microns to few a hundred nanometers [7].

In ECAE (Fig. 6) the material, in the form of square or circular cross-section, is pushed through the extrusion channel by applying a punch load. It is verified [6] that the processed billet (except a small part at ends) is subjected to plastic deformation in the nearly the same way as in the case of simple shear.

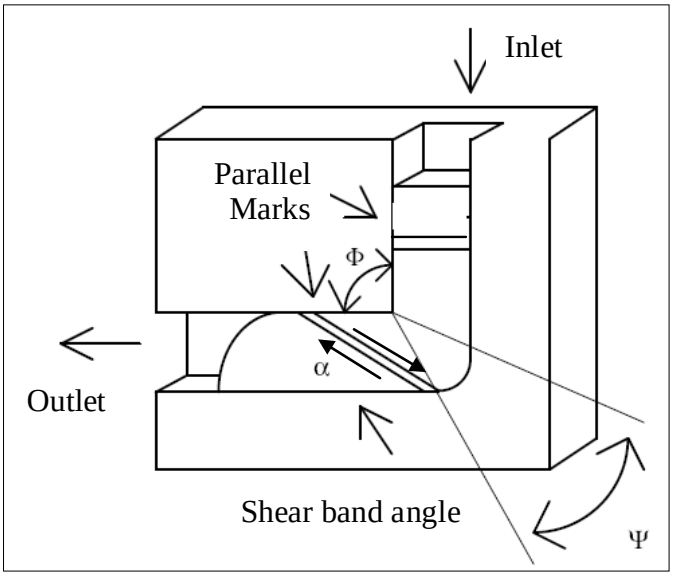

Fig. 6. Illustration of classic ECAE [8].

The prime advantage of ECAE over conventional extrusion is that the cross section of processed billet is same as the initial one. The process is repeatable and hence by subjecting the billet to multiple extrusions, heavy plastic strains can be achieved. In addition, by rotating the billet ($\pm n$ 90°) between subsequent passes, different shear planes can be introduced thus activating different slip systems. There are four different primary routes (A, B_A, B_C, and C) (Fig. 7) based on distinct sequences of the shear plane for multipass processing. This enables one to develop different microstructures and textures. In Route A, the billet orientation is same for all passes. In this case the shear deformation adds strain in the same direction resulting into a lamellar grain structure. For route B_A, and route B_C, after each pass the billet is rotated 90° in alternate or same direction about the extrusion axis. The result for route B_A, is material deformed alternatively in two orthogonal directions, and a distorted fibrous structure is developed. The route B_C restores the original element shape after each two passes and leads to an array of ultrafine equiaxed grain boundaries having high angles of misorientation. In the case of Route C, the billet is rotated through 180° after each extrusion, keeping the shear plane constant but the shear direction is reversed between the two passes. This results in an equiaxed grain structure after each even number of passes. However; since the shear deformation occurs in the same plane (Fig. 8), the developed microstructure is not isotropic. However route B_C produces a more uniform equiaxed grain structure than route C after each of four passes due to alternate changes in slip planes.

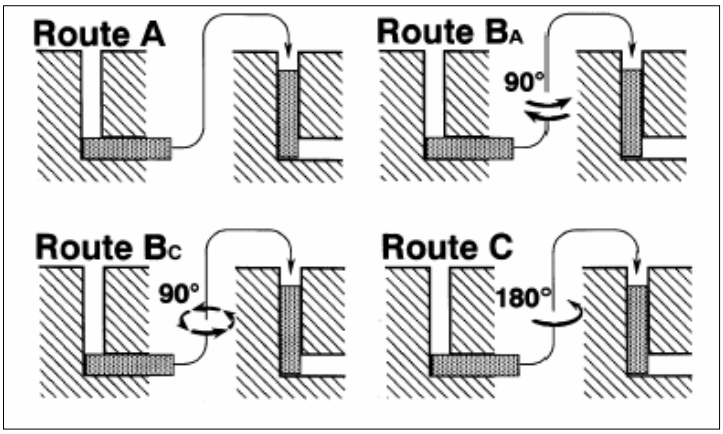

Fig. 7. The primary routes for ECAE processing technique [9].

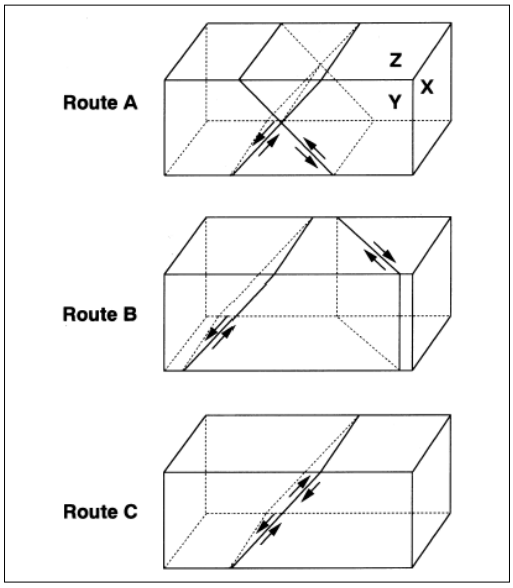

Fig. 8. Shearing patterns for different deformation routes [10].

1.5. Equal Channel Angular Drawing (ECAD)

The idea proposed by Suridi et al. [11] to pull the billet through intersecting channels to eliminate the problems related to compressive loads during ECAE, and having a

potential of producing high plastic strain in a continuous way became popular as ECAD. Thus ECAD offers two major advantages over ECAE [12]: first the length of the specimen is not limited by the buckling instabilities of the extruding ram and secondly, it can be incorporated as one of the intermediate steps in a continuous industrial process. However it is seen that as the billet crosses the shear plane, induced shear strain is also accompanied by a reduction in the cross-section. (Fig. 9) With the increase in the number of passes, the thickness reduction is much more significant thereby reducing practicability of multi-pass ECAD. At the same time equivalent strains developed are much smaller and inhomogeneous as compared to the one developed during classic ECAE. However, the resulting deformation is certainly higher than the deformation achieved by conventional wire/ sheet drawing process, for the same reduction in cross-section.

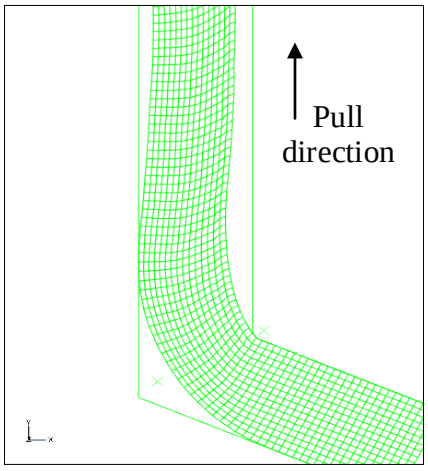

Fig. 9. Illustration of ECAD: deformed shape showing reduction in thickness.

The simple shear (γ) per pass during ECAD is identified as

$$\gamma = 2\tan(90° - \phi/2), \tag{5}$$

where, ϕ is the angle of drawing and the true plastic strain per pass is given by expression;

$$\begin{aligned}\varepsilon &= \frac{\sqrt{2}}{3}\left[\left(\varepsilon_x - \varepsilon_y\right)^2 + \left(\varepsilon_x\right)^2 + \left(\varepsilon_y\right)^2 + \frac{3}{2}\gamma^2\right]^{\frac{1}{2}} \\ &\approx \frac{\gamma}{\sqrt{3}}\left[1 + 2\left(\frac{\varepsilon_y}{\gamma}\right)^2\right] \quad ,\end{aligned} \tag{6}$$

where, ε is the equivalent strain while $\varepsilon_x, \varepsilon_y, \varepsilon_z$ are the strain components along x, y and z axes respectively.

If the $\left(\varepsilon_y / \gamma\right)^2$ ratio is small then the above expression is approximated as,

$$\varepsilon = \gamma / \sqrt{3}. \tag{7}$$

Selection of the channel intersection angle is another prime decision in ECAD. It is seen [13] that if the angle is too sharp then cracks readily appear on the stretched surface. Excessive shearing may even result in tearing of specimen.

1.6. Proposed shear deformation process for continuous ECAE

As seen earlier, ECAE has some important downsides which prevent its wider commercial applications. Firstly, under the application of extrusion pressures, buckling instabilities limit the length of the inlet section. This technique is not suitable for continuous processing of long billets. Also, the technique is only applicable to rectangular or round cross-section bars and cannot be extended directly to sheet metals.

In addition, looking at the cost of the ECAE dies only standard billet dimensions can be easily processed, and any change in cross-section would impose replacement of die components which may be expensive. A main disadvantage of ECAD is that improvement in the mechanical properties is coupled with plastic deformation along the drawing direction causing a reduction in thickness. With a decrease in the die/tool angle (2ϕ), the reduction is more severe and hence imposes a limitation on the sharpness of the die angle. It is seen that for sharper die angles, the otherwise dominant deformation behavior i.e. simple shear, which is responsible for uniform strain through the entire length of specimen, is substituted by bending. In the case of multi-pass processing, the effect becomes aggravate resulting in bending of the specimen making the multi-pass process technically of little importance for grain refinement.

Hence there is a need to make the severe plastic deformation technique a continuous one. It is proposed that by combining ECAE and ECAD, the advantages of both methods are utilized i.e. a process with cumulative strains equivalent to ECAE (and shear angle) can be achieved. In addition, as the continuity of ECAD will be preserved, this process can be effectively applied to both the billets and the sheet-metals.

CHAPTER II

LITERATURE REVIEW

2.1. Properties and applications of interstitial free steel

Interstitial free steels are mild steels in which small quantities of strong carbide-forming elements such as titanium (Ti) or niobium (Nb) are added to precipitate out the interstitials in the form of carbides, nitrides, sulphides or carbosulphides, resulting in an essentially interstitial free matrix. In solid solution, because the levels of carbon and nitrogen are very low (generally, total C content < 0.003 wt. % and total N content < 0.004 wt. %). Such steel is also termed "ultra-low carbon steel". Domestically produced interstitial-free steels typically contain <0.008 to 0.020 wt% C, 0.15 to 0.25 wt% Mn, 0.06 to 0.15 wt% Ti, and 0 to 0.10 wt% Nb. By modern steel making processes such as vacuum degassing these levels of carbon and nitrogen can be reduced to as low as 50 ppm [14].

Interstitial free steels are superformable, i.e. they have excellent deep drawing capabilities. Therefore these steel find wide applications in the automobile and structural industries. Dislocations formed during the forming process within the steels are subsequently pinned by the few remaining carbon atoms. These pinned dislocations make the steels much stronger. Due to carbon strain aging during the paint curing stage this steels exhibits an increase in yield strength (at around 260-355 °F), hence this steel gets its name as the "bake hardening steel" [7]. However, this "bake hardening" has very little affect on tensile strength. IF steels also find wide applications in the areas of tube-

making, tube-bending and hydroforming due to their high ductility and improved strain ageing properties.

A major drawback of IF steels is their low tensile strength (< 360 MPa). This has been addressed to some extent through the application of various metallurgical processes such as solid solution strengthening (using P, Mn and Si), work hardening and strain ageing to achieve strengths of about 450 MPa. Depending on the processing technique the typical properties of IF steel, are tabulated in the following Table 1.

Table 1
Nominal properties of IF steel [14]

	Yield Strength	Tensile Strength	Elongation	r-value	n-value
IF-Steel	19 - 27 ksi 130 - 186 MPa	42 - 46 ksi 290 - 317 MPa	40 - 47%	1.6 – 2.2	0.25 – 0.28

Since, IF steel demonstrates a great potential for various forming operations, and considering its simplicity during metallographic study, it is selected in this study for further investigation.

2.2. Plastic deformation theories

In general polycrystalline metals form are considered to undergo isotropic plastic deformation. However, when considered on a microscopic scale, metals are composed assemblies of single crystals which are anisotropic and it becomes important to consider grain size relative to bulk dimensions in order to specify the plastic deformation mode,

i.e. the smaller the grain size, the more accurate the assumption of isotropic plastic deformation. As the grain size approaches the size of the bulk material, this assumption becomes less valid and the deformation becomes anisotropic. It is also important to consider factors such as grain orientation, grain size distribution, grain morphology and other microstructure details including dislocation sources while choosing the deformation theory because they influence how deformation mechanics affects the grain homogeneity. The assumption of isotropic plastic deformation can be safely applied to homogenous material. As a result, reduction in the grain size not only ensures a more homogenized microstructure, but also yields an increased strength and a more uniform isotropic plastic deformation.

The theory of plastic deformation can further be analyzed either from a microscale view or a macroscale view. The microscale perspective considers the deformation as a discrete process driven by atomic movement and crystal deformation. It assumes the concept of preferential slip i.e. shear deformation takes place along specific crystallographic planes and is always inhomogeneous in nature. At the atomic level, movement of dislocations (which can be considered as a continuous absence of atoms in the crystal structure that results in a stress field along the discontinuity and influences the surrounding region) often results into dislocation tangles and forests. In other words, localized increase in dislocation density (mainly due to an increase in strain) constrains or hinders the movement of other dislocations further thereby increasing the strength of a material. This is also termed as “work hardening”, which is nothing but the change in flow stress with strain.

The macroscopic view formulates the plasticity behavior based on experimental results that relate the stress-strain relationship. As there are many influencing parameters such as temperature effects, strain rate effects, the Bauschinger effect, and work hardening effects, the constitutive relationships are complex. Thus there are some generalized constitutive models available. Some of the important relationships contained in the models are;

$$\begin{aligned}
&\sigma = \sigma_y + H\varepsilon^n && \text{(Ludwick 1909)}\\
&\varepsilon = \sigma / E + H(\sigma / E)^{\upsilon} && \text{(Ramberg and Osgood 1943)}\\
&\sigma = H\varepsilon^n && \text{(Holloman 1944)}\\
&\sigma = \sigma_\psi + (\sigma_y - \sigma_\psi)[1 - e^{n\varepsilon}] && \text{(Voce 1948)}
\end{aligned} \tag{8}$$

where, E, σ_y, H and n are material constants to be determined using experiments.

The Maxwell-Huber-von-Mises and Tresca criteria are very common to approximate work hardening in the case of metals. Two common approximations for work hardening involve isotropic hardening and kinematic hardening. Isotropic hardening assumes the accumulation of forest dislocations that impede further motion of dislocations (neglecting anisotropic effects). Thus it allows the yield surface to change shape without translation. Kinematic models are assumed to have yield surfaces with constant shapes that can translate. In kinematic models it is assumed that accumulation of internal stresses is due to heterogeneity of deformation on a microscopic scale. In other words a dislocation network builds resistance to motion of dislocations which need not be uniform in all directions. As a result, the kinematic model allows for the Bauschinger effect while the isotropic model does not.

2.3. Analytical modeling vs. numerical analysis

Due to the complexity involved in plastic deformation processes, the closed form solutions for governing equation systems usually do not exist. Under certain simplifications, some analytical methods have been developed to obtain partial information about the mechanics of these processes. The slab method seeks to satisfy the force balance and stress equilibrium equations. On the other hand, upper bound analysis focuses on displacement requirements and completely neglects the stress requirements. Slip-line field theory meets both the stress and deformation requirements, but only provides a solution for the plane strain case with regular deformation geometry and a simple material flow rule. Fig. 10 shows components of the mathematical modeling in the deformation process.

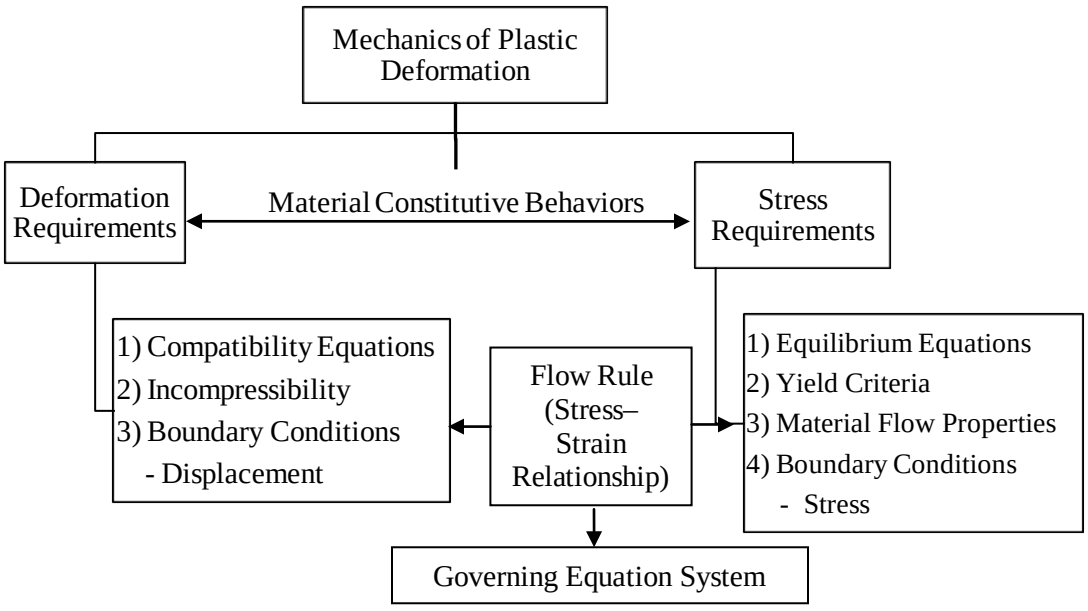

Fig. 10. Components of mathematical modeling of deformation [15].

Compared with the traditional analytical methods, such as upper bound analysis or slip-line field theory, the finite element method can be used to numerically solve governing equations without neglecting complicated but important realistic factors. Provided that the numerical accuracy is guaranteed through using advanced computing technology, computational modeling for forming processes based on finite element methods can provide more reliable stress and strain distributions information, which are crucial to tool-die design and product property estimations. Currently, two kinds of finite element formulations, solid formulation and flow formulation, are widely used in the simulation of forming processes.

2.4. Equal channel angular extrusion: analytical modeling

In the late 1970's, V. M. Segal developed equal channel angular extrusion (ECAE), the most popular plastic deformation method with potential for producing very high true strains and UFG microstructure. The principle involves shear deformation without change in work piece cross-sectional area. Thus, the multi-pass processing of the same billets is feasible. This led to possibility of producing material with grain sizes ranging few microns to few hundred nanometers [7]. Extensive research both experimentally and by numerical simulations has been carried out to analyze and optimize the influencing processing parameters and routes of fabrication. Enhancement in mechanical properties, grain refinement and texture development in deformed material has been studied in detail.

Using the slip-line method, Segal [16] presented the general solutions for uniform and varying friction conditions for sharp and round corner channels. He showed that the

variations in the boundary conditions have moderate effects on equivalent strain and, the strain distribution greatly depends on the friction uniformity and channel geometry. Contact friction plays a very important role in deformation uniformity and degree of plastic zone region developed during shear. For sharp corners and frictionless conditions the plastic zone is a single slip plane and the loading history during the deformation process is monotonic. With an increase in friction, the plastic zone is in the form of a central fan region involving three simple shears along the boundaries. Also, the loading history changes from monotonic to cross loading. Round corner channels seem to have an advantage in reducing the pressure and improving the friction conditions. However the strains generated are lower than in the case of sharp corner channels and with an increase in the outer corner angle, Ψ they are identical to the strains generated for sharp corner and high friction conditions. In other words, the central fan involved in the higher Ψ conditions is equivalent to the sharp corner with high friction. For different friction conditions within channels the deformation obtained is non-uniform and load history is complicated. Providing moving channels eliminates friction and a 'dead metal zone' thereby ensuring ease of metal flow between channels and a more uniform deformation.

Cui H., Goforth R, and Hartwig K. [3] analyzed the metal flow during ECAE process using the slip-line field method. A three dimensional computational model enabled analysis of the flow pattern after different processing routes. A self consistent velocity field is developed assuming a fan-like deformation pattern. In addition based on calculations carried out by Cui, an analytical approach was presented to estimate punch pressures required for non-hardening materials.

D. Lee [17] analyzed ECAE as a special case of channel angular deformation (CAD). He developed an upper bound analysis of CAD to analyze the stresses and strains during the deformation process in which two channels are not equal in cross section. The upper bound analysis was conducted for sharp corner channels (so single shear plane) with a tool angle $\theta=\alpha+\beta$ condition (where α and β are the angles formed by shear plane with inlet and exit sections respectively). Two different coefficients of friction, m_0 and m_f, were considered before and after deformation respectively. The internal power for deformation consists of power dissipated along the slip plane and frictional power dissipation. The internal power for deformation (consisting of power dissipated along the slip plane and frictional power dissipation) is equated to external power. It was concluded that because internal power equals external power, pressing pressure (P) and drawing stress (σ_d) are the same. An expression for shear strain is obtained by taking the ratio of the velocity normal to the shear plane to the velocity parallel to the shear plane. For equal channels (i.e. $\alpha=\beta$) and frictionless conditions, this reduces to strain for the simple shear condition as given by Iwahashi et al. [18] In addition, it is proposed that the maximum drawing stress is limited by flow stress in order to avoid failure due to severe necking.

J. Alkorta and J. Sevillano [19] performed an upper bound analysis which is valid for rigid perfectly plastic (non-hardening) material in frictionless flow conditions. It is extended for strain hardening material by adopting a kinematically valid upper bound flow pattern to compute the deformation energy providing approximate estimates of strains and extrusion forces for these materials. The criterion considered is strain

dependent shear yield strain. The special condition with non-hardening material yields the strain equation proposed Goforth et al. [20]. The mathematical model is then compared with FEM results. It is shown that with an increase in the strain hardening index (n), the die corner gap is increased and in order to avoid this, sufficient back pressure is required, so that both ends are forced to move with the same velocity. In addition, it is reported that strain hardening results in a more heterogeneous plastic strain distribution across the specimen. Again, introducing back pressure reduces heterogeneity.

L. Perez [21] performed an upper bound analysis of a special configuration of die geometry. He assumed equal fillet radii and termed this as equal fillet radii angular pressing (EFRAP). The analytical model can be used to determine the extrusion pressure for non-hardening material for both frictionless and Tresca friction coefficient conditions. It suggested that EFRAP has an advantage over traditional ECAE with regards to the difference in the deformation from the inner part of the die to the outer. In addition, with the variation in outer corner angle ψ deformations are approximately constants, up to a critical value of fillet radius. Beyond this threshold value the effect due to bending is dominant and deformation cannot be assumed to come only from shear. However, an expression for this critical radius is not provided in paper. As equal fillets ensure complete filling of the die (no dead metal zone) the deformations are more uniform across the specimen. FEM simulations were performed to support the analytical model. The model also provides the punch pressure values as a function of tool angle ϕ and fillet radius R. It predicts the strain values and punch forces more accurately at

higher temperatures as the effect of strain hardening is minimal. It is proposed that over prediction of the upper bound results can be minimized by considering non-uniform friction.

Altan et al. [22] performed an upper bound analysis for the 90° ECAE process. His analytical model includes effects due to friction, the inner radius and the dead metal zone. The deformation is assumed to occur at three stages: at the entry surface (1st shear plane), at the exit surface (2nd shear plane), and at the deformation zone (continuous direction change region). In addition to the previous work model that predicts the deformation power, they introduced a component of power dissipated in the dead metal zone and frictional power losses between the transition regions thus providing a more accurate approximation. The model provides a direct relationship between the friction coefficient and radius of inner corner for the deformation zone. The paper also discusses the change in shape of a material flow line as the metal flows through the deformation zone. The normalized plots of the deformed shape of the material line indicate that with increase in the non-dimensional length of the entry zone, the material line deviates more from the straight line. This can also be expressed in terms of the billet thickness to the inner radius ratio and the tool angle ϕ. During early stages the process is assumed to be analogues to forging and the upper bound analysis procedure explained by Avitzur [23] is adopted to analyze the load displacement relationship. The regions dominating static and dynamic friction are identified in these diagrams and use of these diagrams to estimate the friction coefficient is suggested. The diagram has a very close match with ideal conditions.

In addition to providing the total strain relationship the paper also presents the relation between the inner radius and the friction coefficient that governs the size of deformation region. It is concluded that the increase in the friction coefficient results in a larger deformation zone and a more inhomogeneous deformation pattern. The results underline the adverse effect of an increase in fan region (i.e. increasing ψ angle) as indicated by Segal [16]. The use of the deformation model that excludes the velocity discontinuities is proposed to be more accurate at the cost of increasing complexity.

The next section presents a summary of some important strain relations.

2.4.1. Segal's strain model

Segal derived a path independent strain relationship for a sharp corner (i.e. $\psi = 0^\circ$) configuration with a tool angle, ϕ and the number of passes as, n, according to which total strain ε_n is given as:

$$\varepsilon_n = \frac{2N}{\sqrt{3}} \cot\left(\frac{\phi}{2}\right). \tag{9}$$

So for $\phi = 90^\circ$ this equation becomes $\varepsilon_n = \frac{2N}{\sqrt{3}} = 1.155N.$ (10)

2.4.2. Iwahashi's strain model

Iwahashi presented the generalized relation for total strain for a case where $\psi \neq 0$ as:

$$\varepsilon_n = \frac{2N}{\sqrt{3}}\left[\cot\left(\frac{\phi}{2}+\frac{\psi}{2}\right)+\frac{\psi}{2}\cos ec\left(\frac{\phi}{2}+\frac{\psi}{2}\right)\right]. \tag{11}$$

2.4.3. Goforth's strain model

Goforth R, Hartwig K. and Cui H. analyzed metal flow during the ECAE process using a slip plane method and estimated the punch pressures required for non-hardening materials. According to this equation:

$$\varepsilon_n = \frac{N}{\sqrt{3}}\left[2\cot\left(\frac{\phi}{2}+\frac{\psi}{2}\right)+\psi\right]. \tag{12}$$

2.5. Previous work on processing metals by Equal Channel Angular Drawing

Another near analogue process is equal channel angular drawing (ECAD). This was reported as an alternative to ECAE by Suriadi, Chakkingal and Thomson et al. [11]. In this process the specimen was drawn through a constant cross-section channel as compared to extrusion of a workpiece in ECAE. The study consists of effects of different routes on resulting microstructure, texture and mechanical properties using pure aluminum during Equal Channel Angular Drawing (ECAD) process. Micro-bending was reported as a significant mode of plastic deformation. The processing routes differs with respect to shear planes i.e. in route I with each pass shear takes plane along the same macroscopic shear plane, while in route II the shear occurs alternately on two intersecting shear planes. These planes make an angle of 135°. In route III deformation occurs on four different shear planes with very complicated deformation geometry. It is seen that though there is significant improvement in the mechanical properties in all three routes, the decrease in the drawing stress, which is observed continuously from one pass to next, is different for different routes. It is a maximum for route I and the least for route III. It is verified that the strain path along which the material deforms can be

effectively changed by changing the processing route. Studies of the microstructure reveal that route I results into elongated subgrains while route II and III result into equiaxed subgrains. It is concluded that ECAD alone cannot produce ultrafine grains separated by high angle boundaries irrespective of the processing routes. Moreover, processing material by ECAD through two or more passes has no practical advantage on improvement in properties.

J. Alkorta and J. Sevillano [24] performed numerical calculations on multi-pass ECAD, and it is concluded that as the shear deformation process in ECAD is associated with significant reduction in the thickness. It appears that the multi-pass ECAD process will be technically of little importance.

Zisman et al. presents the application of the ECAD technique to thin sheet metals [13], and provides a comparison with the ECAD of rods. Experimental results show that ECAD on sheet metal provided similar results on microstructure and improvement in mechanical properties as provided by other SPD techniques, used on sheet metals such as C2S2 and CONFORM [13]. The initial yield strength increases by 1.6 after two passes with a reduction in the thickness of less than 16%. Despite the reduction in thickness, the process can be effectively applied to control the resulting texture. In addition it was demonstrated that both equivalent strain per pass and total strain accumulated both are related to the sheet thickness reduction in multi-pass processing. This means industrial implementation of multi-pass processing may be limited. In addition the resulting microstructures show reduced or no high-angle boundaries after two or three passes. It is encouraged to explore the possibilities of producing a high-

angle microstructure with uniform sub-grain crystalline structure while at the same time keeping reduction in thickness a minimum.

P. Chaudhury et al. [25] introduced a method for continuous processing of billets using a severe plastic deformation technique based on ECAE. In this manifestation of the process use of a set of rollers or a conveyor system is suggested to grip and feed the metal stock into the ECAE dies while another set will pull them from the exit channel. Because buckling instabilities while feeding the billets are greatly reduced or almost eliminated the continuous process may work.

The present work utilizes the same principal introduced by Chaudhury et al. [25] where an effort is made to combine the processes of ECAE and ECAD. It is proposed that this method has the potential of producing shear deformation which is very similar to ECAE while retaining the continuous nature of the drawing process. The process is then analyzed for its industrial implementation by performing numerical simulations and comparing the results with experiment. The objectives of the research are:

1) Demonstrate the feasibility of the process obtained by combining the ECAE and ECAD processes. Show that by doing this, the ECAE process can be extended for continuous processing of sheet metals.
2) Compare the performance of the proposed process with existing ECAE and ECAD techniques using Finite Element (FE) analysis.
3) Perform experimental study to analyze the mechanical response of sheet metal subjected to ECAE and ECAD techniques.

CHAPTER III

NUMERICAL SIMULATIONS

3.1. Introduction to numerical simulation

As mentioned before, major work dealing with deformation techniques is focused on microstructural aspects of the refinement, resulting texture and enhancement in mechanical properties. Analytical models have been developed for Equal Channel Angular Extrusion (ECAE) and other SPD techniques using slip-line field theory, and upper-bound approach. There have been some studies reported on finite element models primarily on ECAE. However, fewer efforts have been made on finite element studies of the closed channel sheet drawing process and comparing its performance with classic ECAE.

In this study, FEM simulations of Equal Channel Angular Drawing (ECAD) and ECAE are presented. The plane-stress FEM simulations of ECAD and plane-strain simulations of ECAE were performed using the commercial analysis package ABAQUS 6.7.1. This chapter presents numerical analyses of four problems which collectively achieve the objectives. First the modeling of ECAD process, with conventional open and close channel configuration is provided. Secondly, ECAE analysis of IF steel sheet specimens embedded in an IF steel container is used to support the hypothesis that ECAE has the edge over the drawing process. This analysis compares the non-uniformity in strain and stress developed during both processes. Next, the analysis of combined drawing and ECAE is presented along with various process parameters and their influence. This combined ECAD-ECAE process is compared with drawing and

ECAE alone and it constitutes the major part of the simulation work. In the end, the feasibility analysis of the combined process for industrial application is presented by modeling the feeder mechanism using rollers and comments on some of the process requirements.

3.2. Simulations of the sheet metal drawing process

Conventional drawing is referred to as an open channel configuration wherein the sheet metal is drawn over a sharp corner without any support from the top. The closed channel configuration resembles the flow of sheet metal when it is drawn through completely confined channels of equal cross-sectional areas. This is also referred as equal channel angular drawing (ECAD). This section presents the work done on these two processes, and presents confidence for a slight edge that ECAD has over conventional drawing.

3.2.1. Geometry and model

As described in the section *1.5*, during the drawing process, sheet metal is essentially drawn over a sharp corner to induce plastic strains by the process of simple shear. The initial configuration of analysis is as shown in Fig. 11 The radius of the die insert, r is 0.7 mm. The initial thickness of the sheet t_0 is 0.7 mm. The analysis is conducted dynamically in ABAQUS/Explicit as it can be efficiently applied to quasi-static problems such as sheet metal drawing/ forming wherein contact dominates the solution and local instabilities may form due to wrinkling of sheets. The sheet, the drawpunch, the support plate, and the die are modeled as separate parts. The rigid punch, support plate, and die are modeled in ABAQUS/Explicit as discrete rigid surfaces with the

*RIGID BODY option. The sheet metal is modeled using 3672 4-node bilinear plane stress quadrilateral elements with reduced integration (CPS4R). Reduced integration avoids the issue of volumetric locking which may occur in full integration when the strains developed are on the order of the plastic strain (which is very common in sheet metal drawing/forming processes).

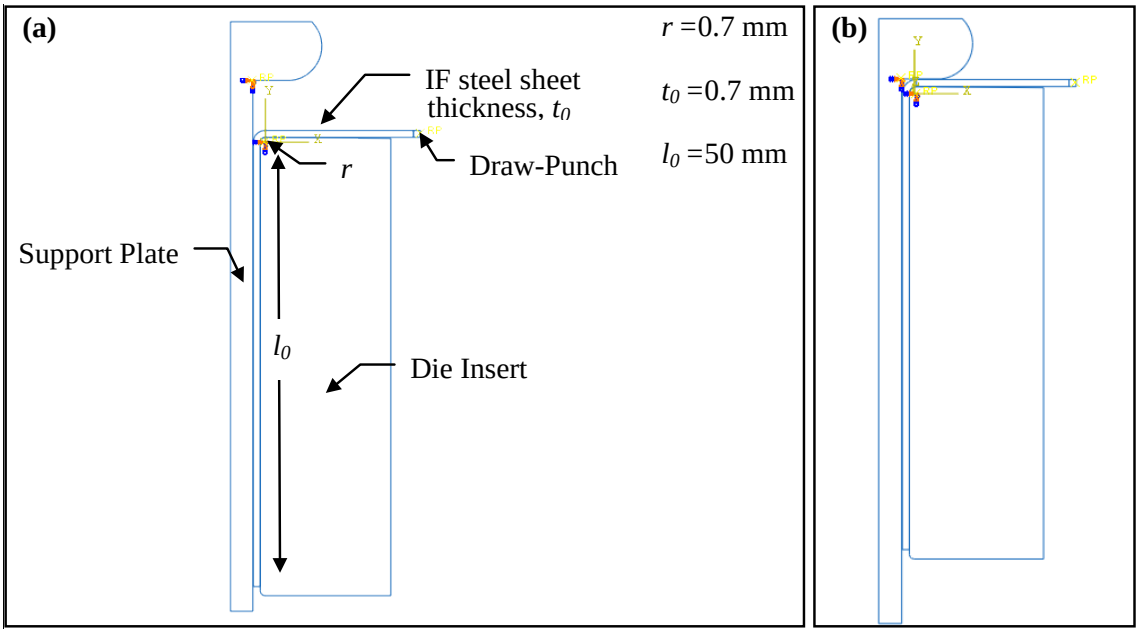

Fig. 11. Schematic of the initial configuration: (a) open channel drawing, (b) closed channel drawing (ECAD).

3.2.2. Material properties

An elastic-plastic isotropic model is assumed for the material in the sheet and the properties are those of commercially manufactured Interstitial-Free (IF) steel (obtained from the tensile tests on as-received samples). The properties used for simulations are

presented in Table 2 Values beyond the yield point are approximated as linear segments using the *PLASTIC option.

Table 2
Material properties of sheet metal

Properties	Value
Material	Interstitial-Free (IF) steel
Density, ρ (tones/mm^3)	7.85 x 10^{-9}
Young's modulus, E (MPa)	210000
Poisson's ratio, ν	0.3
Plastic Properties	
True Yield Stress (MPa)	True Plastic Strain (%)
125.60	0.000
137.21	0.078
163.33	0.82
200.00	2.580
232.56	4.800
250.00	5.970
264.83	7.580
281.395	9.800
300.00	12.760
309.30	14.800
323.29	17.000
332.50	19.800
350.00	24.800
358.14	29.800

3.2.3. Contact interaction

The contact between the sheet metal and the rigid die is modeled using the *CONTACT PAIR option. The mechanical interaction between the contact surfaces was assumed to be a friction contact, with a coefficient of friction of 0.08 (which is assumed to be the friction during experimental analysis). A hard contact model was used to define the contact pressure-overclosure relationship with the kinematic contact constraint method, which prevents any penetration of sheet metal into the die at each constraint load. A similar contact interaction was applied between the sheet metal and the support plate with a gap of 0.05 mm between these two surfaces. This gap minimizes the thickness reduction which is a characteristic feature of conventional drawing. A surface to surface tie constraint is applied between the drawpunch and leading edge of the sheet metal using the *TIE option. This allows the sheet metal to follow the motion of the punch enabling the measurement of drawing force (requirement).

3.2.4. Loading

In ABAQUS/Explicit the displacement of the drawpunch is specified using the *BOUNDARY option, the magnitude of which is specified with the *AMPLITUDE option. This enables the displacement to be ramped up to 51 mm (which is slightly larger than the length of the sheet metal in the inlet region.) during the total time step of four seconds. This approximates the strain rate of 0.5 inches per second used during the experimental study.

Initially, conventional open channel drawing was modeled wherein the sheet metal is not supported from the top as it flows through the exit channel. Later, the closed channel

configuration, wherein the sheet metal is continuously supported, was modeled. The second configuration gives a slight advantage as it minimizes the reduction in thickness without a significant increase in drawing force. Detailed results are presented in next section.

3.2.5. Results and discussion

Figs. 12 and 13 present the contour plots of the von-Mises stress and equivalent strain (PEEQ) along with the deformed mesh for sheet (thickness to die radius ratio, t/r = 1) drawn over a 90º die in the case of the open channel configuration. As seen from these contours higher stresses are developed near the sharp corner (die insert). They are subsequently reduced as flow takes place in the exit plane. However, they are not uniform.

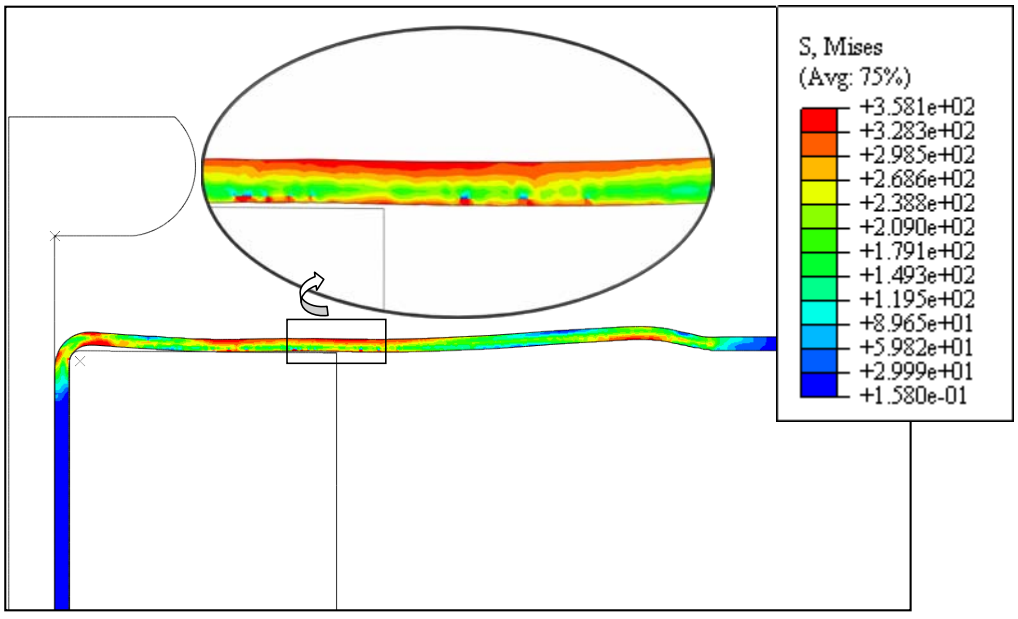

Fig. 12. Model results for open channel configuration: von-Mises stress contours.

This non-uniformity is more significant in strain and as demonstrated by the deformed mesh, where strains are higher near the contact areas (die-metal contact) and less near the central region across the thickness.

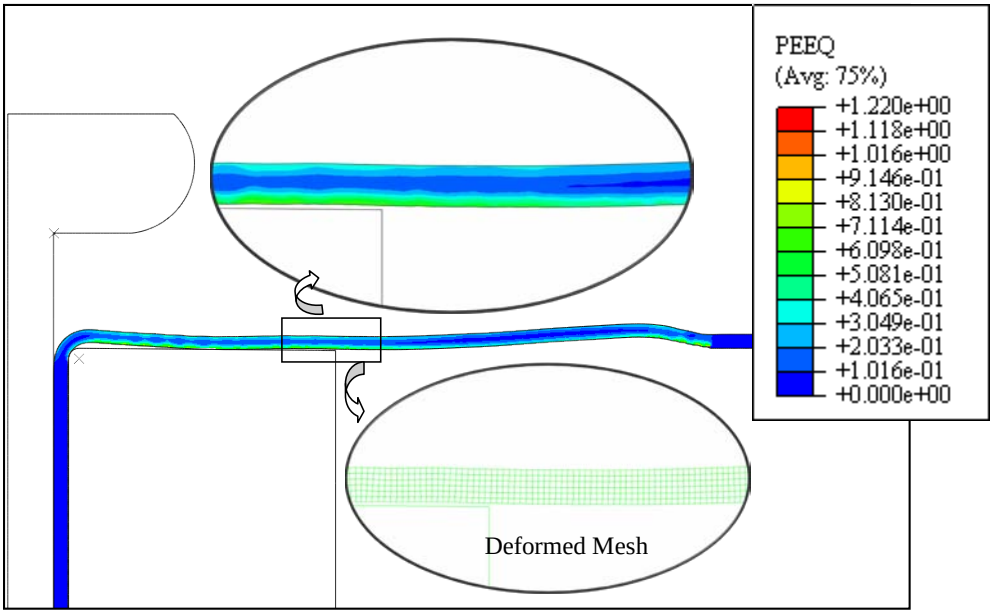

Fig. 13. Model results for open channel configuration: equivalent strain contour (PEEQ).

Figs. 14 and 15 present strain and stress distributions across thickness. The distance is measured from the farthest point from the die radius. Thus near the die radius the strain is 0.66, which reduces to 0.14 at the mid section and again increases to 0.34 near outer surface. A strain distribution is observed for the closed channel configuration with little advantage over the conventional process. However, at the same location across the thickness the stresses are observed to be much higher as compared to conventional drawing. When compared to the strain distribution after one pass of ECAE, these strains

are very low and hence multi-passing is important. When the strain history (i.e. how the strains are developed with respect to time) is plotted (Fig. 16)for the open and the closed channel configuration, interestingly the later one demonstrates beginning of strain evolution at slightly earlier timeframe and are seen to be slightly higher at all locations across the thickness as compared to the open channel configuration.

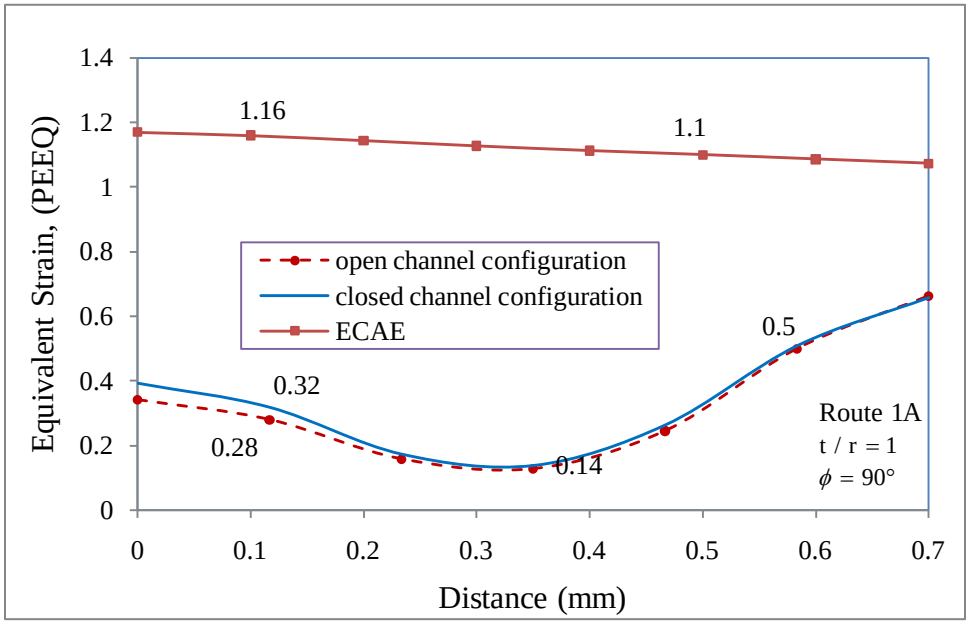

Fig. 14. Model results for comparison of equivalent strain (PEEQ) distribution across the thickness.

Though, the drawing force requirement from Fig. 17 is almost the same for both arrangements, a major advantage is gained with respect to the reduction in thickness.

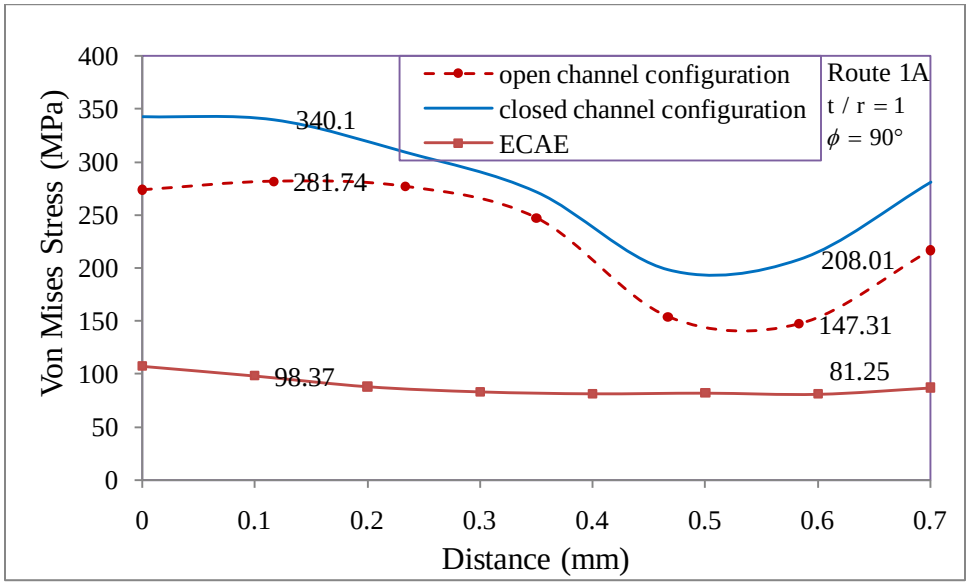

Fig. 15. Model results for comparison of von-Mises stress distribution across the thickness.

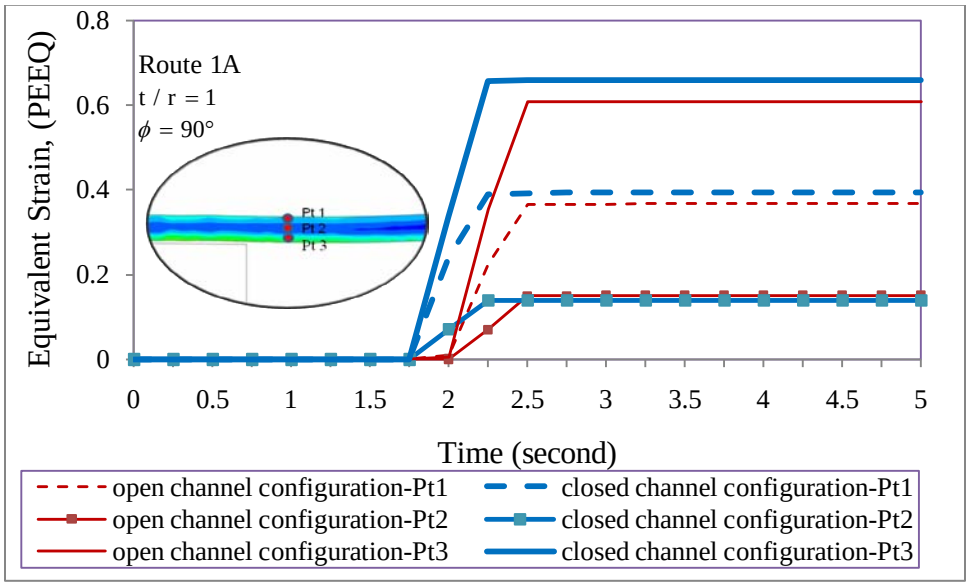

Fig. 16. Model results for comparison of equivalent strain (PEEQ) history.

As seen in Fig. 18 for the open channel configuration, the reduction in thickness varies from 9.05% to 11.1% for (t/r = 1), while for the closed channel configuration it is 7.6% to 8.86%. This is a significant improvement. For higher t/r ratios the results are more encouraging and could be exploited for commercial use. Another interesting fact is that instead of constraining the sheet metal in closed channels, if a small gap is maintained, then this reduction in thickness can be further reduced. However this will be at the cost of a smaller equivalent strain.

Once it is confirmed that equal channel angular drawing (ECAD), i.e. the close channel configuration, offers advantages with respect to equivalent strain and minimization in reduction in thickness, it will be interesting to analyze different processing parameters that influence the grain refinement process. One of the parameters studied is the effect of drawing angle. Three different angles, namely 90º, 115º and 135º degrees were evaluated.

Fig. 19 presents a comparison of the drawing force requirement for these three angles, and it is observed that though there is little difference, the peak force requirement for 90º is higher compared to 135º. In other words, with the increase in the angle of drawing, the drawing process becomes easier and drawing force requirement is reduced.

However, as discussed before, this minimization in the drawing force is at the cost of equivalent strain. As with the increase in the drawing angle where the area of contact at the sharp corner increases, the strains are reduced at any given location across the thickness. This is as illustrated in Fig.20.

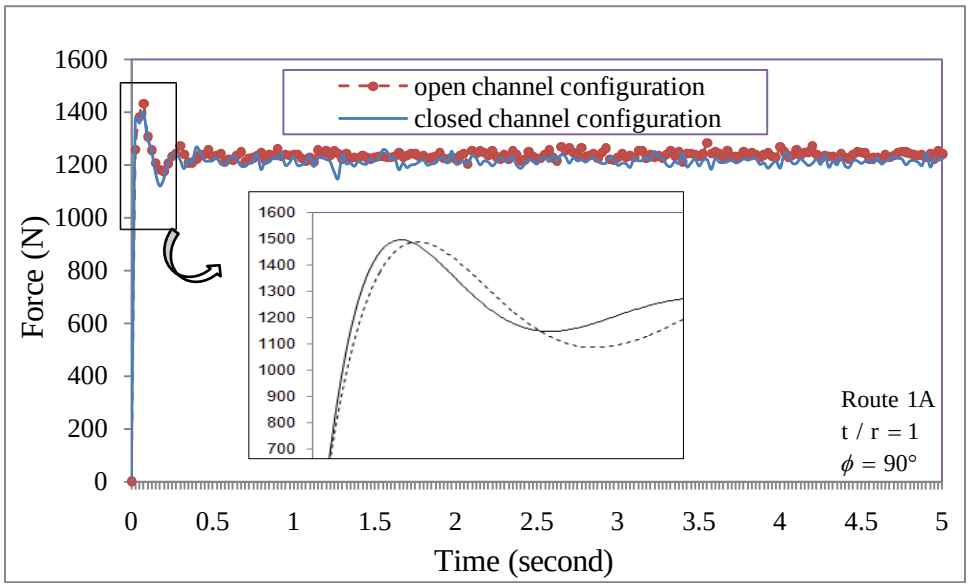

Fig. 17. Model results for comparison of drawing force requirements.

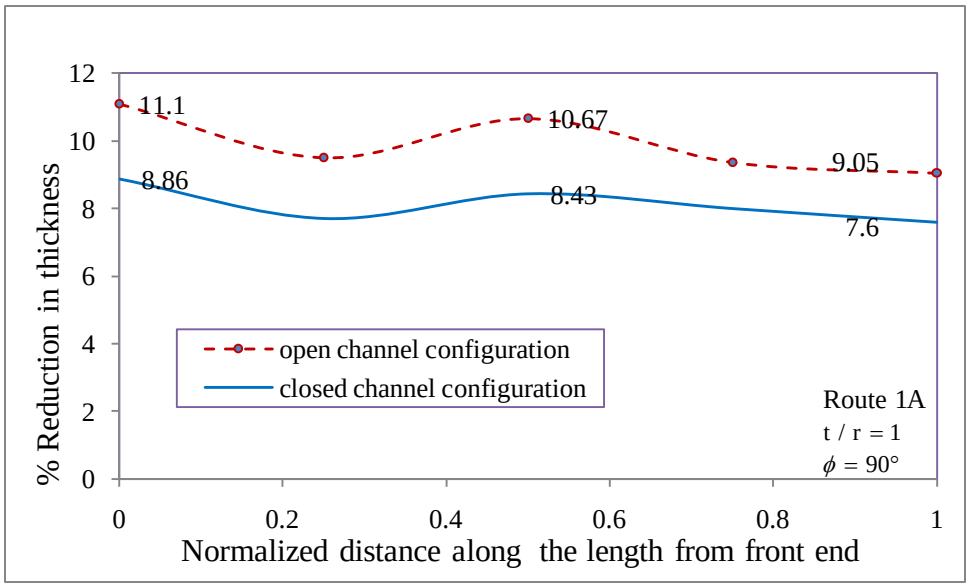

Fig. 18. Model results for comparison of percent reduction in thickness.

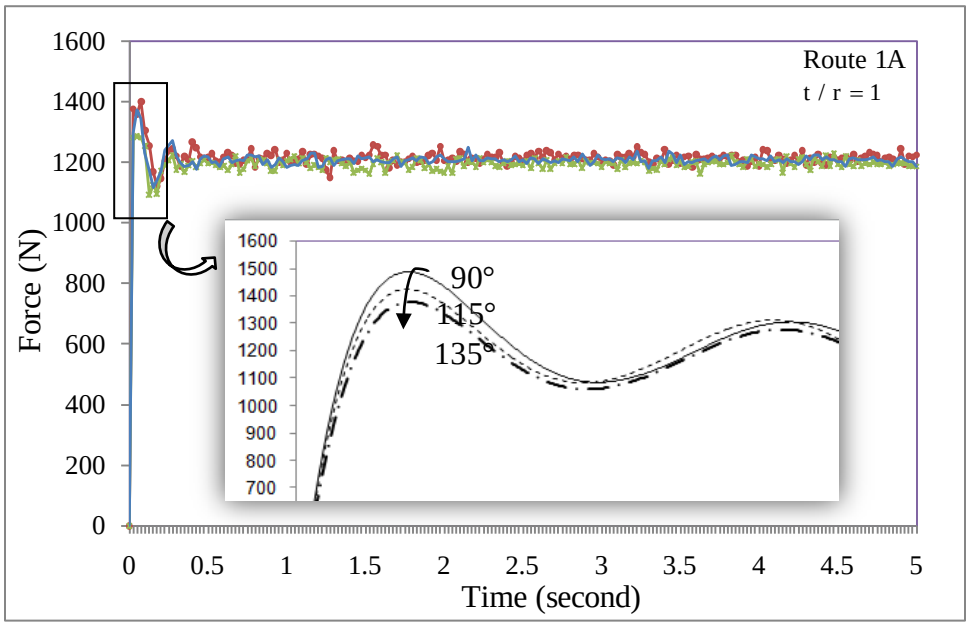

Fig. 19. Model results for closed channel configuration: comparison of drawing force requirement at different drawing angles.

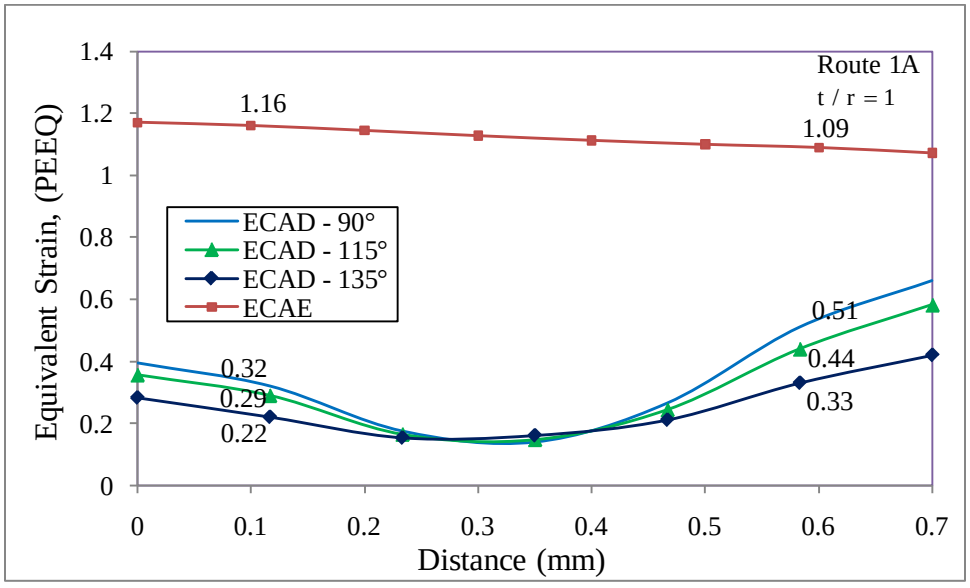

Fig. 20. Model results for closed channel drawing: comparison of equivalent strain (PEEQ) across the thickness.

Two important conclusions are obtained from the equivalent strain history for these three angles (Fig. 21). First, with the increase in angle, the equivalent strains are significantly reduced. Secondly an increased angle reduces the strain non-uniformity. This means the strain distribution along the thickness in the case of 135º is more uniform as compared to the one obtained at 90º. This aspect could be very important when implementing the design of the closed channel configuration for commercialization. This is because the uniform strain distribution implies the possibility of uniform microstructure and isotropic mechanical properties.

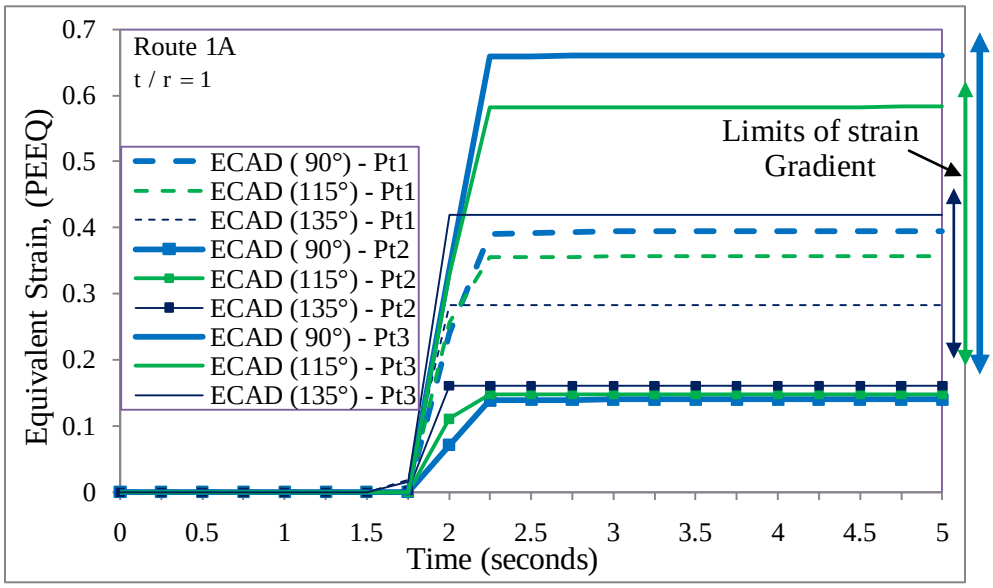

Fig. 21. Model results for closed channel configuration: comparison of strain history at different angles.

3.3. Simulations of Equal Channel Angular Extrusion (ECAE)

3.3.1. Geometry and model

The initial configuration used during modeling of the ECAE process is shown in Fig. 22 wherein twelve IF-steel sheets are embedded in IF-steel cans outer dimensions 1”x1”x10” size. This model stimulates the experimental study. For simplicity, it is assumed that all the sheets follow the same strain history, so the entire group of sheets is modeled as a single region. The die geometry plays an important role on material flow during this process. In this study the dies have an angle of intersection of the channels equal to $\phi = 90°$, and have an angle of the outer arc of curvature $\psi = 0°$ is used.

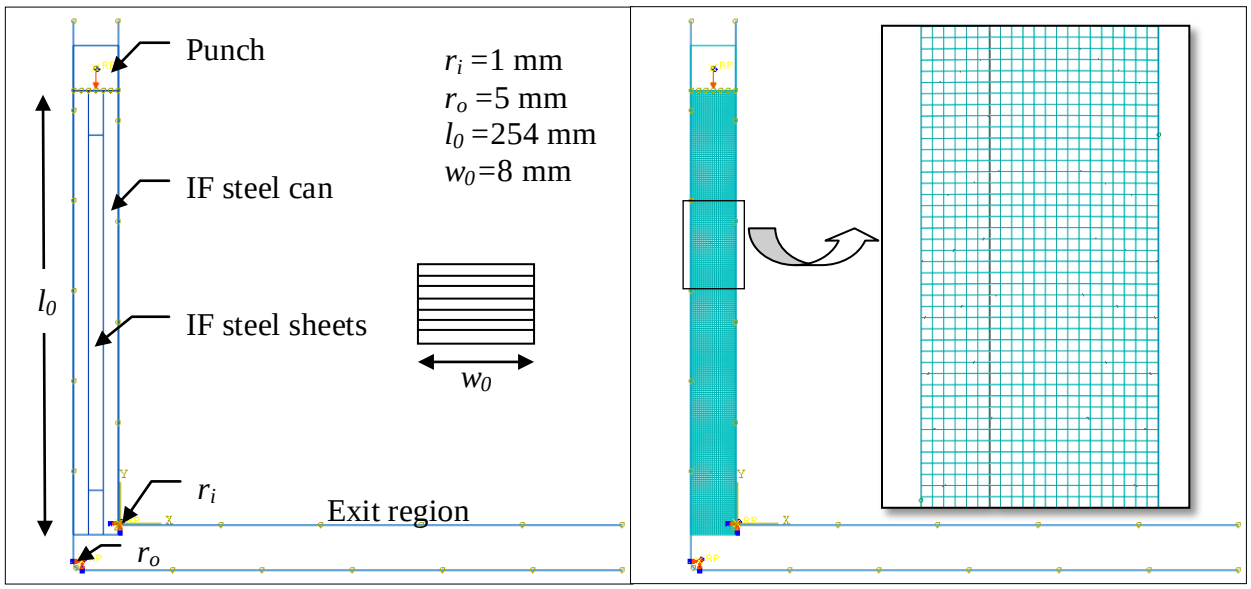

Fig. 22. Initial configuration for ECAE of IF steel sheets.

Channels of intersection are rounded-off with the inner radius r_i =1 mm and outer radius r_o =5 mm, to avoid the numerical singularity problem as the material flows plastically around the corners. The punch, and die channels are modeled as discrete rigid surfaces while the embedded IF steel sheets and billet are modeled using 4389 4-node bilinear plane strain quadrilateral elements with reduced integration (CPE4R).

Similarly, to understand the response of these canned IF steel samples after two passes of ECAE, a small change in die geometry is implemented. It is illustrated in Figs. 23 and 24, which present the initial configuration. The response is analyzed after 2A and 2C passes respectively. During route 2A, the sheet orientation is kept the same from one pass to other, while in route 2C the sheet was rotated by 180° in between two passes.

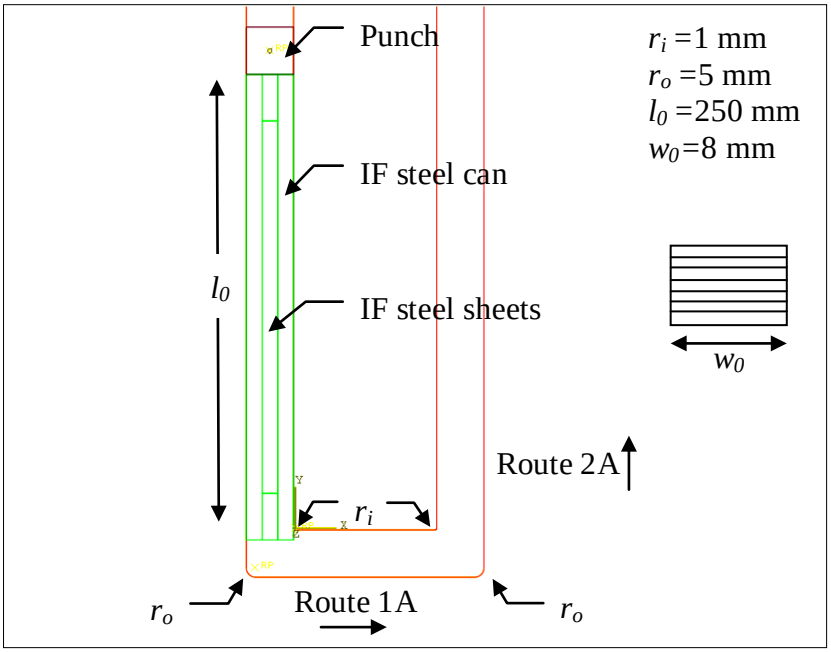

Fig. 23. Schematic of initial configuration for ECAE route 2A.

3.3.2. *Material properties*

Similar to drawing simulation, an elastic-plastic model is assumed for the IF-steel billet. The properties are as discussed before in Table 2.

3.3.3. *Contact interaction*

To model the plastic flow of the billet through the die including the initial upsetting of billet, a surface to surface contact interaction is defined between the die-bottom surface and the leading edge of the billet in addition to direct contact between the dies and billet surfaces. The friction coefficient of 0.08 is assumed at all the contact surfaces.

3.3.4. *Loading*

A displacement boundary condition is defined for the extrusion punch using the *BOUNDARY option, with an amplitude of 200 mm, which ramps continuously through the complete time step of 60 seconds.

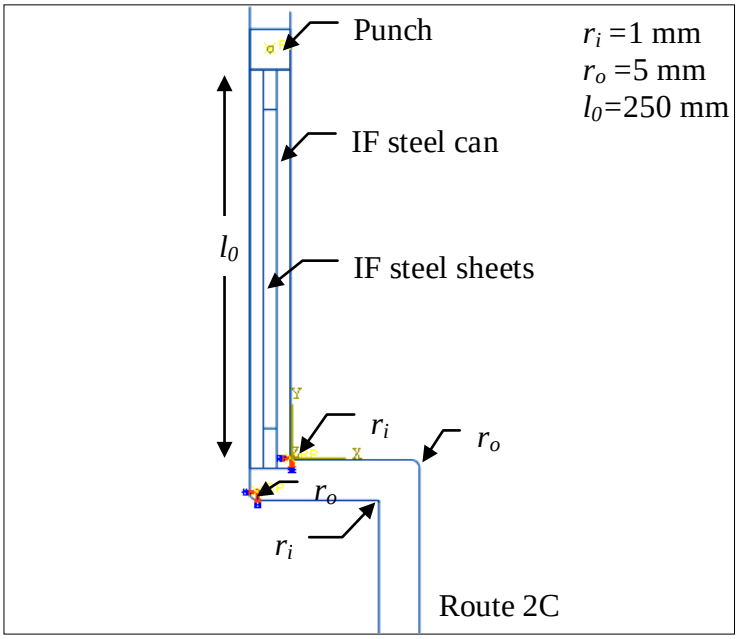

Fig. 24. Schematic of initial configuration for ECAE route 2C.

3.3.5. Results and discussion

Fig. 25 presents the von-Mises stress developed in the IF steel billet after one complete pass, while Fig. 26 presents the progressive evolution of stresses showing the upsetting phenomenon, resulting high stressed shear zone at the front of exit angle, and then development of steady stabilized stress contours. Thus after 20% of stroke length, the process reaches a steady state resulting in uniform stress along the length. The results of similar study are provided in Figs. 27 and 28 which illustrate the evolution of equivalent strain in the billet after one pass.

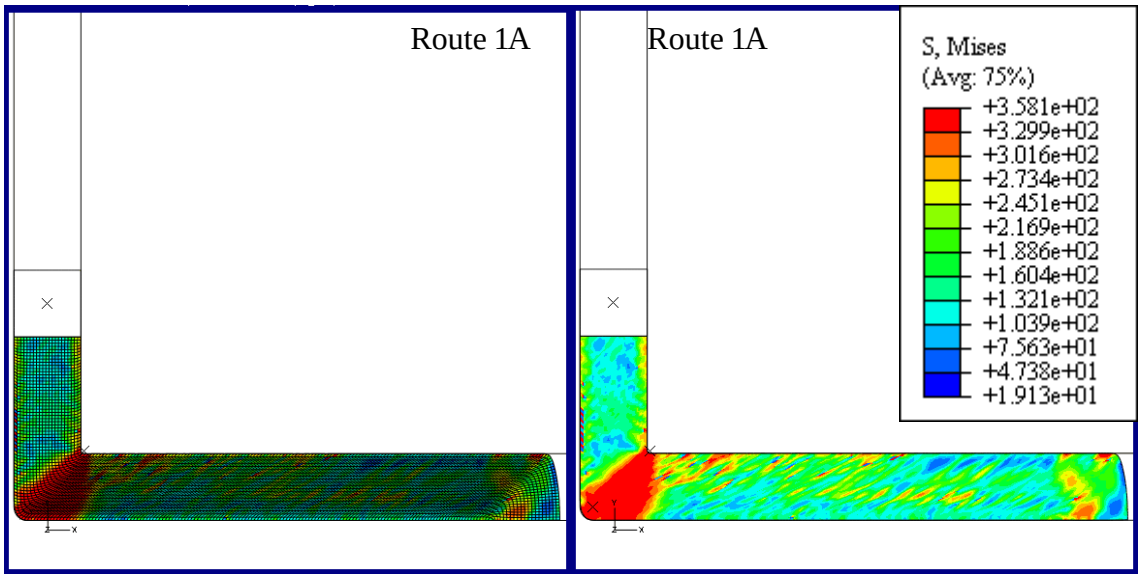

Fig. 25. Model results for ECAE: von-Mises stress contours (with μ=0.08).

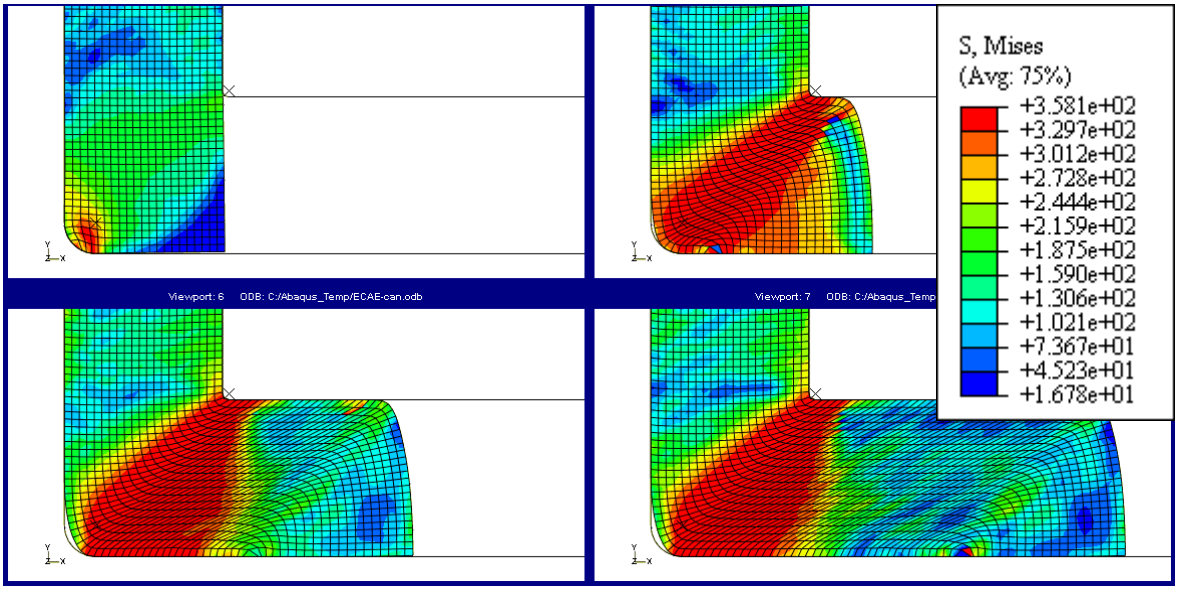

Fig. 26. Model results for ECAE: stress evolution during upsetting (with μ=0.08).

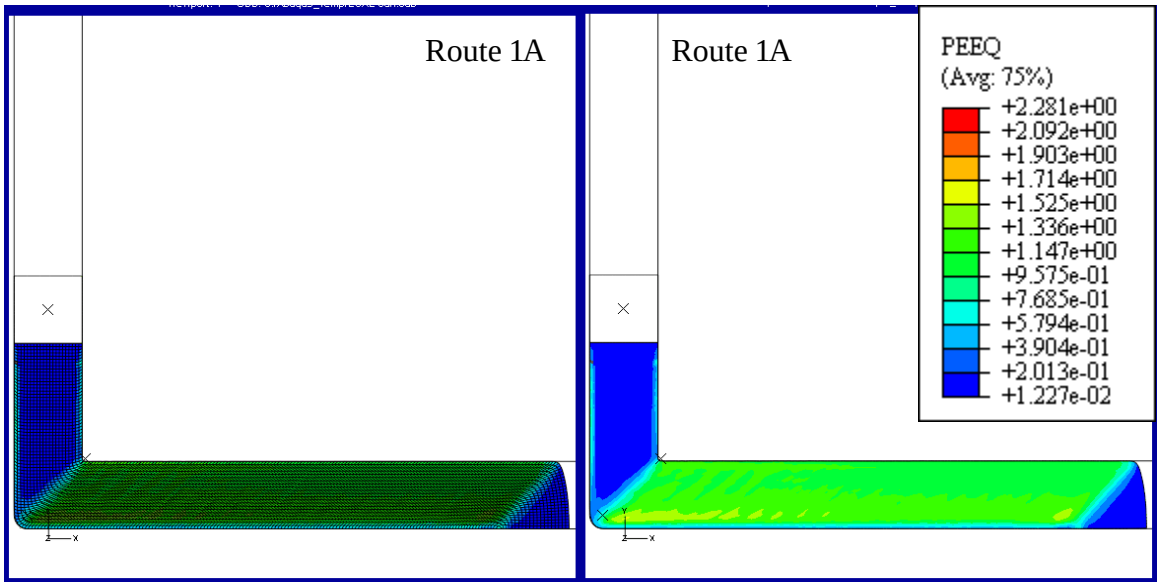

Fig. 27. Model results for ECAE: equivalent strain (PEEQ) contours (with μ=0.08).

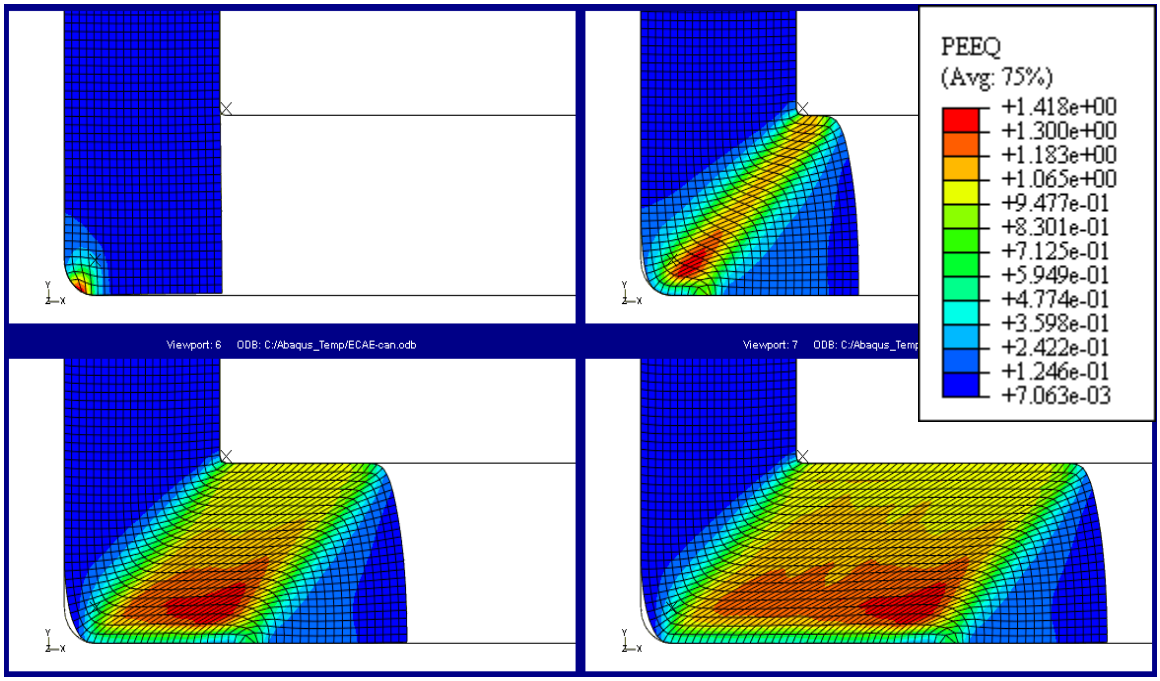

Fig. 28. Model results for ECAE: equivalent strain history (with μ=0.08).

For a better understanding of resulting equivalent strains in IF steel sheets embedded within the billet, only the section containing sheet samples is evaluated for further analysis. Fig. 29 shows the development of uniform equivalent strains across the thickness and along the length for this section. Fig. 30 explains the strain history for three points across the thickness. Slightly higher strains are observed at point 1. It is believed that this difference may be due to influence of friction and dead metal zone at the bottom surface. So, the average equivalent strain across the thickness after one pass of ECAE is 1.156 (point 2 and point 3). This is in conformity with the equivalent strains obtained by Segal's strain model [6], according to which the strains are given by the relation:

$$\varepsilon_n = \frac{2\,N}{\sqrt{3}} = 1.155\,N\,. \qquad (10)$$

The expression is applicable for $\phi = 90^{\circ}$ and where, N = No. of passes.

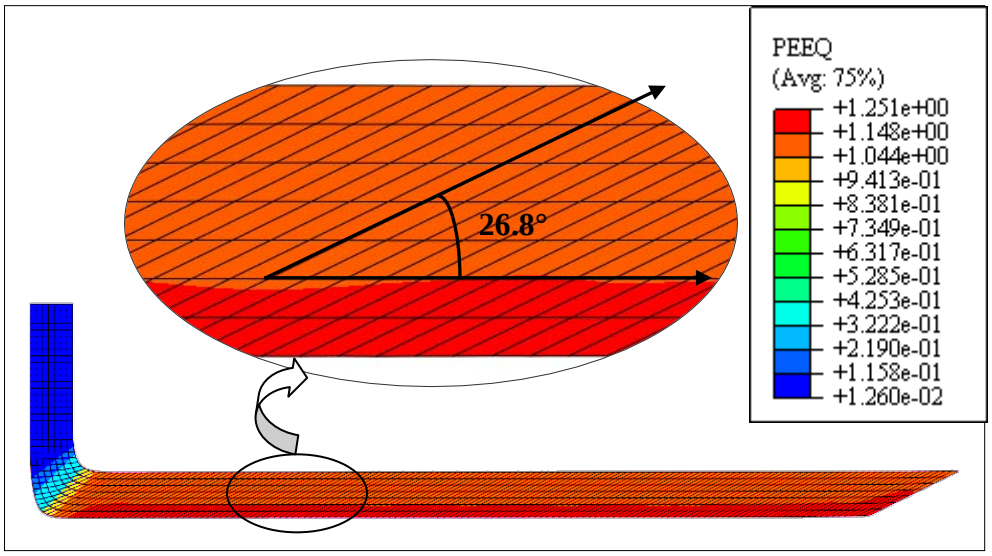

Fig. 29. Model results for ECAE: equivalent strain in canned IF steel sheets without friction.

A quick study was performed to realize the influence of friction. It is seen that if the friction between the die-metal contact surfaces is completely eliminated then it results in a slight reduction in strain. However, the uniformity of strain improves across the thickness. It is illustrated in Fig. 31.

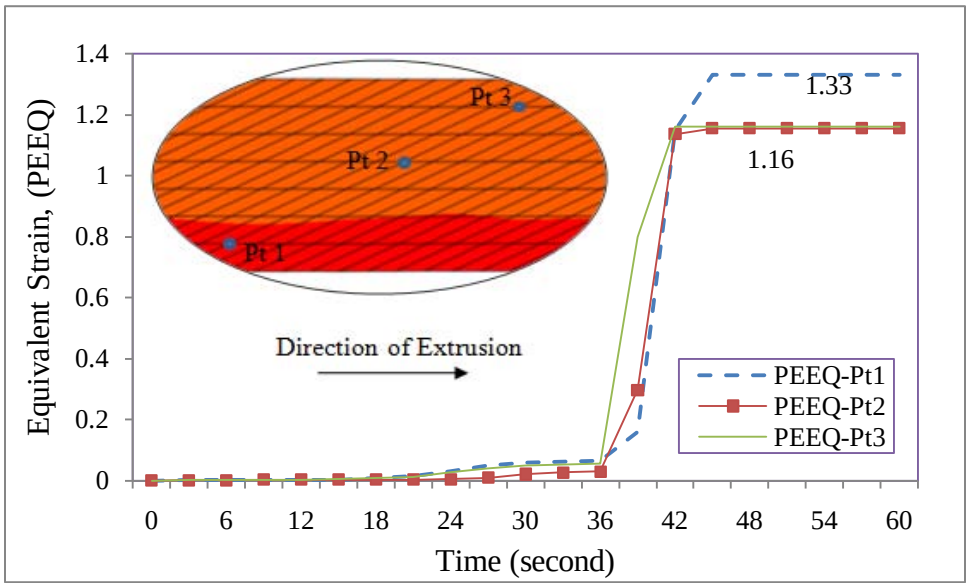

Fig. 30. Model results for ECAE: equivalent strain history in IF steel sheets (with μ=0.08).

After analyzing the response of IF steel sheet samples subjected to ECAE after one pass, a study was performed to explore it further for two passes, route 2A and route 2C. As presented in Fig. 32 during route 2A, the mesh elements are elongated in the direction of extrusion, while after route 2C the deformed elements regain an aspect ratio of almost one. This simulates the experimental behavior that in route 2A grains are refined by elongating in the direction of extrusion.

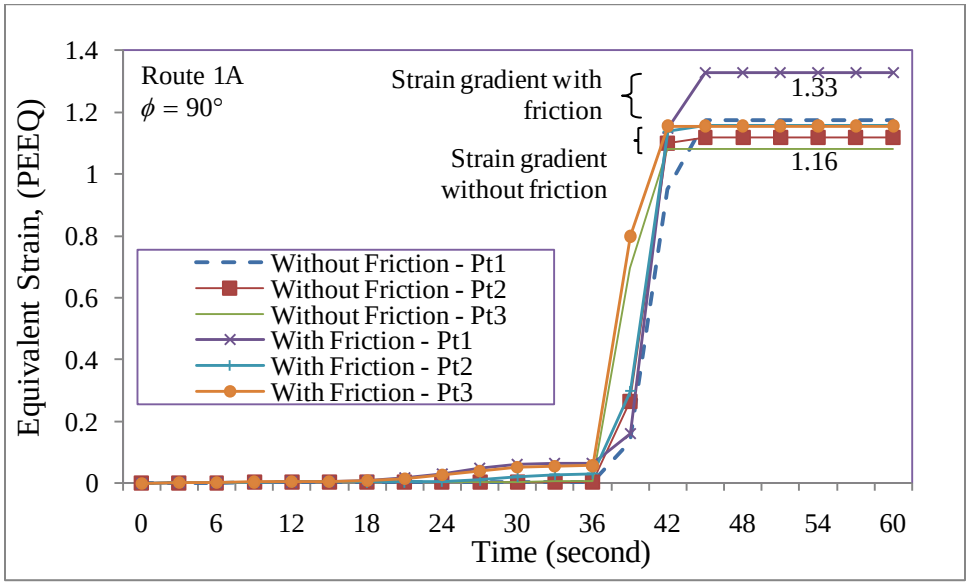

Fig. 31. Model results for ECAE: comparison of strain history in IF steel sheets with and without friction.

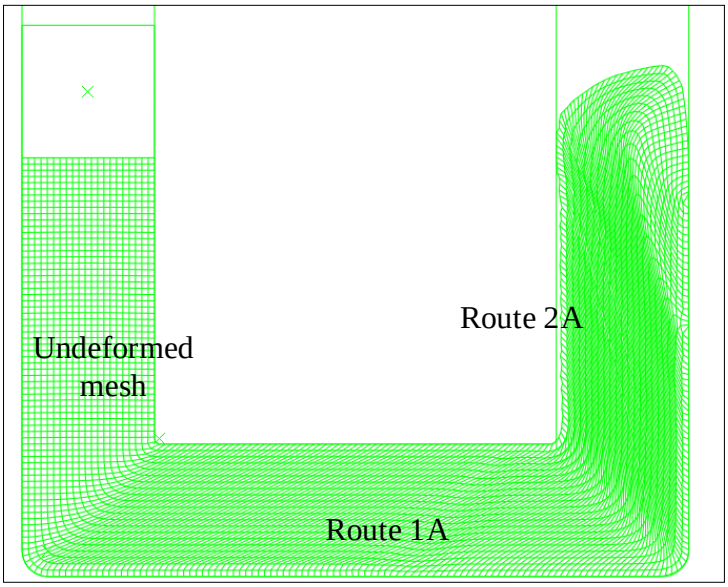

Fig. 32. Model results for ECAE route 2A: deformed mesh without friction.

Figs. 33 and 34 present the von-Mises stress contours and equivalent strain contours for the billet, while Fig. 35 presents strain contours for embedded IF steel samples after route 2A. Similarly, Figs. 36 through Fig. 38 present these contours for route 2C. It is evident that in route 2C, the grains regain their original orientation.

The extrusion force requirement for route 1A, 2A and 2C are presented in Fig. 39 As expected for the second pass, the force requirements are almost twice with route 2A which are slightly higher compared to the requirement of route 2C. This increase is primarily due to work hardening of material during first pass.

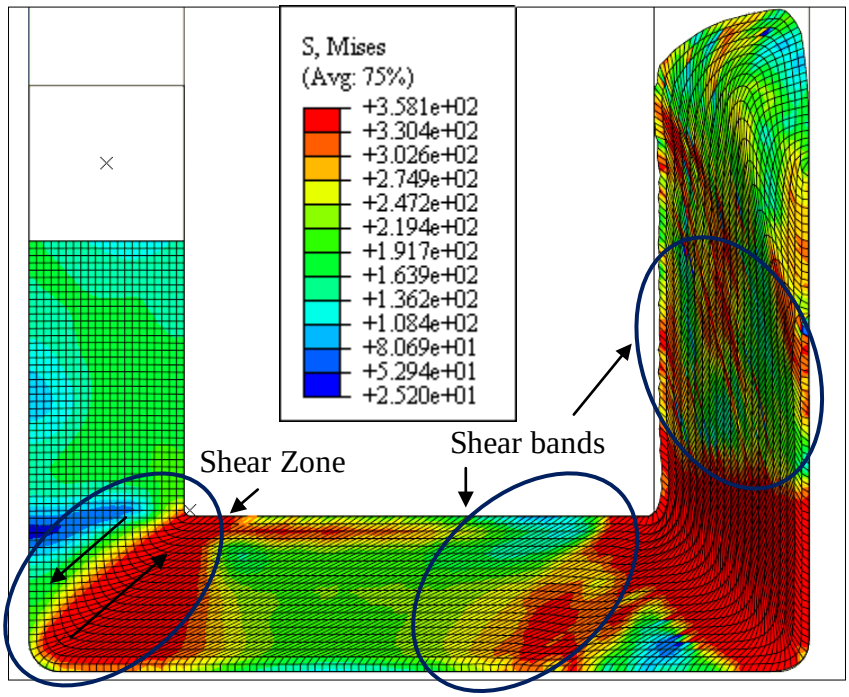

Fig. 33. Model results for ECAE route 2A: von-Mises stress contours without friction.

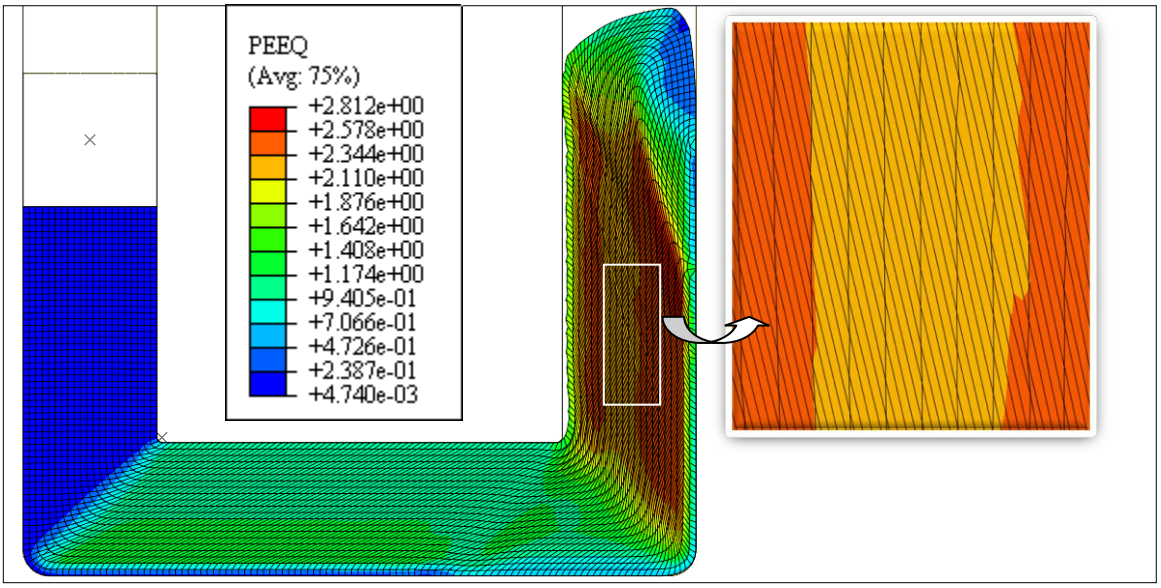

Fig. 34. Model results for ECAE route 2A: equivalent strain contours without friction.

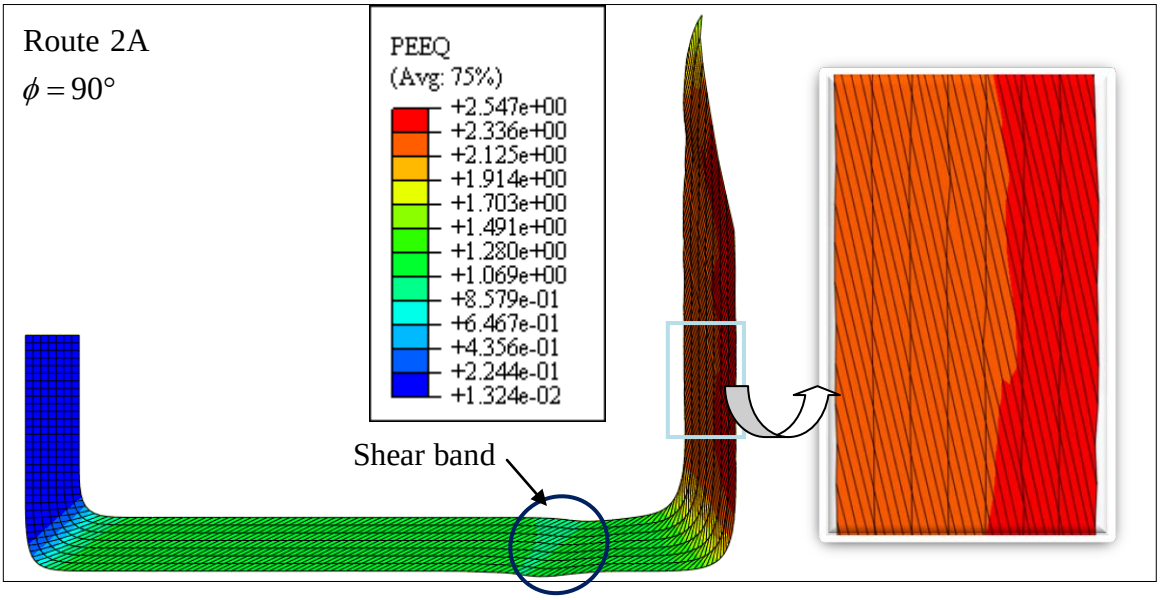

Fig. 35. Model results for ECAE: equivalent strain in IF steel sheets without friction.

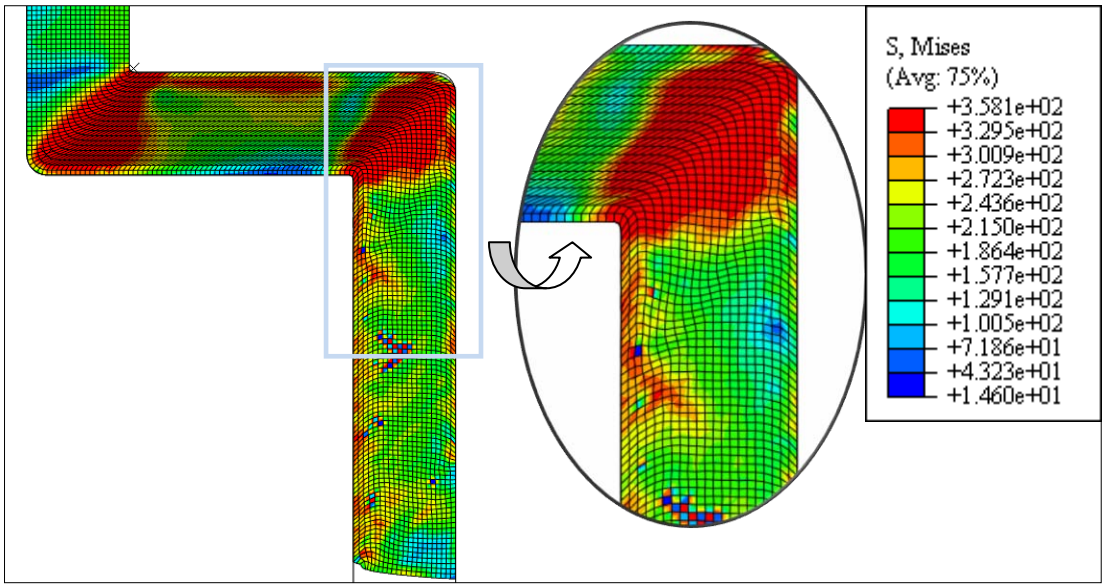

Fig. 36. Model results for ECAE: von-Mises stress contours without friction.

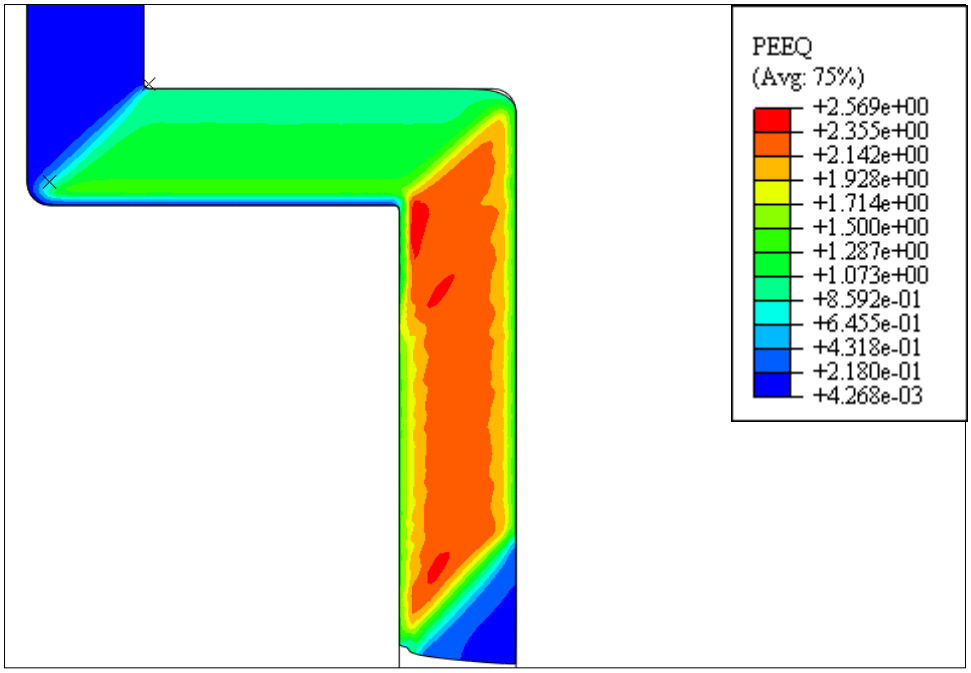

Fig. 37. Model results for ECAE: equivalent strain (PEEQ) contours without friction.

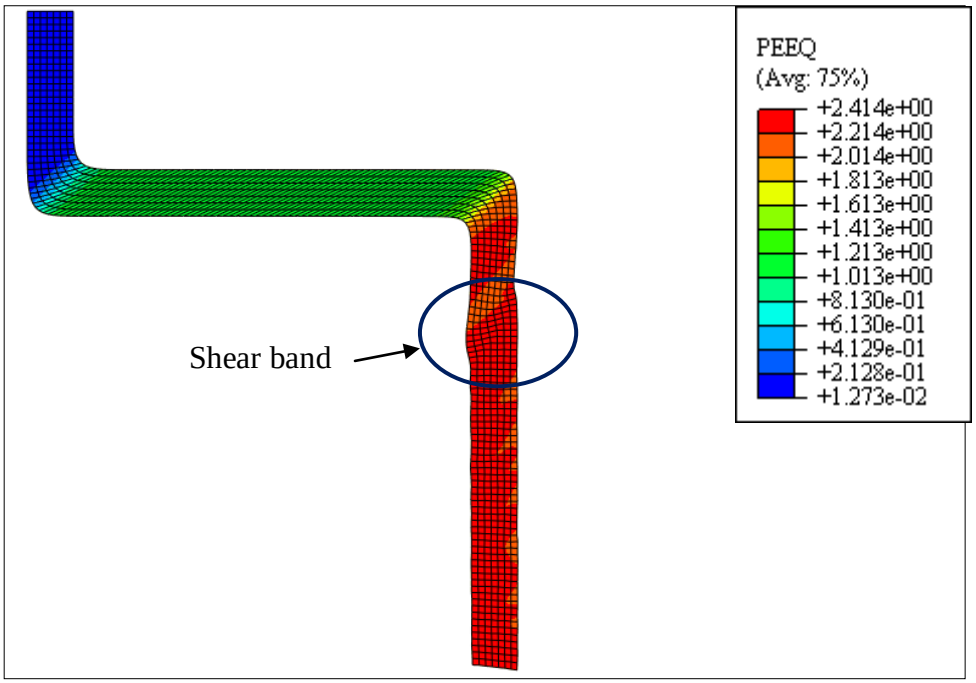

Fig. 38. Model results for ECAE: equivalent strain (PEEQ) in IF steel sheets without friction.

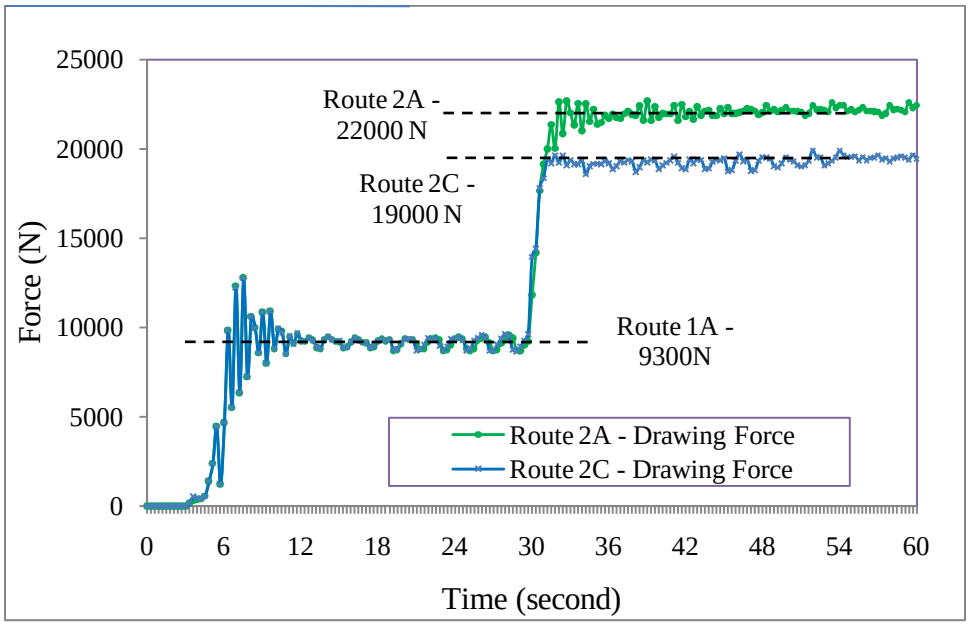

Fig. 39. Model results for ECAE: extrusion force measurement without friction.

Fig. 40 represents a comparison of stress distribution across the thickness for these three routes; while Fig. 41 illustrates the strain distribution across the thickness. For all routes the strain distribution is fairly uniform across the thickness. Localized shear bands are seen in route 2A and 2C (Fig. 35 and 38). This was little surprising; as the assumption of an isotropic material model should have resulted in homogeneous shear. However it is believed that these are mainly due to simulation issues: sharp corners present singularity points; increasing the channel radii may eliminate shear band effects. Route 2A shows a slight edge over route 2C with respect to the strain; particularly along the edge closer to the bottom die wall of the exit channel. Table 3 presents a comparison of equivalent strain results obtained from numerical analysis with the strains predicted by Segal's strain model for $\phi = 90°$. The results match very closely. The strain history for route 2A and route 2C are presented in Figs. 42 and 43.

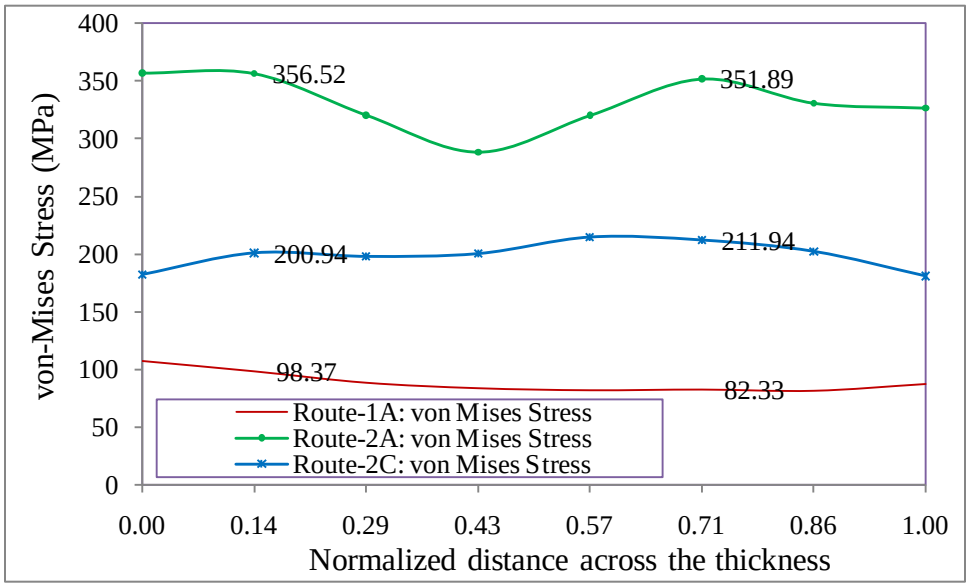

Fig. 40. Model results for ECAE: von-Mises stress distribution across the thickness.

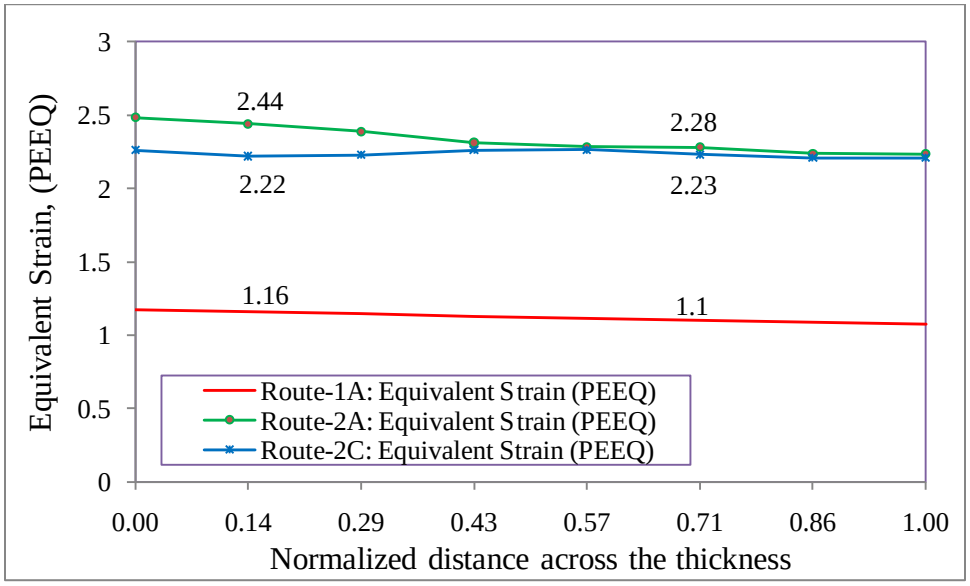

Fig. 41. Model results for ECAE: equivalent strain distribution across the thickness.

Table 3
Comparison of numerical results: equivalent strain values

ECAE Route	Strain value from Segal's strain Model	Equivalent Strain value from numerical simulations
1A	1.155	1.156
2A	2.311	2.304
2C	2.311	2.262

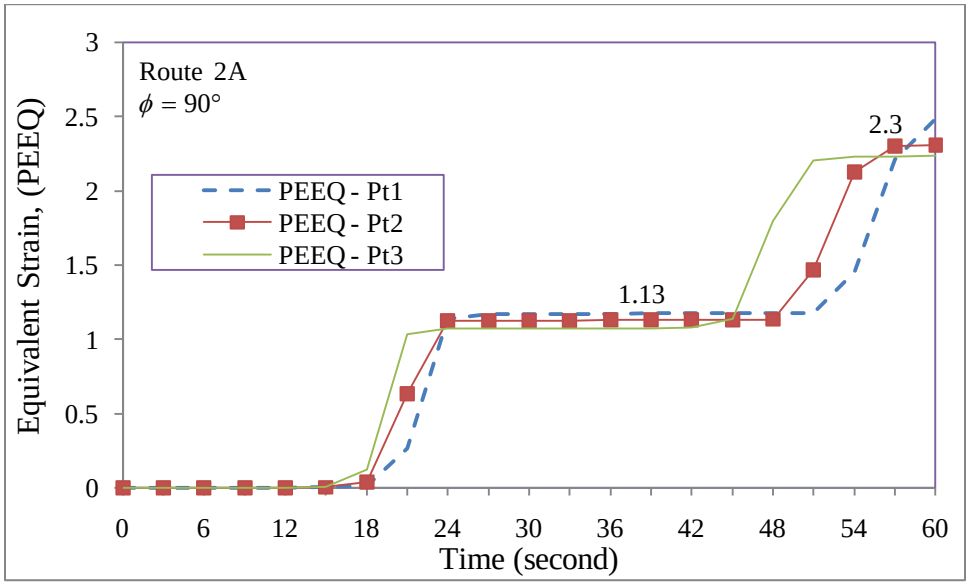

Fig. 42. Model results for ECAE route 2A: equivalent strain (PEEQ) history.

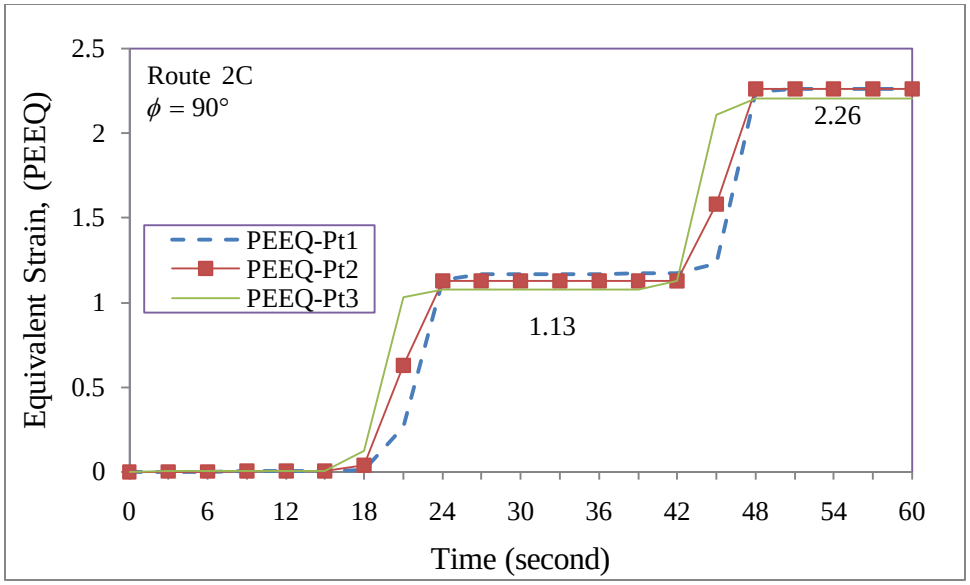

Fig. 43. Model results for ECAE route 2C: equivalent strain (PEEQ) history.

3.4. Simulations of combined drawing and extrusion process: shear deformation

3.4.1. Geometry and model

To analyze the performance of the proposed process (the combination of drawing and extrusion) as compared to the ECAD and ECAE techniques, a simplified geometry model was assumed wherein the initial configuration is same. All die surfaces are modeled using an analytical rigid surface while punches are discrete rigid surfaces. To retain the conformity of results material properties, contact interactions, and other numerical details are retained as in the earlier sections, with little variation in loading conditions.

3.4.2. Loading

To analyze the drawing process, a displacement boundary condition was applied to the reference point of the drawpunch, which is in turn was tied to the leading surface of the plate using *TIE option. Similarly, applying a displacement boundary condition to the reference point of the punch tied to the rear end of the plate approximates ECAE. However, it is to be noticed that this does not model the initial upsetting process. For the shear deformation process, the same displacement is applied at both ends.

Numerical studies were performed to compare the response of IF steel samples subjected to ECAD, ECAE, and the shear deformation processes. The results are interpreted in terms of the equivalent strain distribution across the specimen. The results are validated by comparing with analytical models.

3.4.3. Results and discussion

Fig. 44 provides the comparison of equivalent strain contours obtained after three processes: ECAD, ECAE and shear deformation. In the case of ECAD higher strains are observed near the two edges, with the maximum being near the edge closest to the inner corner. For ECAE and shear deformation the strains are fairly uniform across the thickness of the sheet specimens.

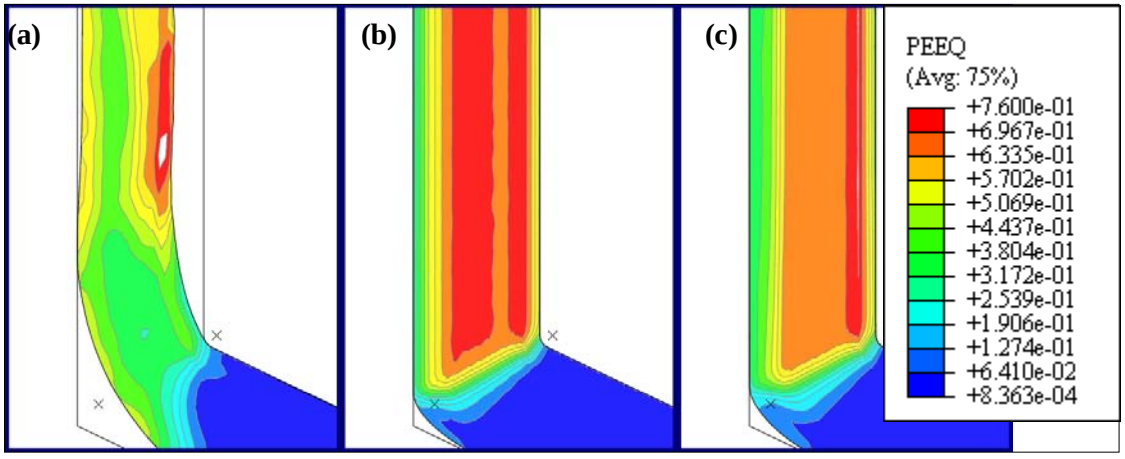

Fig. 44. Model results for comparison of equivalent strain (PEEQ) at 115º: (a) ECAD, (b) ECAE, (c) shear deformation.

From Fig. 45 it is seen that in ECAD higher stresses are observed near the surfaces. This is expected, because as the plate flows through closed channels, due to the sudden change in direction of flow, it initially experiences a higher compressive stress at the corner and then tries to flow through the exit channel along the opposite side (support surface).

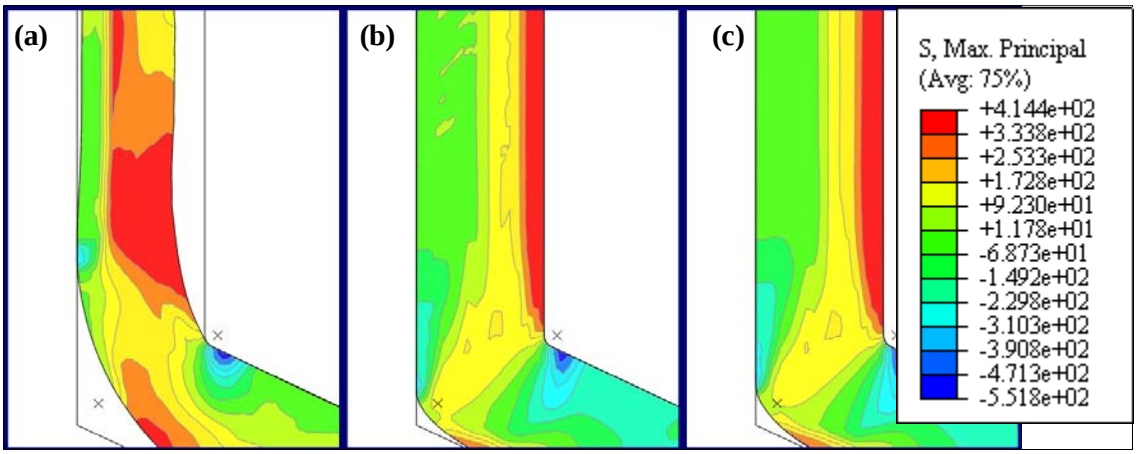

Fig. 45. Model results for comparison of maximum principal stress at 115°: (a) ECAD, (b) ECAE, (c) shear deformation.

In this study for a higher thickness to die radius ratio (*t/r* = 10) the reduction in thickness is also higher (23%). In addition, as illustrated in Fig. 44 (a), the strain distribution (and stress distribution) is not uniform. As observed from Table 4 ECAD alone cannot provide a satisfactory solution imparting a higher strain and thereby improving material properties. This is mainly because at lower *t/r* ratios average equivalent strains are lower and though with higher *t/r* ratios higher strains can be gained, this increase also results in a higher percent reduction in thickness.

On the other hand, the stress contours of the ECAE process (Fig. 44 (b)) and shear deformation process (Fig. 44 (C)) seem to have a similar and uniform profile. The strain contours of ECAE and shear deformation (Fig. 44 (b) and (c) respectively) confirm the uniformity of strain across the thickness. It is illustrated in Fig. 46, which compares the distribution of equivalent strain across the thickness for all three processes

Table 4
Model results of ECAD: influence of *t/r* ratio at 115° after one pass

Thickness to die radius ratio, *t/r*	Average equivalent strain (PEEQ) at centerline	Reduction in thickness
1	0.366	8.42%
10	0.584	23.02%

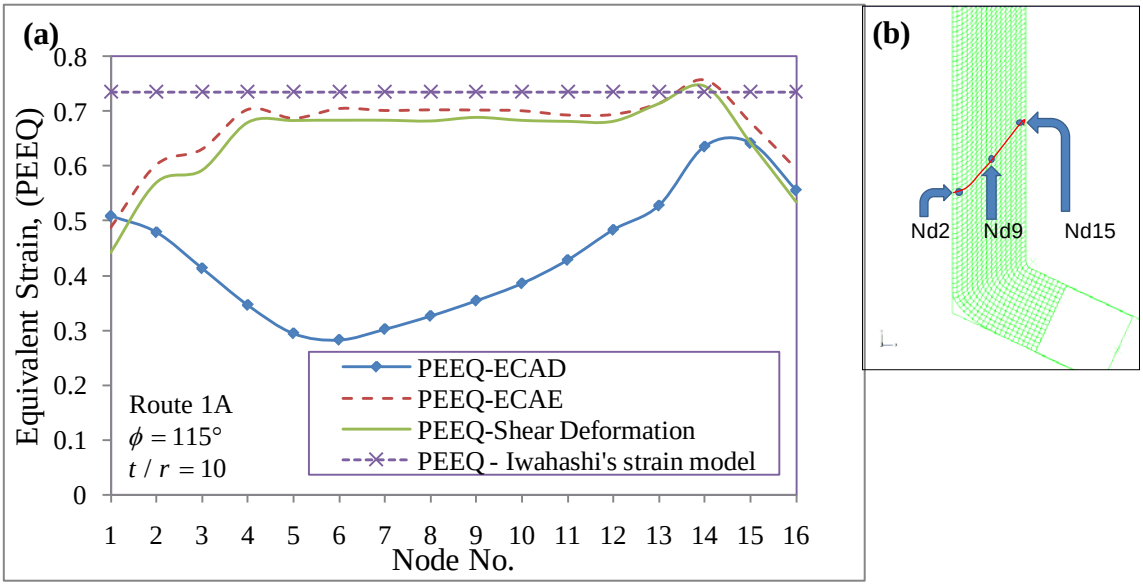

Fig. 46. (a) Model results for comparison of equivalent strain (PEEQ), (b) node location.

It is observed that, strains developed in the shear deformation process are very close to the ones developed during ECAE and are uniform over almost the entire thickness. However, with ECAD, strains are very small and non-uniform. The numerical results are very close to the equivalent strain predicted by Iwahashi's strain model. Figs. 47 through

49 present the strain history. It is evident that ECAD results in large strain gradient, while ECAE and shear deformation result in fairly uniform strains.

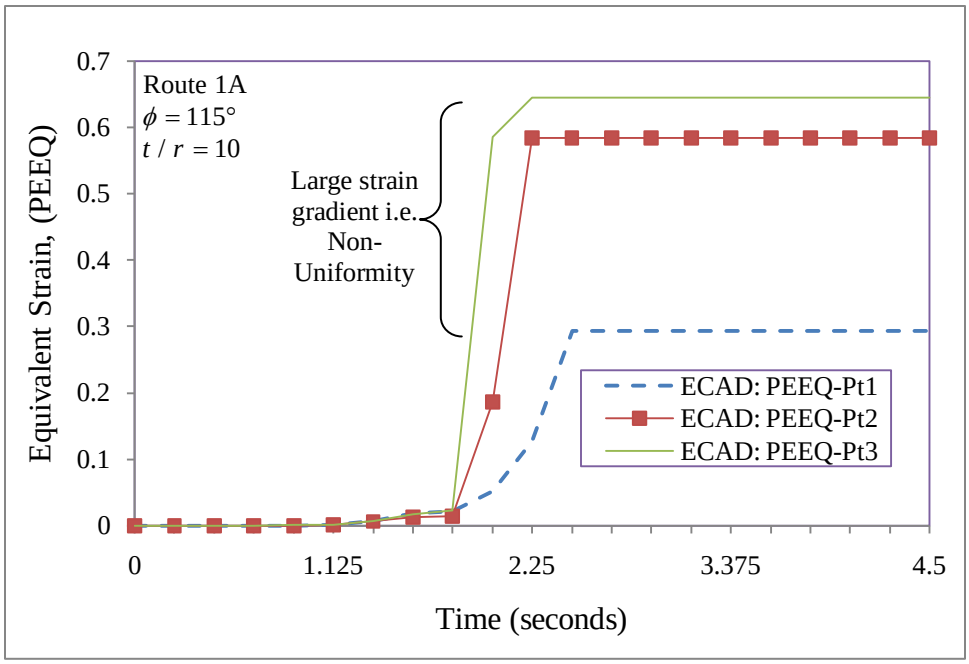

Fig. 47. Model results for ECAD: equivalent strain (PEEQ) history.

Fig. 50 presents the deformed mesh and Table 5 shows the comparison of shear angle and analytical solutions, validating the results. The variation is also presented in Fig. 51. This supports the hypothesis that combining ECAE and drawing results in strains of the order of those developed in classic ECAE.

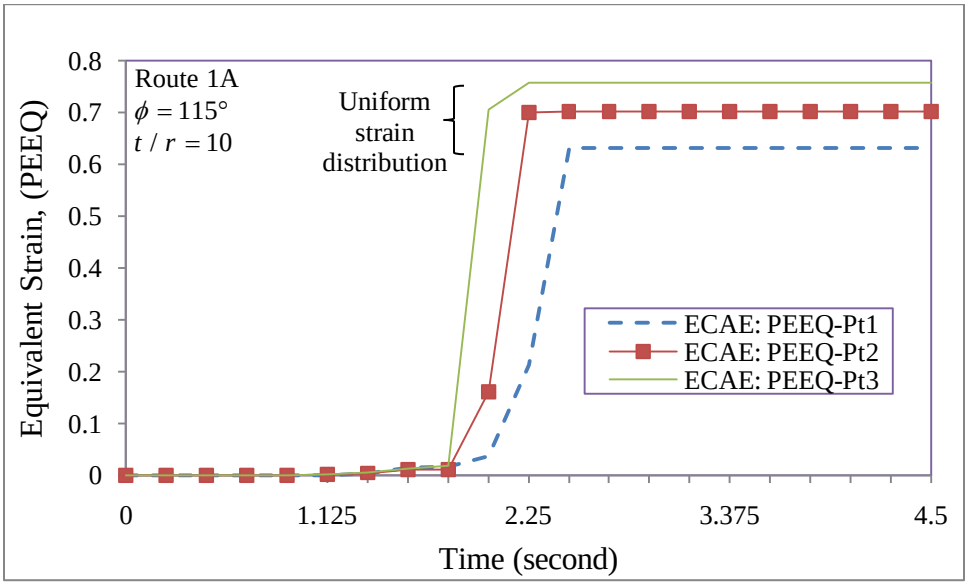

Fig. 48. Model results for ECAE: equivalent strain (PEEQ) history.

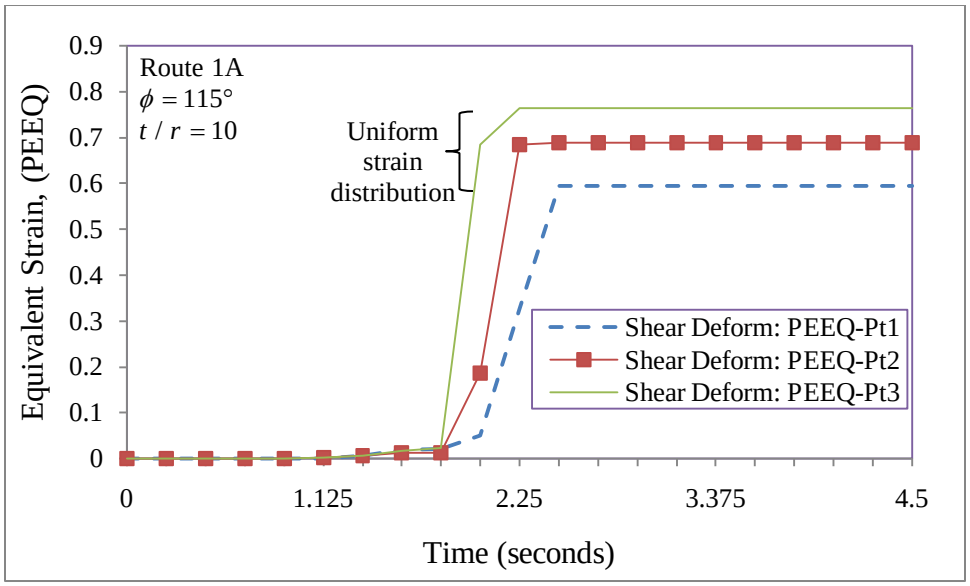

Fig. 49. Mode results for shear deformation: equivalent strain (PEEQ) history.

This indicates that the potential of shear deformation for developing the strain is equivalent to the one developed in classic ECAE.

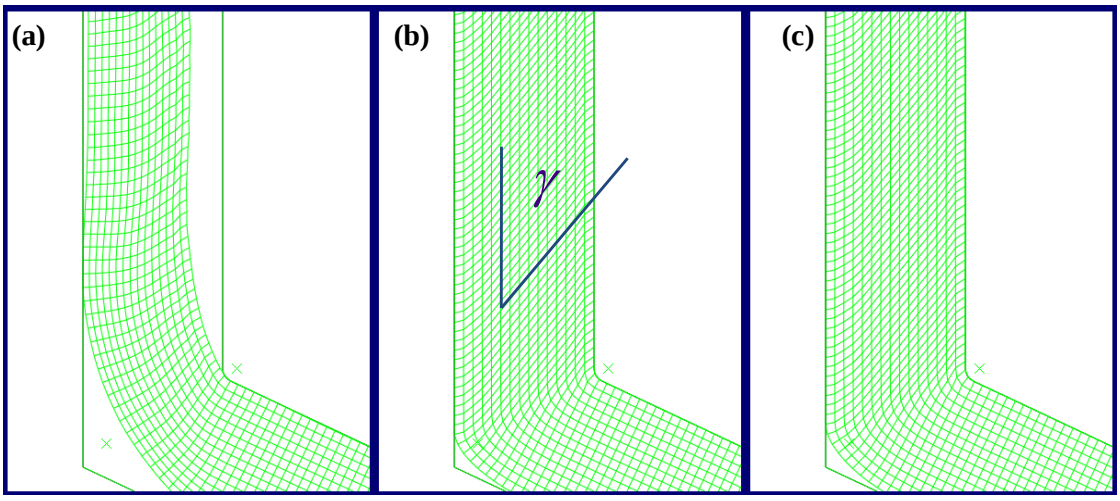

Fig. 50. Model results for comparison of deformed mesh at 115º: (a) ECAD, (b) ECAE, (c) shear deformation (t/r = 10).

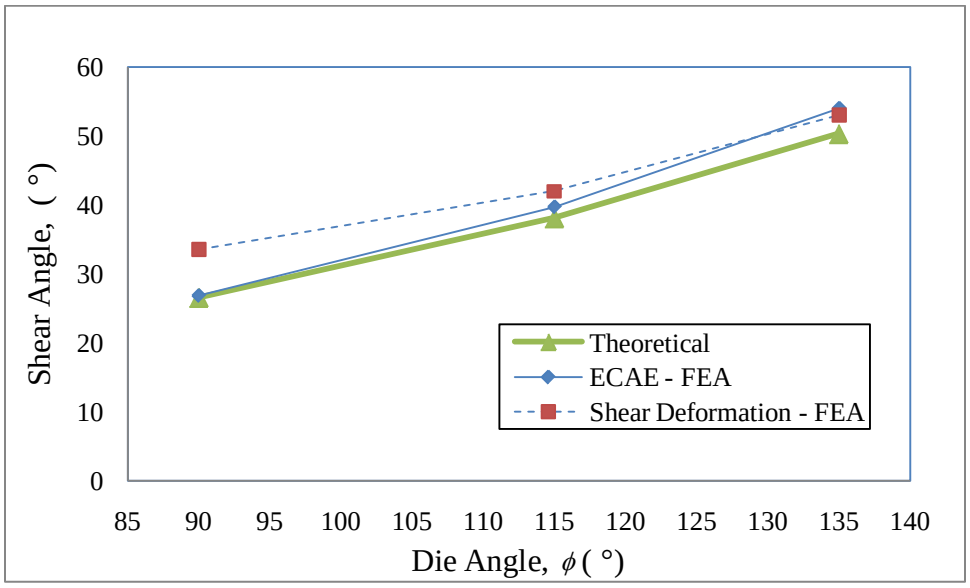

Fig. 51. Model results for comparison of shear angle with analytical results.

Table 5
Shear angle: comparison with analytical model

Die Angle, ϕ	Shear angle from Iwahashi's strain model	Shear angle from ECAE-FEA	Shear angle from shear deformation-FEA
90°	26.6°	26.8°	33.5°
115°	38.1°	39.7°	42.0°
135°	50.4°	54.0°	53.0°

3.5. Simulations of proposed continuous shear deformation process

3.5.1. Geometry and model

As discussed in previous section 2.5, by combining ECAE and drawing a continuous shear deformation technique can be achieved. For continuity of the operation one needs to feed the strip/ billet from one end into the dies while pulling it out from the other end. Different mechanisms can be used to achieve this effect. In this study rollers are used to model both a feeder mechanism and a drawing mechanism. The initial configuration with an angle of channel intersection of 115° is considered for this study (Fig. 52).

The IF steel sheet of original dimensions 3.5 mm x 250 mm is fed through the ECAE dies using a feeder mechanism consisting of two sets of rollers. During the feeding stage, the strip is reduced to approximately 3.2 mm in thickness (approx. 8.5% reduction). Another roller mechanism at the exit section pulls the plate out. The radius of the rollers,

R_o is 25 mm. The rollers are modeled as discrete rigid surfaces while dies are modeled as analytical rigid surfaces. The IF steel sheet is modeled using 3336, 4-node bilinear plane strain quadrilateral elements with reduced integration (CPE4R).

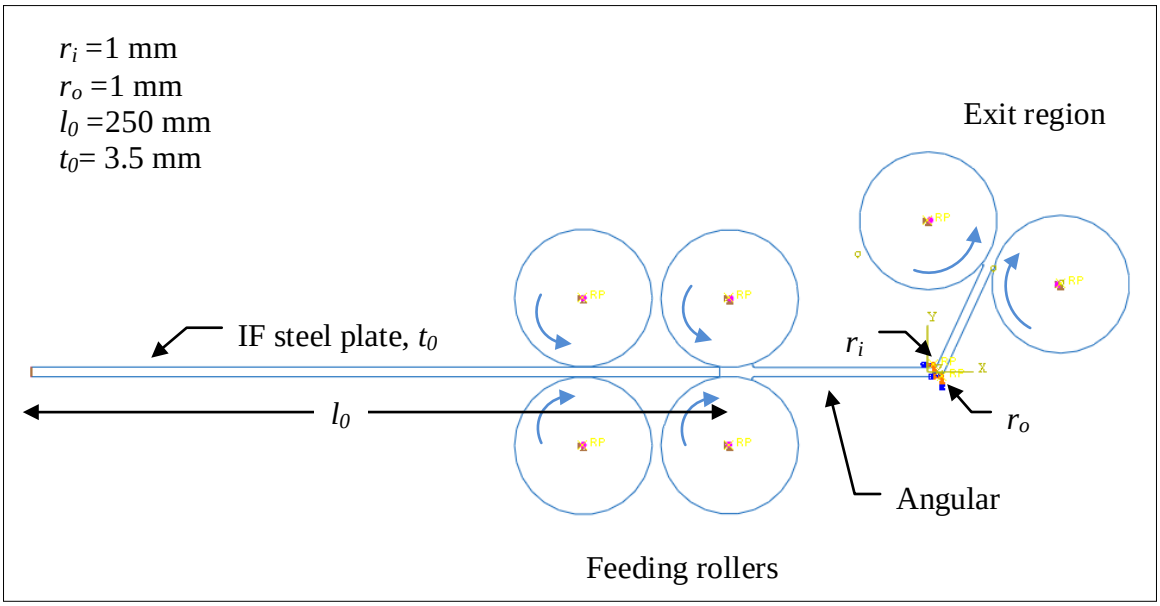

Fig. 52. Schematic of initial configuration for continuous shear deformation.

3.5.2. Material properties

The isotropic hardening curve of IF steel is described using 15 points on the stress strain plastic curve as presented in Table 2.

3.5.3. Contact interaction

Coulomb friction is assumed between the rollers and the plate, with a friction coefficient of 0.45. As friction is the only factor responsible for the plate into the rollers, it is an important parameter. The contact interaction between the roller and sheet

surfaces, and the die and sheet surfaces are defined using a surface-to-surface type kinematic contact method.

3.5.4. Loading

For a quasi-static study of the feeding operation, the rollers are rotated at a constant angular velocity of 0.628 rad/sec, which corresponds to a roller surface velocity of 15.7 mm/second. To initiate the rolling process, at the rear end the sheet is given an initial velocity of 1.0 mm/second in the x-direction for an initial 5% of the time step defined using the *AMPLITUDE option.

3.5.5. Results and discussion

Fig. 53 presents the deformed mesh pattern clearly showing the effects due to both the rolling deformation (with reduction of 8.5%) and shear deformation. The shear deformation is of the same degree as observed as in the case of ECAE route 1A.

The stress contour (Fig. 54) shows some non-uniformity and localized regions with low stresses. However, as seen in Fig. 55, strains are very uniform over a major portion across the thickness. This is further supported by comparing equivalent strain (PEEQ) presented in Fig. 56 It is seen that though the strain distribution is uniform across the thickness in the shear deformation process, it is slightly lower compared to the ECAE process. However, a major advantage is improvement in the equivalent strain as compared to conventional drawing. Fig. 57 presents the equivalent strain history identifying effects of rolling and shear deformation processes. As illustrated shear deformation develops a fairly uniform strain across the thickness.

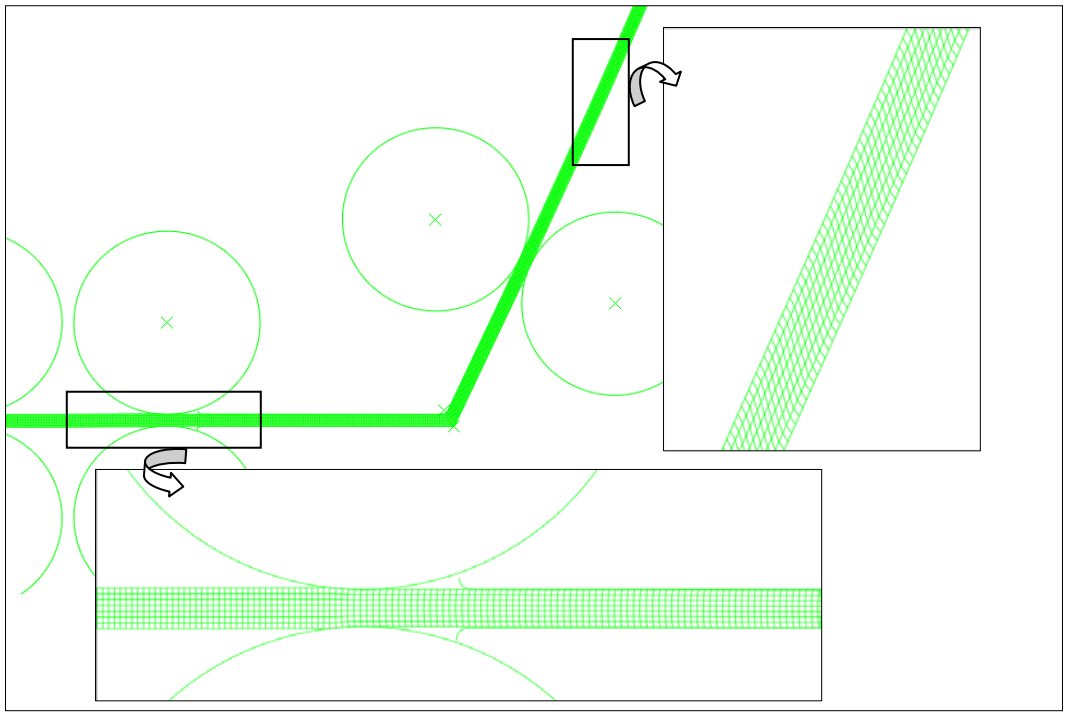

Fig. 53. Model results for continuous shear deformation: deformed mesh.

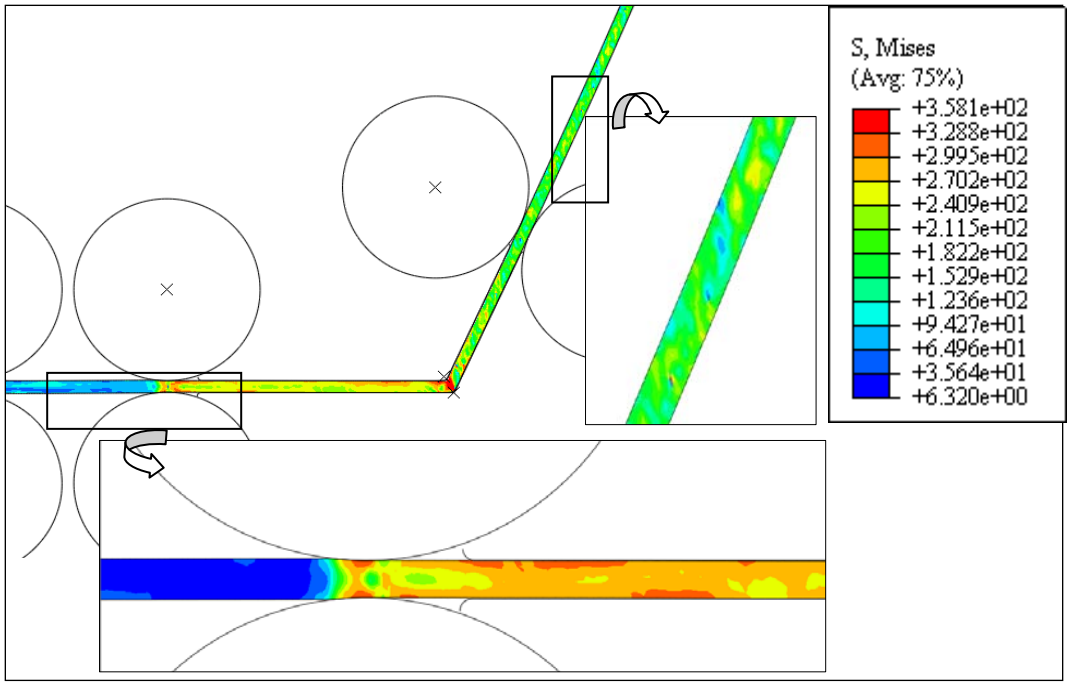

Fig. 54. Model results for continuous shear deformation: von-Mises stress contours.

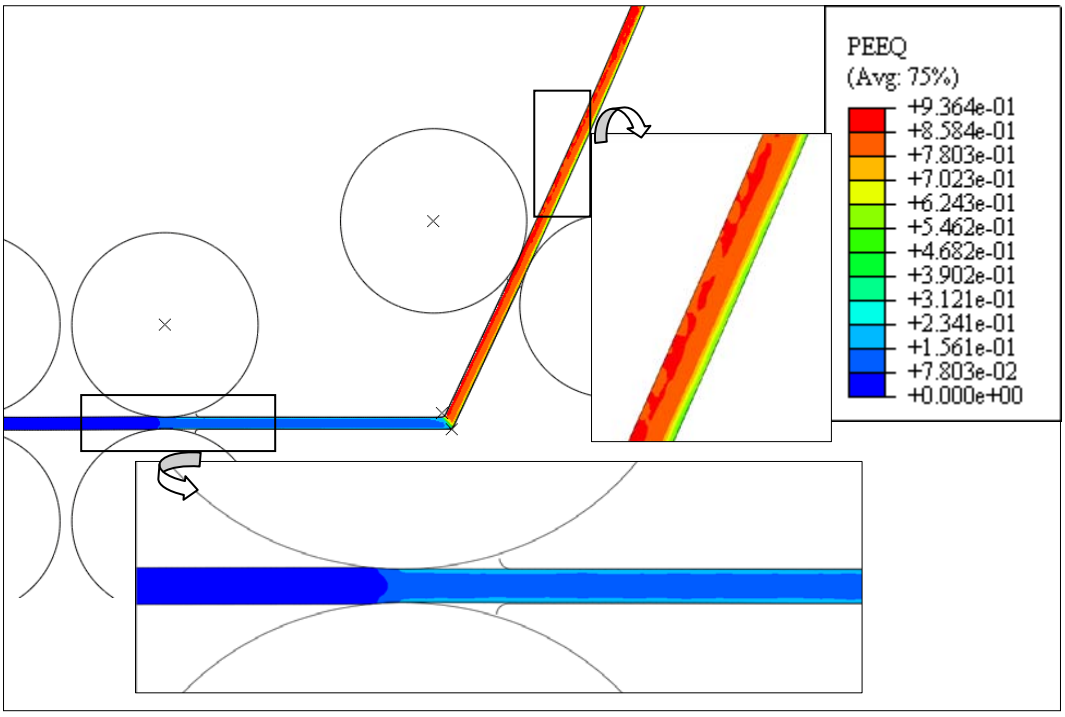

Fig. 55. Model results for continuous shear deformation: equivalent strain contours.

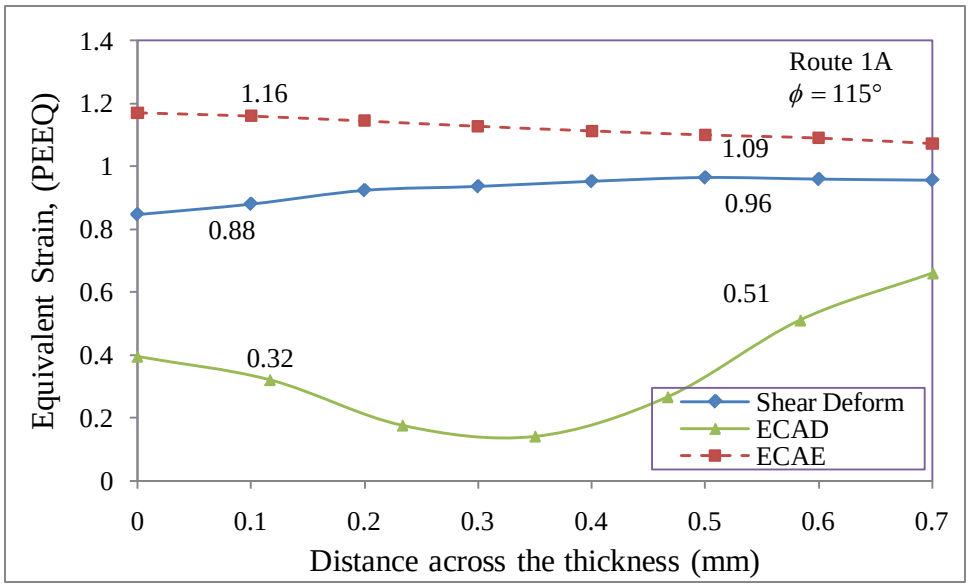

Fig. 56. Model results for comparison of equivalent strain distribution across the thickness.

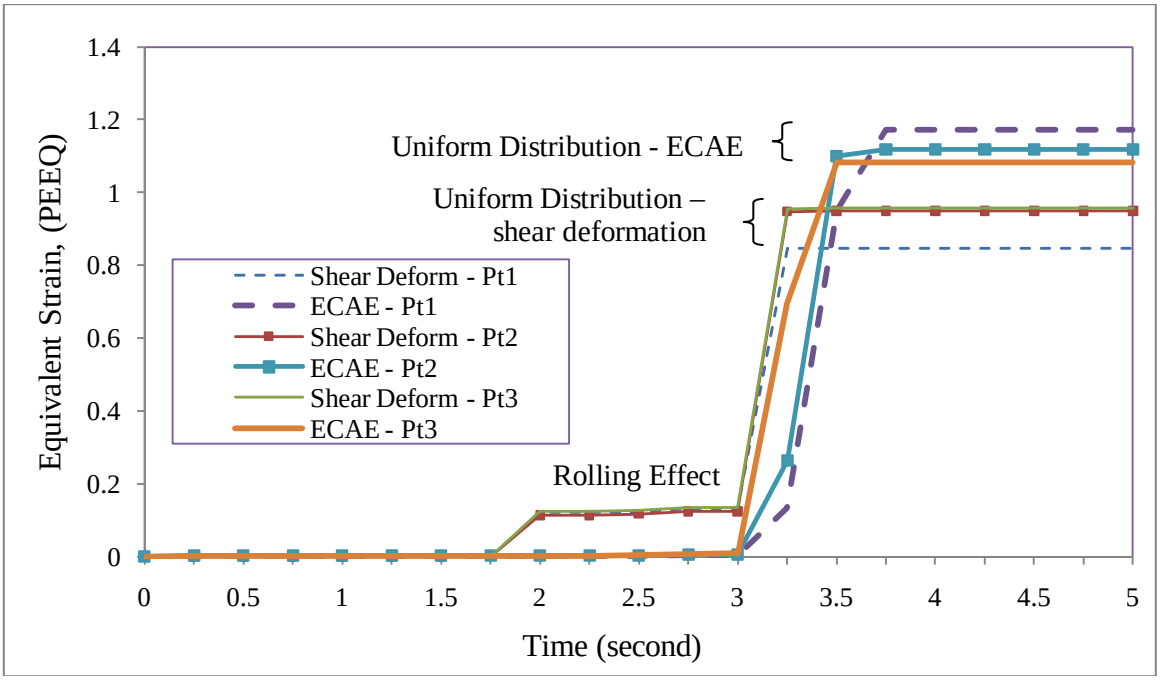

Fig. 57. Model results for continuous shear deformation: equivalent strain (PEEQ) history showing uniform strain distribution.

As mentioned earlier, friction between the plate and the rollers plays a vital role. Table 6 presents the influence of friction.

Table 6
Numerical results for continuous shear deformation: effect of friction coefficient

Friction coefficient		Results
Roll friction	Die-material friction	
0.3	0.0	Roll friction is not sufficient enough to feed the plate into the dies.
0.4	0.0	Rolls feed the plate into the dies however at the exit metal flow is not smooth and consistent.
0.4	0.08	Rolls feed the plate into the dies; however at the exit section the friction resistance is significantly high and the plate does not flow out.
0.45	0.08	Very smooth and uniform material flow is observed.

Thus the shear deformation process is shown to be effective in retaining continuity of the drawing operation, minimizing percent reduction in thickness even at high *t/r* ratios, and imparting higher strain values.

CHAPTER IV

EXPERIMENTAL PROCEDURES

4.1. As-received material

The interstitial free steel used in this research was received from the R&D Department of ArcelorMittal in the form of a 16” (406.4 mm) x 2” (50.8 mm) x 0.028” (0.7 mm) sheet. These steels are often produced in sheet form in two stages: initial rolling of continuous cast slabs on a hot strip mill followed by cold rolling on a tandem mill or cold mills.

4.2. Annealing of IF steels

To soften the IF steel sheets a continuous annealing treatment was applied. During annealing, the steel was held at a temperature above the recrystallization temperature typically about 800 ℃ (1470 F) for 10 minutes and then slowly cooled. This precipitates the carbides and results in large ferrite grains.

In case of IF steel the recrystallization temperature is greatly influenced by the microalloying additions (titanium, niobium, or titanium plus niobium). A higher cooling temperature lowers the recrystallization temperature and, in conjunction with heavy cold reduction ($\sim$80%), results in superior forming properties. A high annealing temperature is preferred for increased grain growth and high mean Lankford value ($\bar{r}$ -values) [14]. (Lankford values are primary indicators of the formability of low carbon steels.) The cooling rate after annealing is not critical, and there is no need of an overaging treatment. This processing makes the IF steel suitable for the production of highly formable, automotive cold-rolled sheet grades.

4.3. Experimental setup and die design

To compare the results of numerical analysis from ABAQUS and for a better understanding of the sheet metal drawing and extrusion processes, an experimental study was performed. This study consisted of three tasks: design and manufacturing of die components, performing drawing experiments on IF steel sheet samples at various angles and Equal Channel Angular Extrusions of IF steel samples canned in IF steel bars.

4.3.1. Sheet metal drawing: design and manufacturing

A special drawing die assembly was designed and built to study the Equal Channel Angular Drawing (ECAD) process applied to sheet metal. The existing die block assembly with aid of a hydraulic drawbench had the capability of conventional drawing metal strips at right angle alone (i.e. open channel configuration). Hence the new die assembly was designed with the aim to extend the flexibility of the drawing process for any draw angle, compliant with variable thickness and drawn over variable die-nose radii.

The die drawing assembly along with their different components is presented in Figs. 58 and 59, while engineering drawings of all major components are presented in Appendix. The prime functions of various components are described in Table 7.

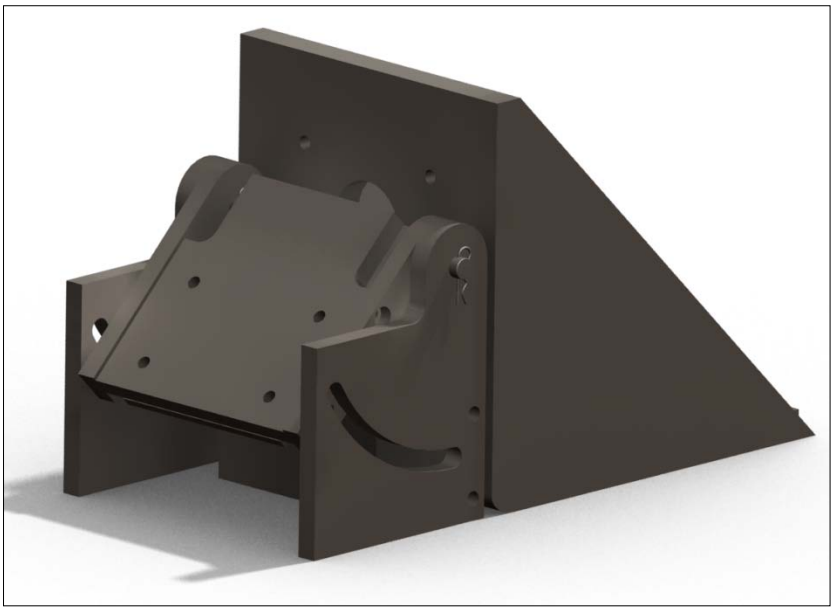

Fig. 58. Schematic of die assembly used for sheet metal drawing.

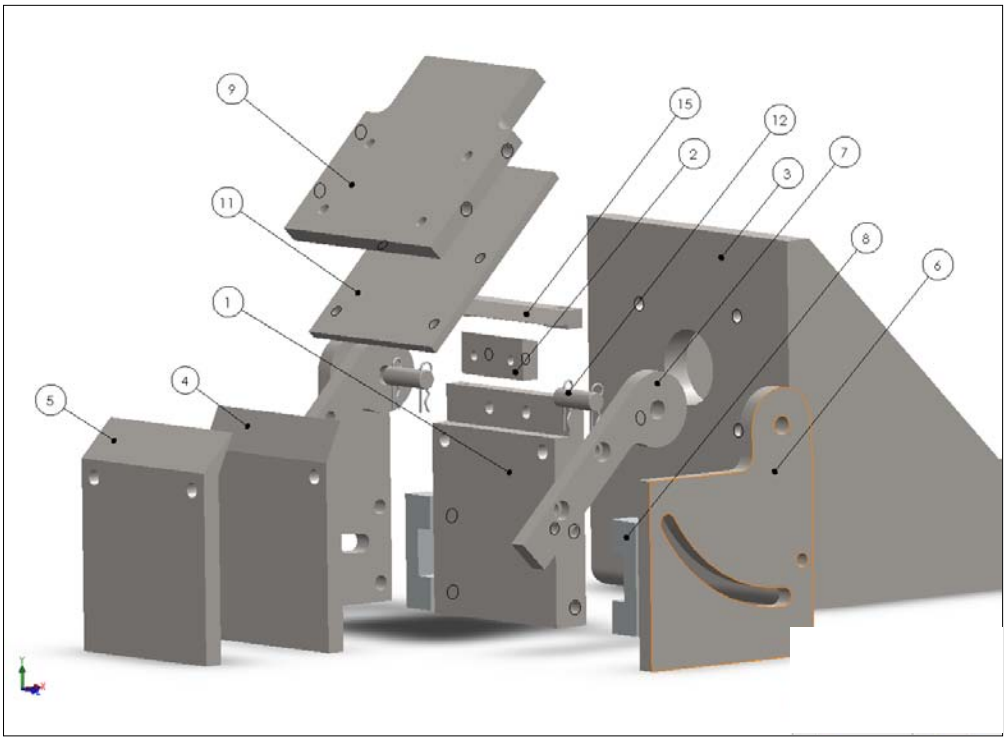

Fig. 59. Schematic of die assembly used for sheet metal drawing: exploded view.

Table 7
Functions of different components of die assembly (component numbers from Fig. 59)

Sr. No.	Component (No.)	Function
1	90 Degree Adapter (1)	It holds the die inserts and also supports the sheet metal when angle of drawing is 90º
2	Die Insert (2)	Die insert provides the sharp corner over which the sheet metal is drawn. The sharp edge is maintained along the line of action of draw-bench.
3	115 Degree Adapter (4)	It supports the sheet metal at drawing angle of 115º.
4	135 Degree Adapter (5)	It supports the sheet metal at drawing angle of 135º.
5	Side Support Plate (6)	It provides the flexibility of changing angle of drawing, retaining a close channel configuration.
6	Rotating Support Plate (7)	It allows holding the support plate and wearing plate assembly at various angles.
7	Support Plate (9)	It basically provides the link between rotating support and a wear plate by holding them together. In addition, sheet metal of any thickness can be constrained within the close channels by varying the gap between support plate and wear plate.
8	Wear Plate (11)	It acts as a supporting back plate to reduce the bending of sheet specimen as it passes over a sharp corner.
9	Top Support Plate (15)	It supports the plate as it flows through the exit channel

Because the die inserts are subjected to high contact stresses, shock resistant S7 tool steel, which also holds high wear resistant was selected for making these die inserts.

4140 steel was used for making most of the die assembly components. Bulk material was in the heat treated (annealed) form. The annealing heat treatment prior to machining reduces the material's yield strength and hardness, thereby enhancing its ductility and machinability. Often 4140 steel is full annealed (austenite structure) by heating to a temperature range of 790-845℃ (1450-1550°F), followed by slow cooling, resulting a hardness of nominally 197 HB [14].

The shock resistant S7 tool steel used for making the die inserts was hardened after machining on EDM by austenitizing to 925-955℃ (1700-1750°F), holding for 15-45 minutes, and slowly cooled in air. The resulting quenched hardness is nominally 60-61 HRC.

A summary of the heat treatments required for tool materials before the machining, and the mechanical properties after machining and heat treatment are presented in Tables 8 and 9.

Table 8
Summary of heat treatment before machining

Material	Components	Heat Treatment	Hardness (HB)
4140 Steel	Tool adapters, Support Plates and Wear Plate	Full Annealing 790-845℃ Air cooled	HB 197
S7 Tool Steel	Die-inserts	Annealing 815-845℃	HB 187 - 223

Table 9
Mechanical properties of materials after machining and hardening

Material	Hardening Temperature	Yield Strength (ksi)	Tensile Strength (ksi)	Elongation	Hardness
4140 Steel	480	175	188	16%	HB 388
S7 Tool Steel	425	205	275	10%	HRC 53

4.3.2. Sheet metal drawing: experimental study

IF steel sheet with an initial thickness of 0.7 mm (0.027”) were first cut from as-received material to the dimension of 44 mm x 200 mm (1.725”x8”) and then annealed at 800 ℃ for 10 minutes under Argon gas. These sheets were then bent and placed in the closed channels. The front flat region before bending was approximately 2” long and fed into the draw-bench clamp. Prior to drawing, to reduce frictional effects, lubrication was applied to both the sheet specimen and the die inserts. IF-steel sheet specimens were then drawn easily at room temperature with a draw-bench speed of approximately 12 mm per second (0.5 inches per second). Table 10 presents the test matrix used for experimental analysis of the drawing process.

The drawing process causes reduction in the sheet thickness as the sheet passes over the sharp corner. In addition, the trailing region is observed to have a little bump. Hence, to make the sheet metal ready for next drawing pass, this small bump was flattened out

and then sheet sample was again replaced in the closed channels. After each pass of drawing, % reduction in thickness is recorded using a micrometer.

Table 10
Test matrix for drawing analysis of IF steel

Sample ID	Drawing Route	Process Parameters			Vickers Hardness	Optical Microscopy
		Radius of die insert, *r*	Thickness to Radius ratio, *t/r*	Angle of drawing, *θ*		
(A)As-received samples						
0	0	-	-	-	√	√
(B)To study effect of routes and number of passes						
1	1A	0.7	1	90°	√	√
2	2A	0.7	1	90°	√	√
3	2C	0.7	1	90°	√	√
4	4A	0.7	1	90°	√	√
5	4C	0.7	1	90°	√	√
6	8A	0.7	1	90°	√	√
7	8C	0.7	1	90°	√	√
(C)To study effect of sheet metal thickness to die radius ratio						
8	1A	0.14	5	90°	√	-
9	2A	0.14	5	90°	√	-
10	4A	0.14	5	90°	√	-
(D)To study effect of drawing angle,						
10	4A	0.14	5	90°	√	-
11	4A	0.14	5	115°	√	-
12	4A	0.14	5	135°	√	-

For the approximate measurement of the drawing force, a small assembly was made using a digital fish scale. As shown in Fig. 60 at one end of the assembly a fish scale is

mounted while another end is connected using a rigid rod. This divides the connector in a ratio1:3. Thus fish scale actually measures one fourth of the total drawing force. Also, for a better approximation of strain rate at any given time, a digital caliper was used. Thus, recording the stroke length and drawing force at different time frames, a force against displacement curve was obtained.

Fig. 60. Schematic of assembly used for drawing force measurement.

4.3.3. Equal Channel Angular Extrusion (ECAE): experimental study

IF steel sheets were embedded in IF-steel billets to analyze their response to ECAE. The IF steel cans were cut from bulk plate and prepared to the dimensions 25mm x 25mm x 210mm (1”x1”x8.25”). The longitudinal axis of each billet is in the same direction of rolling. A through 0.25” diameter hole was then drilled in each billet can and a dimension slot of 8.4mm x16.5mm (0.33”x0.65”) cut using EDM. Twelve IF-steel

sheets with dimension 8mm x 16mm x 200mm (0.027”x0.645”x8” were then pressed into the slot. The ends were closed using IF steel plugs. Billets were then extruded at room temperature at an extrusion rate 2.5 mm per second (0.1 inches per second). The details of the different routes used in this study are presented in Table 11.

Table 11
Test Matrix for ECAE processing of IF steel sheets canned in IF steel

Sample ID	ECAE Route	Vickers Hardness	Optical Microscopy
0	As-received	√	√
E1	1A	√	√
E2	2A	√	√
E3	2C	√	√
E4	4A	√	√
E5	4C	√	√

To reduce the frictional effects, the billet and moving bottom channel walls were lubricated prior to extrusion. Because the extruded billet shows some dimensional change, the billets were reshaped using combined rolling and machining. After 1, and 2 passes, a 50 mm (2”) section was cut from the rear end of the processed billet for microstructure analysis and hardness measurements.

4.4. Hardness measurement

Another method of measuring the improvement in mechanical strength is measurement of hardness. Hardness is an indirect measurement of strain hardening. There are many hardness methods including Rockwell, Brinell, Vickers, and Knoop.

With different methods there are differences in process variables including indenter shape, load, duration of application of load, and the formula that provides the hardness number. In this study the Vickers micro-hardness test was used to analyze the effects of the drawing process on strengthening of the specimens.

The Vickers test utilizes various sized pyramidal shape diamond indenters (Fig. 61) and the hardness value is defined as the ratio of load to the surface area of indentation. The expression that relates the hardness value HV with applied load and surface area of indentation is given by [15],

$$HV = \frac{P}{A} = \frac{2P\sin\left(\frac{\theta}{2}\right)}{D^2} \quad , \tag{13}$$

where, P is the applied load in kgf, A is the unrecovered projected area of the indentation (mm^2), and D is the diagonal length of the indentation (usually arithmetic mean of two diagonals D_1 and D_2) in mm.

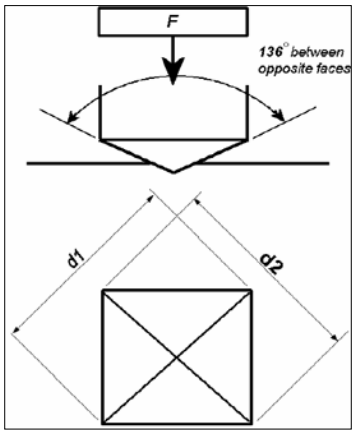

Fig. 61. Indenter geometry for Vickers micro-hardness test.

In this study hardness tests were performed on the Microhardness Tester LM300AT with a load of 300 gf applied for duration of 13 seconds. An indenter with a pyramidal shape has an angle between opposite sides of 136°. To ensure that the hardness value is not influenced by previously marked indentations, the distance between indentations should be three times the indentation diagonal. In addition the specimens are grinded before measuring the hardness to avoid the influence of any impurities or residual stress. Approximately 8-10 readings are recorded and averaged for each specimen to ensure reasonable statistics for accuracy.

The yield strength and Vickers hardness value (H_V) are related by expression [26]:

$$\sigma_y = HV_{Mpa} / 3 . \tag{14}$$

4.5. Optical microscopy

To study the effect of the drawing process on the microstructure of processed specimens optical microscopy was performed using a Nikon Epiphot metallograph equipped with a Polaroid DMC digital camera and polarizing filters. The process of optical microscopy was subdivided into four parts which include sectioning, mounting, grinding, polishing, and etching.

Sectioning refers to cutting the samples from processed material. Though shearing the specimen on a tabletop hand shear appeared to be the quickest method of sectioning, the shear burrs result which received excessive metal deformation, care was needed to remove this excessive deformation region by rough grinding. On the other hand, specimens cut with an abrasive wheel with proper lubrication result in a smooth cutting edge with minimal deformation. This results in minimal microstructural change due to

overheating. In this study samples were cut using self lubricating Buehler Isomet 1000 diamond saw for Vickers hardness, and optical microscopy. To keep the material temperature low, the saw blade was cooled continuously with an oil-water lubricant. This reduce mechanical loading and localized annealing effects due to heating.

For optical microscopy the samples were mounted in thermosetting resin, Bakelite. To ensure that the high curing temperature (approximately 150 °C) do not have any adverse effects on cold-drawn specimens; a quick comparative study was performed. Wherein two samples; one mounted in castable epoxy and the other in bakelite were tested for micro-hardness. As the results were consistent, the use of bakelite mounting was assumed to be suitable, as it is quick and easy for polishing. Since, only the cross-section of the sheet was of interest for micro-structural study, the stack of sheets was mounted perpendicular to prepared surface. To ensure that the stack remains in the correct alignment during mounting, a metal binder clip was used to secure the stack at one end.

Surface grinding and polishing of the bakelite mounted samples were then performed to remove any impurity or scale developed during cutting operations. This also improves the surface finish and prepares the samples for metallography. Grinding was performed using traditional method of abrasive removal of material from the surface where the samples were pressed against the grinding wheel with an attached silicon carbide grinding of selected grit size and rotating at a set speed. This was the initial rough surface grinding stage. During polishing, the abrasive particles are so small that it is difficult to hold them on grinding pads. Hence, these particles are often suspended in

liquid slurry or as a paste and then applied on soft polishing pads rather than directly bonding them on the grinding surface.

In this study the initial grinding was performed by hand on a Buehler Ecomet 3 machine with a 120-grit grinding disk at a preset speed. This removed any thin film of bakelite that might have accumulated on the specimen during mounting. Because the specimens are thin they can change orientation during curing. The advantage of using an automated grinding machine is that a uniform finish on multiple (six) samples can be obtained at the same time. Initially a chamfer of 45° was made on the corner edge of the sample surface to be polished. This reduces the friction during successive specimen preparation stages.

In the next stage samples were then taken to the Buehler automatic grinding machine. This allowed control of grinding time, grinding force and direction of circular motion between the polishing platen and specimens. In this study for the initial grinding on disks of 400-grit surfaces, the total grinding time was set as 20 minutes. A grinding force as 36 lbs with the platen rotating in a counter-clockwise direction with 210 rpm was selected. A continuous stream of water was used to flush the abrasive disk and keep the specimens cool. Before proceeding to the next stage at 600-grit, specimens were flushed with running water to prevent contamination of succeeding abrasive papers. After final grinding on a 1200-grit surface, specimens were cleaned with cotton and water, flushed with water to prevent watermarks, and then dried under a heater. The surface finish resulting after this initial grinding was suitable for Vickers micro-hardness measurements.

It is important to have a scratch free mirror-like surface finish. This is important because a mirror-like surface can reflect large amounts of light resulting into a high quality image. Scratches have negative impact on the results. The grinding stage is often followed by a polishing stage. Both processes are carried out in multiple steps by using progressively finer grits.

During the polishing stage the specimens are polished first using glycol based 9-µm diamond paste applied on Ultra-Pol cloth with a force of 36 lbs with platen rotating counter-clockwise direction at 150 rpm. This step is performed for 12 to 15 minutes in the presence of Metadi fluid as a lubricant. The platen was then removed from the power head and rinsed with water. Next, the specimens are polished with 3-µm diamond paste and Metadi Fluid lubricant on a Trident cloth. This stage is performed for approximately 10 minutes with the wheel rotating counter-clockwise at 120 rpm. For better results, a similar stage with 1-µm diamond paste followed by polishing with 0.05-µm MasterPrep Alumina slurry on wet MicroCloth for 2-3 minutes is performed for ultra-low carbon IF steel samples [14]. During grinding and polishing stages, to ensure the complete removal of trapped pockets of foreign material, routine cleaning with distilled water followed by subsequent ultrasonic cleaning may be carried out.

For IF steel the incoming light is reflected uniformly and a polished surface alone does not result in good grain boundary discrimination for optical microscopy. Hence polishing stage is followed by chemical etching which will expose grain boundaries and produce contrast between grains. To prevent the formation of a passive layer on the polished surfaces, the material is etched immediately after polishing. Low carbon

content in IF steel (with ferrite grain boundaries) makes it less practical to use conventional etchants such as nital. Marshall's reagent is more effective as an etching agent to reveal the microstructure of IF steel specimens. Table 12 presents the composition of Marshall's reagent.

Table 12
Composition of Marshall's reagent

Etchant	Chemical	Quantity	Part by volume
Marshall's Reagent	Solution A		
	Water	100 mL	1
	Oxalic Acid	8 gm	
	Sulfuric Acid	5 ml (conc.)	
	Solution B		1
	Hydrogen Peroxide	30%	

The addition of 1 mL hydrofluoric acid per 100 mL of Marshall's solution provides a deeper etching response. Hence in this study a mixture of Marshall's reagent with hydrofluoric acid in the ratio 100:1 ml was used for etching. For better results still specimens were sometimes pre-etched in 2% nital. To minimize pitting, polished surfaces should be held vertically. Table 13 presents the composition of 2% nital.

Table 13
Composition of 2% nital

Etchant	Chemical	Quantity
2% nital	Nitric Acid	2 mL (conc.)
	Ethyl Alcohol	98 mL

Our experience has been that for an IF steel Marshall's reagent delineates all ferrite boundaries and i.e. more effective than 2% nital alone. [14]

CHAPTER V

EXPERIMENTAL RESULTS AND DISCUSSIONS

The goal of the experimental study was to characterize the mechanical response of IF steel sheet specimens subjected to ECAD and ECAE processes and validate the deformation process analyzed using numerical analysis. Testing included, Vickers micro-hardness, and optical microscopy. Independent process variables during the ECAE processing included route and number of passes (N), and initial grain size. While for ECAD experiments along with drawing route and number of passes, drawing angle (ϕ), and the ratio of initial thickness of the specimen to the drawing die radius (t/r) are expected to influence plastic strain, grain morphology and enhancement in mechanical properties.

Next few sections present the experimental results describing the influence of process variables on thickness reduction, hardness and microstructure. This is followed by a discussion section, which address issue of the resulting microstructure, drawing force and validation of numerical results.

5.1. Reduction in thickness

As discussed in section 3.2.5 the major concern during ECAD, is that a reduction in thickness accompanies the induced plastic strain. As reported by Alkorta, et al. [27] the industrial application of pure ECAD will be limited by a higher reduction in thickness per pass, for an effective increase in strain. In this study a detailed analysis of the reduction in thickness and the influencing process variables, during ECAD are presented.

5.1.1. Effect of routes and number of passes

Fig. 62 shows the thickness reduction pattern with the same die configuration ($\phi = 90°$ and t/r =1) for an increasing number of passes, and for route A and route C. As expected the thinning effect is more significant, as the number of passes increase. A quick summary is presented in Table 14.

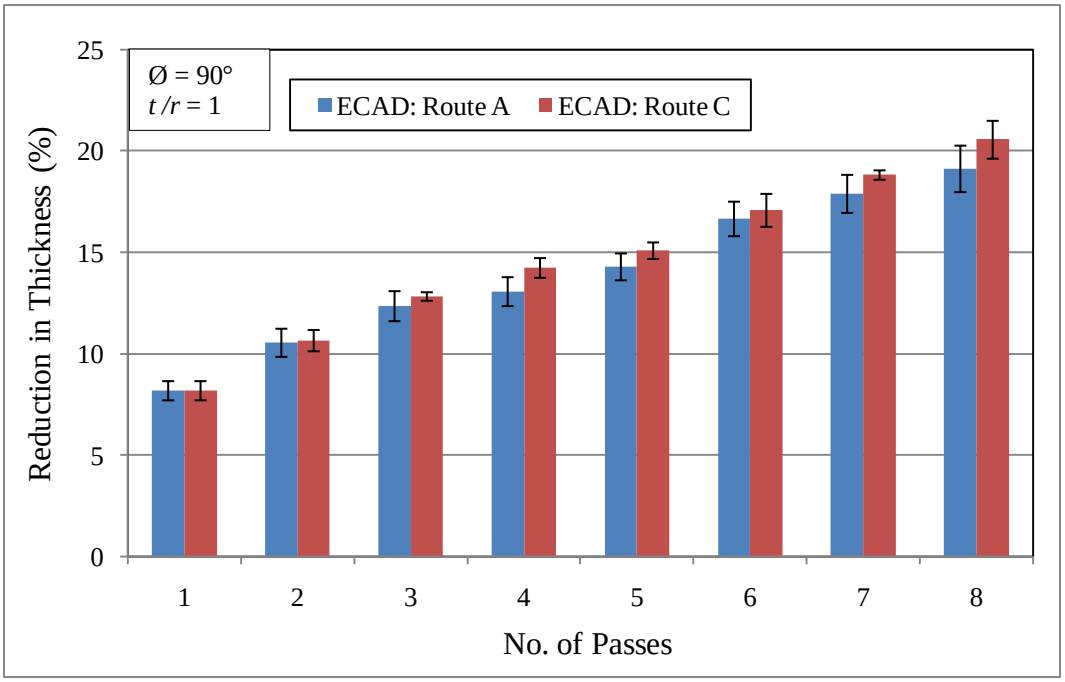

Fig. 62. Experimental results for ECAD: effect of routes on reduction in thickness.

Also in route C, as the steel sheets are rotated through 180° between successive processing, the thinning effects are observed at both top and bottom surfaces and hence reduction is slightly higher as compared to route A.

Table 14
ECAD: affects of route and number of passes on reduction in thickness

Route	Average Reduction (%)	Deviation	Increase per pass	Route	Average reduction (%)	Deviation	Increase per pass
1A	8.20	0.47	-	1C	8.20	0.47	-
2A	10.56	0.69	2.36	2C	10.67	0.53	2.47
4A	13.08	0.71	2.52	4C	14.25	0.49	3.58
6A	16.66	0.85	3.58	6C	17.09	0.81	2.84
8A	19.13	1.14	2.47	8C	20.56	0.93	3.48

5.1.2. Effect of sheet thickness to die radius ratio, t/r

Fig. 63 presents the variation in thickness reduction with *t/r* ratio for different routes for the same configuration discussed before. It is apparent that with an increase in *t/r* ratio, there is an equivalent increase in reduction of thickness.

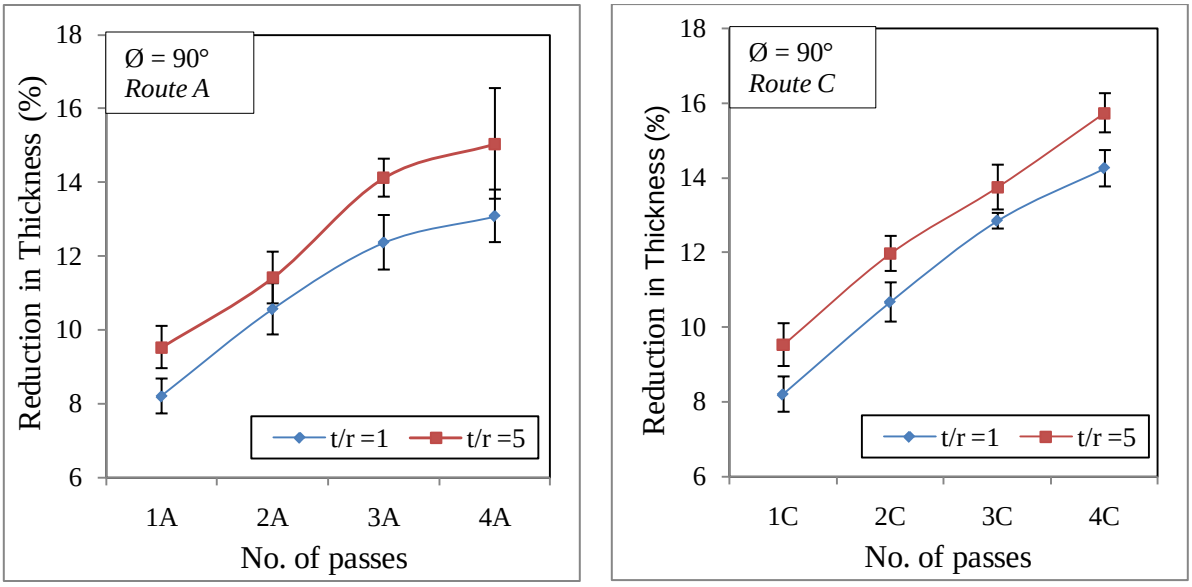

Fig. 63. Experimental results for ECAD: effect of *t/r* ratio among different routes on reduction in thickness.

Fig. 64 presents the similar variation in thickness profile considering additional effects due to drawing angle. It is seen that the influence of *t*/r ratio on thickness reduction decreases (though with slight increase in deviation) with increase in drawing angle.

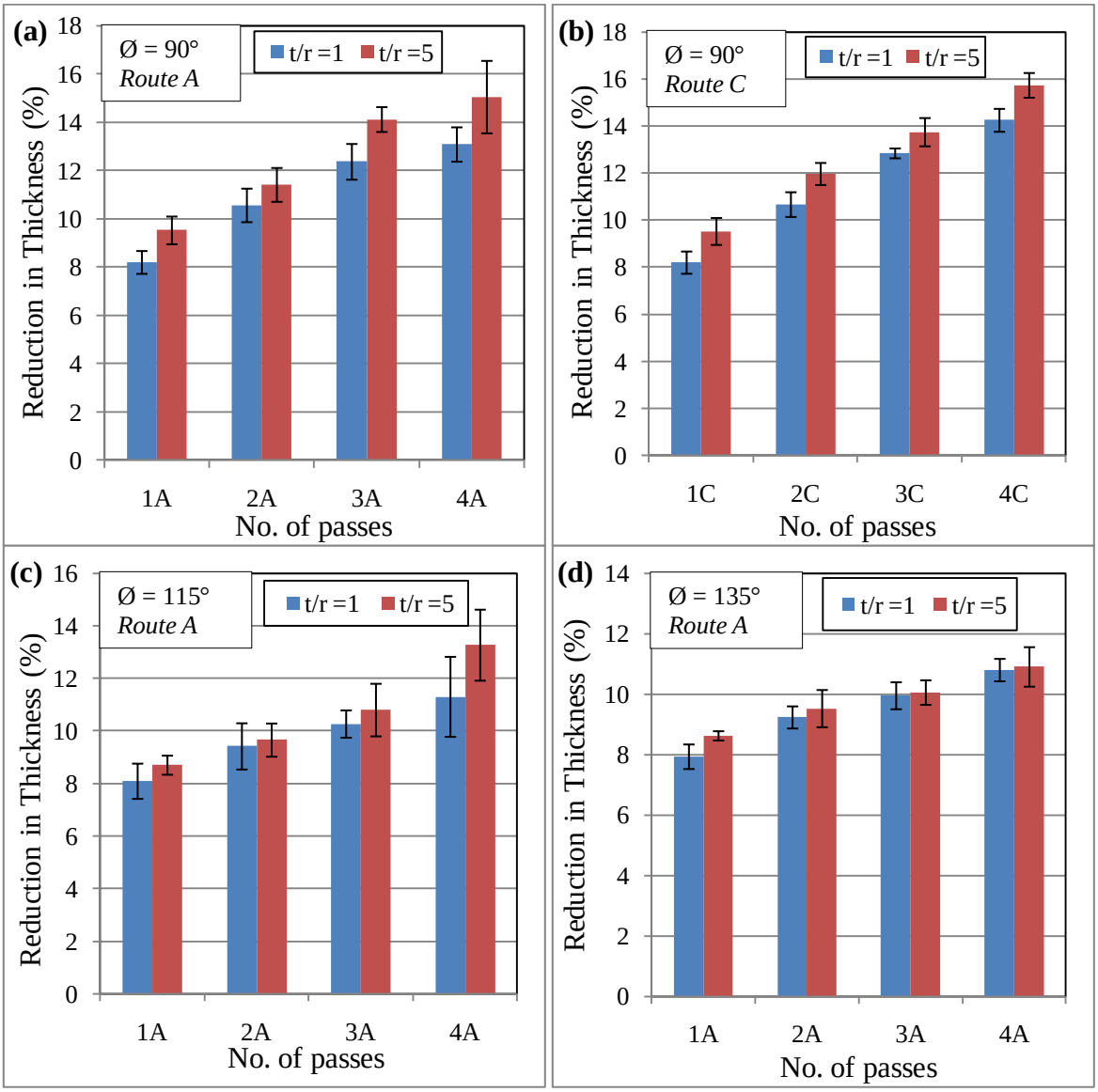

Fig. 64. Experimental results for ECAD: effect of *t/r* ratio on reduction in the thickness (a) and (b) show variation with route A and C, (c) and (d) present the variation for different drawing angles.

5.1.3. *Effect of drawing angle, ϕ*

Fig. 65 presents the influence of drawing angle on the reduction in thickness. As noticed, with the increase in the drawing angle, the metal sheet flows easier around the die corner and thereby reduce the thinning effect.

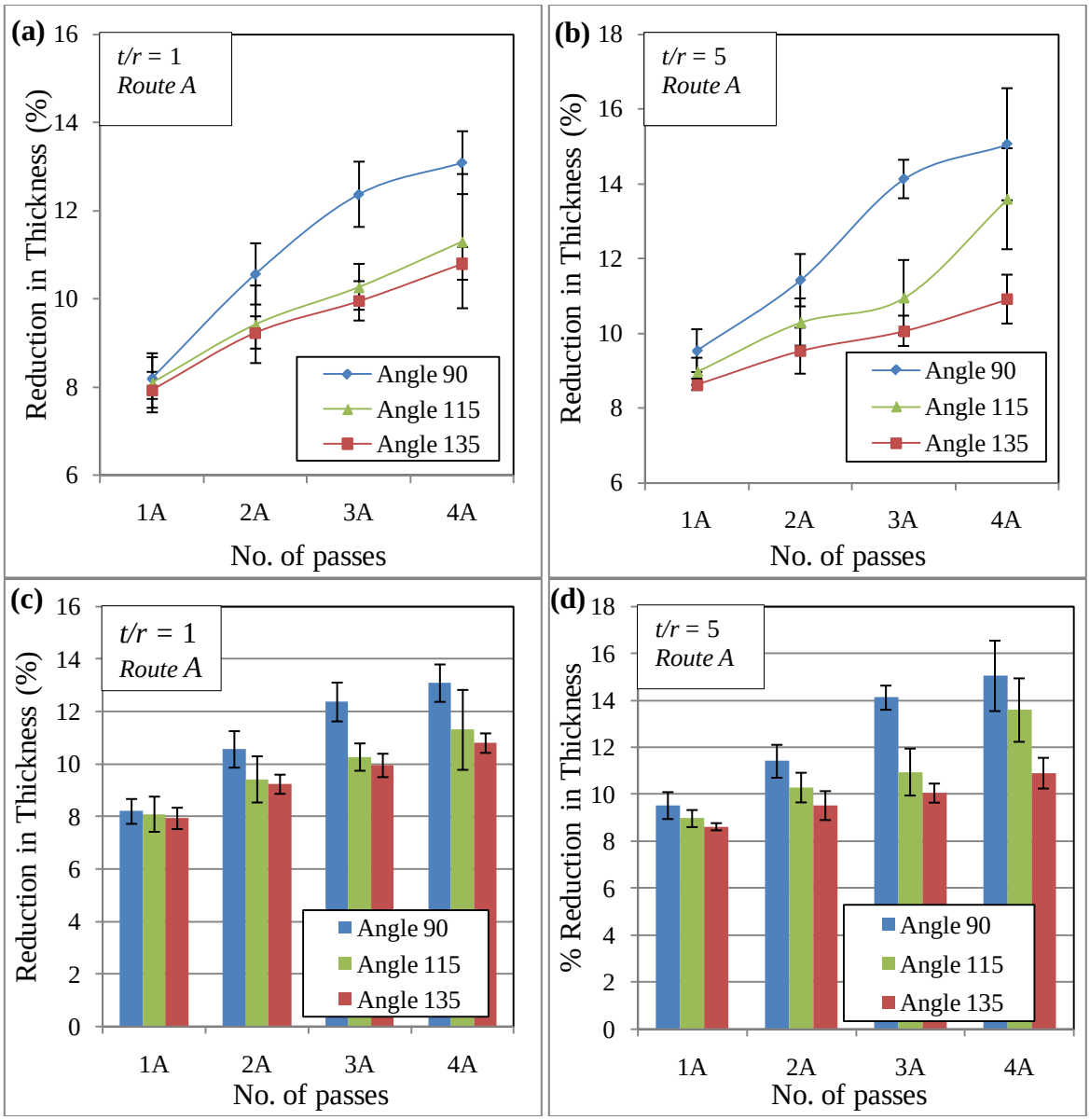

Fig. 65. Experimental results for ECAD: e5ffect of drawing angle, ϕ on reduction in the thickness (a) t/r=1 (b) t/r=5 (c) and (d) present bar charts.

As seen from Fig. 64 (a), for route A, with the increase in number of passes, the influence of lowering the die angle is much more significant as compared to earlier passes. The same is the case with route C (Fig. 64 (b)). However, once again, route C presents more deviation in results compared to route A.

Thus, it may be verified that, during the experimental setup, provision of top and back support plates, with a little spacing from sheet metal, shows significant improvement in minimizing reduction in thickness as compared to the results presented by Alkorta et al. [27]. This is further illustrated in Tables 15 and 16.

Table 15
Thickness reductions obtained from experimental results of Cu samples [27]

Drawing angle, ϕ	Sheet thickness to die radius ratio, *t/r*	Reduction in thickness (%)	
		After first pass	After second pass
115	3	16.2%	Fracture
135	3	14.4%	29%

Table 16
Thickness reductions obtained from experimental results of IF steel samples in the present study

Drawing angle, ϕ	Sheet thickness to die radius ratio, *t/r*	Reduction in thickness (%)	
		After first pass	After second pass
90	5	9.5%	11.41%
115	5	8.7%	9.66%
135	5	8.62%	9.53%

In conclusion, the reduction in the sheet thickness can be effectively minimized by either lowering *t/r* ratio or increasing the drawing angle.

5.2. Hardness measurements

Vickers micro-hardness measurements were performed to study how different ECAD process variables impact the mechanical behavior of the IF steel sheet. Additionally we compared the sheet property changes performance with ECAE-processed samples. Hardness is presented for flow plane (F), transverse plane (T) and longitudinal plane (L).

Table 17
Vickers hardness measurement taken to study effect of process variables

Specimen ID	Route	Plane*	1	2	3	4	5	6	7	8	Avg.	Std. Dev.
ECAD: For Ø=90° and *t/r* =1												
0	0*	F	74.8	78.0	78.5	77.8	76.9	76.5	74.7	75.6	76.6	1.5
0	0	T	83.4	88.0	82.3	85.0	90.2	72.5	91.4	94.8	85.9	6.9
1	1A	F	93.4	88.8	87.6	92.0	87.1	87.6	87.1	87.6	88.9	2.4
1	1A	T	98.3	92.8	96.8	93.2	99.0	96.6	93.3	109.4	97.4	5.4
2	2A	F	105.0	100.5	98.5	110.1	107.1	107.8	111.6	106.9	105.9	4.5
2	2A	T	102.8	106.5	105.9	106.8	109.0	113.7	107.7	111.7	108.0	3.4
3	2C	F	104.6	99.9	103.3	101.1	101.6	108.2	106.1	109.2	104.2	3.4
3	2C	T	105.9	102.4	105.7	100.2	100.7	103.4	111.9	112.4	105.3	4.7
4	4A	F	119.2	120.2	123.5	127.5	123.1	127.8	125.8	127.0	124.3	3.3
5	4C	F	130.6	126.9	120.3	122.1	127.6	130.0	122.5	123.5	125.4	3.9
6	8A	F	146.4	146.7	153.1	143.0	146.5	144.3	146.0	149.9	147.0	3.2
7	8C	F	148.7	145.0	153.2	147.9	146.1	154.3	147.0	143.4	148.2	3.8
ECAD: For Ø=90° and *t/r* =5												
8	1A	F	97.6	95.2	94.0	89.6	95.9	94.0	92.5	98.8	94.7	2.9
9	2A	F	103.5	108.2	109.8	104.5	107.5	108.3	107.4	105.5	106.8	2.1
10	4A	F	133.3	132.6	133.6	128.7	132.6	123.5	137.5	139.1	132.6	4.9
ECAD: For Route 4A and *t/r* =5												
10	90°	F	133.3	132.6	133.6	128.7	132.6	123.5	137.5	139.1	132.6	4.9
11	115°	F	122.2	127.5	123.5	123.5	129.8	125.5	118.4	128.1	124.8	3.7
12	135°	F	106.7	105.7	109.2	111.7	104.5	110.2	103.0	108.3	107.4	3.0

Table 17 continued

Specimen ID	Route	Plane*	1	2	3	4	5	6	7	8	Avg.	Std. Dev.
ECAD: Ø=90° and *t/r* =1 Variation across thickness measured from bottom (contact) surface												
0	0	F	80.2	77.6	78.3	80.8	81.7					
1	1A	F	106.4	102.4	91.8	95.3	102.0					
2	2A	F	126.4	116.4	103.0	111.5	115.4					
4	4A	F	143.6	137.6	123.0	132.7	140.4					
6	8A	F	151.3	142.9	139.0	146.9	149.0					
ECAE experiments												
E1	1A	F	202.0	200.9	192.8	193	197.8	202.3	205.1	203.3	199.6	4.7
E2	2A	F	200.9	197.3	207.2	200.1	201.2	195.8	205.7	205.5	201.7	4.1
E3	2C	F	219.4	222.9	213.7	224.9	227.2	219.7	223.9	216.6	221.0	4.5
E4	4A	F	229.4	220.5	225.7	224.8	214.8	216.8	218.8	229.6	222.6	5.6
E5	4C	F	234.8	228.6	227.4	229.3	222.6	217.9	227.0	229.2	227.1	5.0
E1	1A	L	168.0	189.4	183.5	190.6	190.4	193.9	188.1	191.9	187.0	8.3
E2	2A	L	197.7	196.4	191.7	191.8	192.2	195.0	197.6	194.3	194.6	2.5
E3	2C	L	211.7	208.6	199.2	201.9	205.7	206.4	213.2	208.1	206.9	4.7
E4	4A	L	219.6	210.5	220.1	212.8	223.3	225.4	209.0	217.3	217.3	6.0
E5	4C	L	206.9	210.9	219.1	219.5	210.6	208.9	214.4	213.5	213.0	4.6

The hardness measurement results for various combinations of process variables are presented in Table 17. To analyze the influence of the process parameters on hardness, average values are taken into consideration, while standard deviation indicates the uniformity of results.

5.2.1. Influence of route and number of passes

Fig. 66 presents the variation of hardness with increasing number of passes and different routes. It shows that for as-received specimen hardness values along the length of transverse plane are higher as compared to values along the flow plane. However, this tendency decreases with an increase in the number of passes. It is believed that rolling

during earlier manufacturing stages imparts higher hardness along the transverse plane, as compared to along the length of flow plane. Also with an increase in the number of passes during ECAD, the combined effects of stretching and work hardening along the length of the flow plane, improve the homogeneity thereby reducing the differences in hardness.

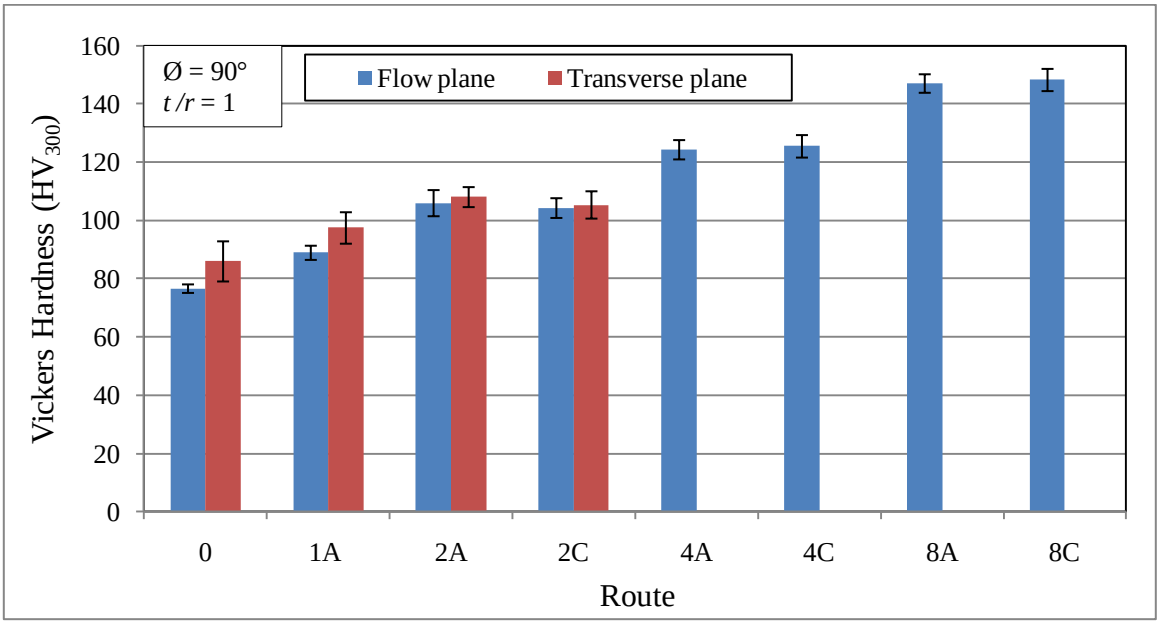

Fig. 66. Experimental results for ECAD: affect of routes on hardness.

Also, in general, it is observed that hardness increases with an increase in the number of passes.

Fig. 67 presents a comparison between the response of sheet samples subjected to ECAD and ECAE. For each pass, the average hardness value of samples from ECAE is almost twice than of corresponding ECAD samples. In addition, it is expected that with

this trend, approximately 10-12 passes of ECAD will be required to generate the same hardness increase as seen after one pass of ECAE.

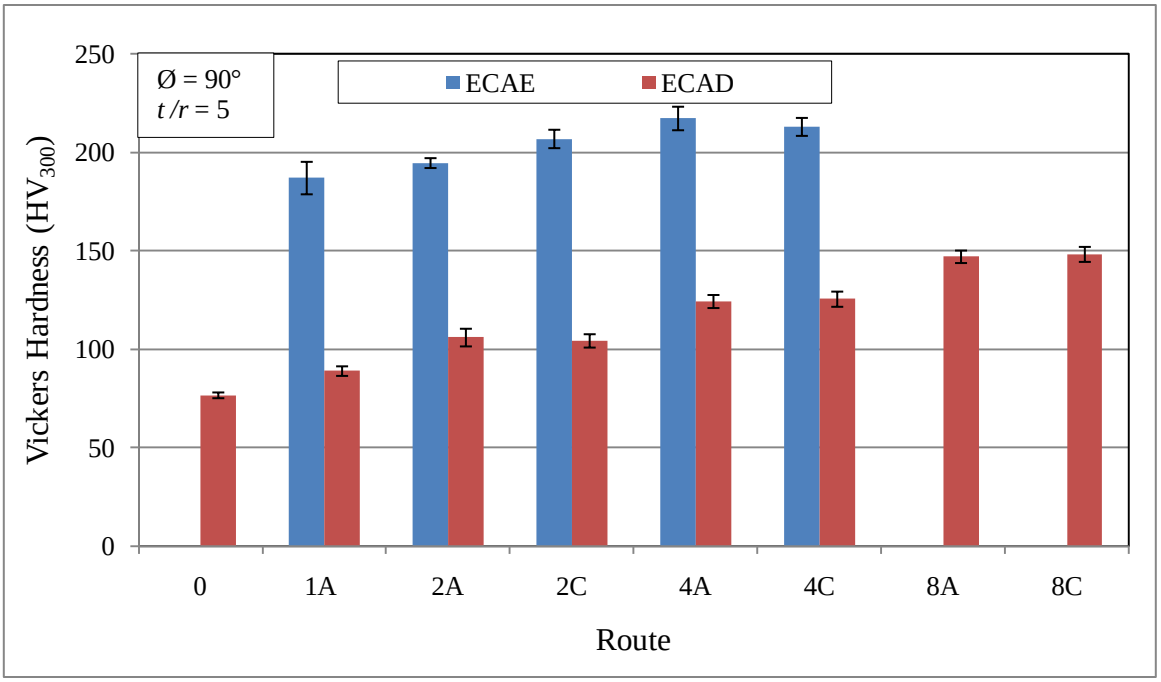

Fig. 67. Comparison of hardness values in IF steel samples subjected to ECAE and ECAD process.

In conclusion, though with subsequent passes of ECAD, improvement in the hardness value is recorded, the pure ECAD process appears to be less potential for industrial implementation. This is because of the large reduction in thickness expected after 10-12 ECAD passes. (A way to achieve equivalent strain at lower pass, is to use a die with a higher *t/r* ratio, say 10, this will again result in increased thinning effect and thus gives less control on thickness reduction).

5.2.2. *Effect of drawing angle, ϕ*

During the experimental study of the ECAD process, it is expected that the use of a higher channel intersection angle (i.e. drawing angle) will result in a lower the plastic strain and thereby a reduced hardness. Fig. 68 confirms the same and presents this trend for two different *t/r* ratios for route 4A. As witnessed for a *t/r* ratio of 5, with the increase in the drawing angle, the hardness value reduces significantly.

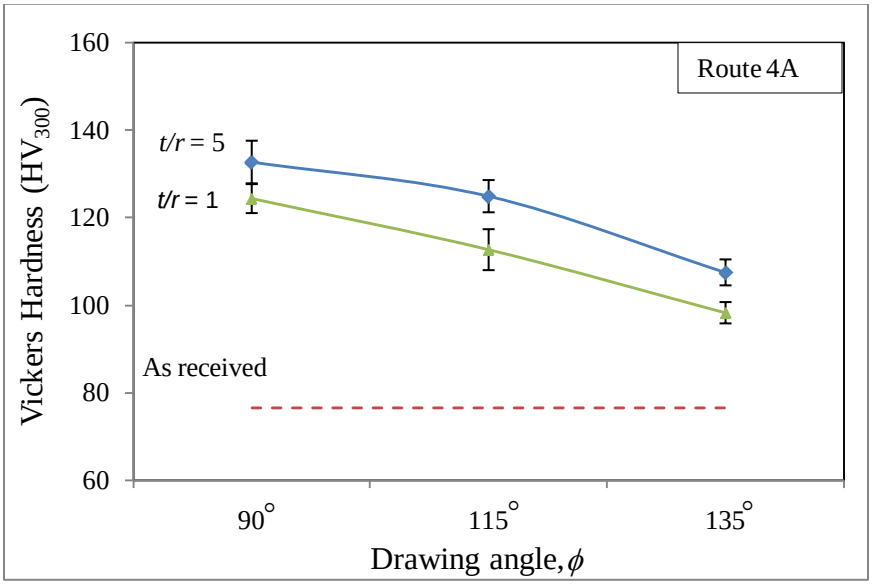

Fig. 68. Experimental results for ECAD: effect of drawing angle, and *t/r* ratio on hardness.

5.3. *Optical microscopy*

As in the case of most low-carbon steels, the ferrite in IF steel appears as equiaxed (equal dimensions in all directions). The bcc ferrite structure in the annealed material (800 °C for 10 minutes) is characterized by an average grain size of 18 μm (ASTM size

8.9) without any preferred orientation. The microstructures of as-received material across the thickness after annealing (along the length of flow plane and transverse plane) are presented in Fig. 69 (a) and Fig. 69 (b). Along the flow plane a fairly uniform microstructure is seen, while the grains show slight elongation along the transverse plane.

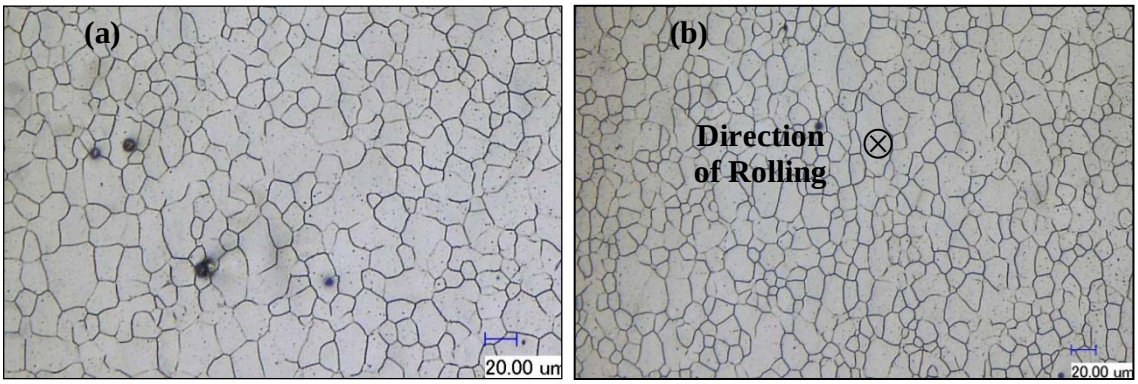

Fig. 69. Optical Micrographs of as-received IF sheet samples across the thickness (a) along the flow plane, and (b) across transverse plane.

5.3.1. Microstructure evolution of IF steel sheet samples during ECAD

During ECAD route A and route C were studied. In route A - ECAE, the billet orientation is same for all passes; the shear deformation takes place continuously in the same direction resulting in elongation of subgrains. As similar evolution is believed to take place during ECAD, i.e. it is expected that subgrains will elongate more predominantly along the edge that passes over the sharp radii of the die. With increase in number of passes, elongation will progressively move towards the opposite edge.

On the other hand, since during route C - ECAE, the billet is rotated through 180° after each extrusion. This keeps the shear plane constant but reverses the shear direction between two successive passes. The result is equiaxed grain structures after each even pass. However, during route C - ECAD, it is believed that during the initial few passes, the subgrains continue to elongate along both edges and rapidly form a laminar structure along the entire thickness. If the process is further continued, it would then start reducing the elongated structure, generating a fairly equal dimensional morphology. Thus it is assumed that, during the initial few passes of route C, the lamellar structure will be predominant and at a higher number of passes an equiaxed grain structure will evolve after the even passes. Figs. 70 to 78 present optical micrographs of IF steel samples obtained through ECAD experiments.

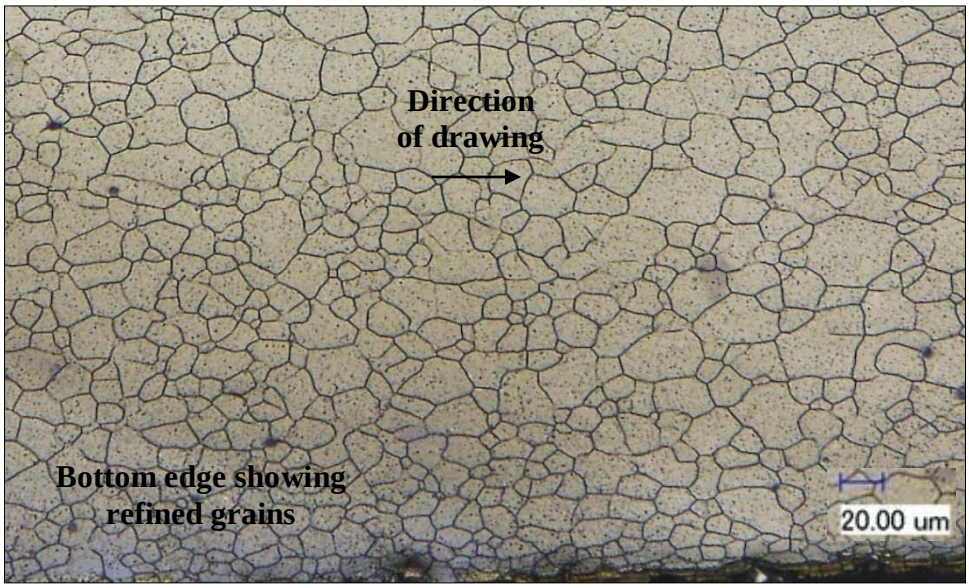

Fig. 70. Optical micrograph of ECAD: IF steel sheet (route 1A) flow plane view.

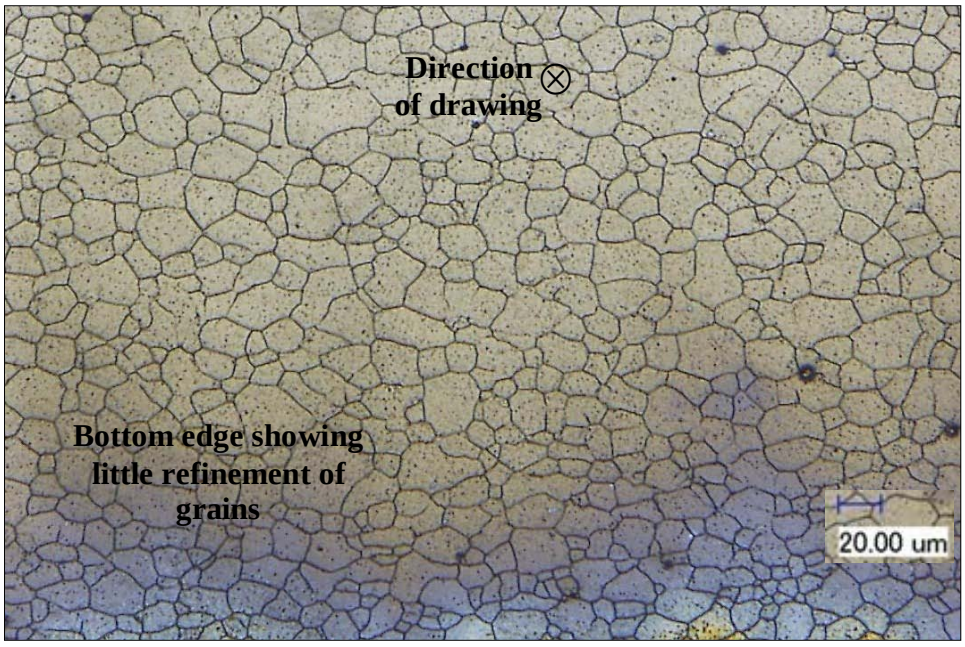

Fig. 71. Optical micrograph of ECAD: IF steel sheet (route 1A) transverse plane view.

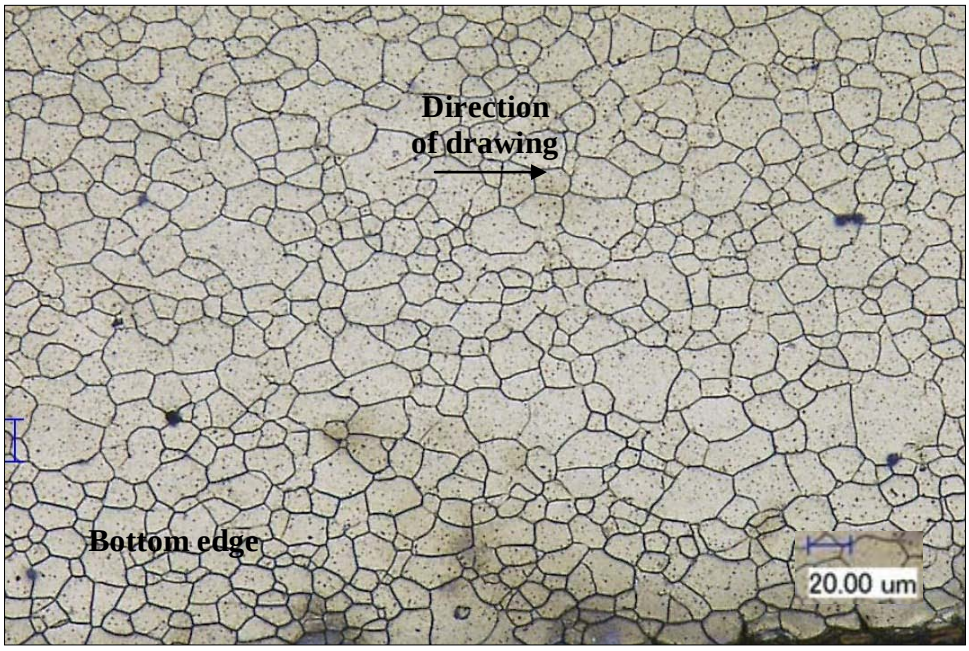

Fig. 72. Optical micrograph of ECAD: IF steel sheet (route 2A) flow plane view.

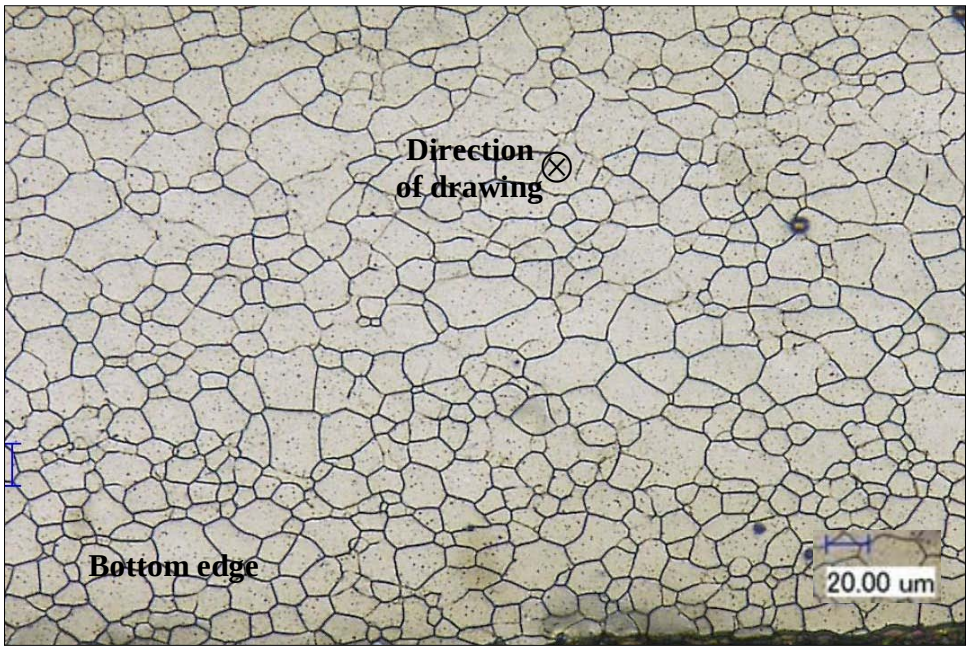

Fig. 73. Optical micrograph of ECAD: IF steel sheet (route 2A) transverse plane view.

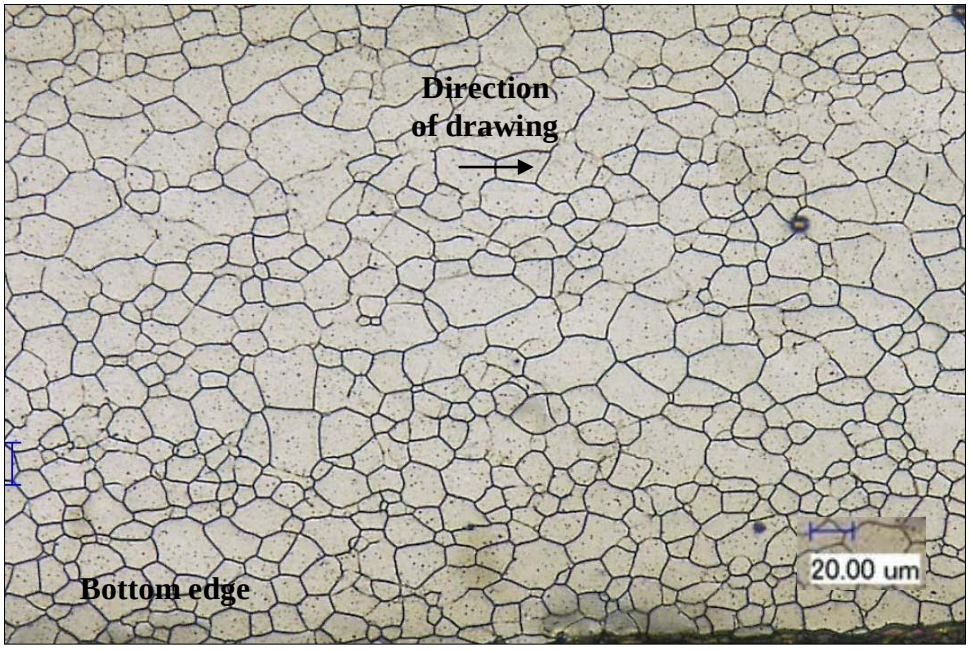

Fig. 74. Optical micrograph of ECAD: IF steel sheet (route 2C) flow plane view.

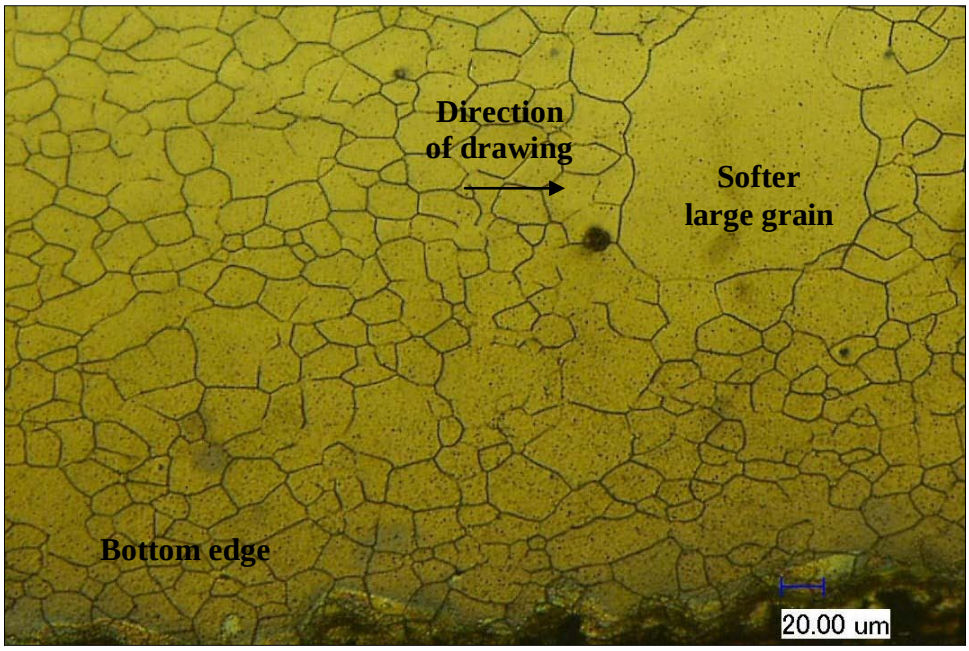

Fig. 75. Optical micrograph of ECAD: IF steel sheet (route 4A) flow plane view.

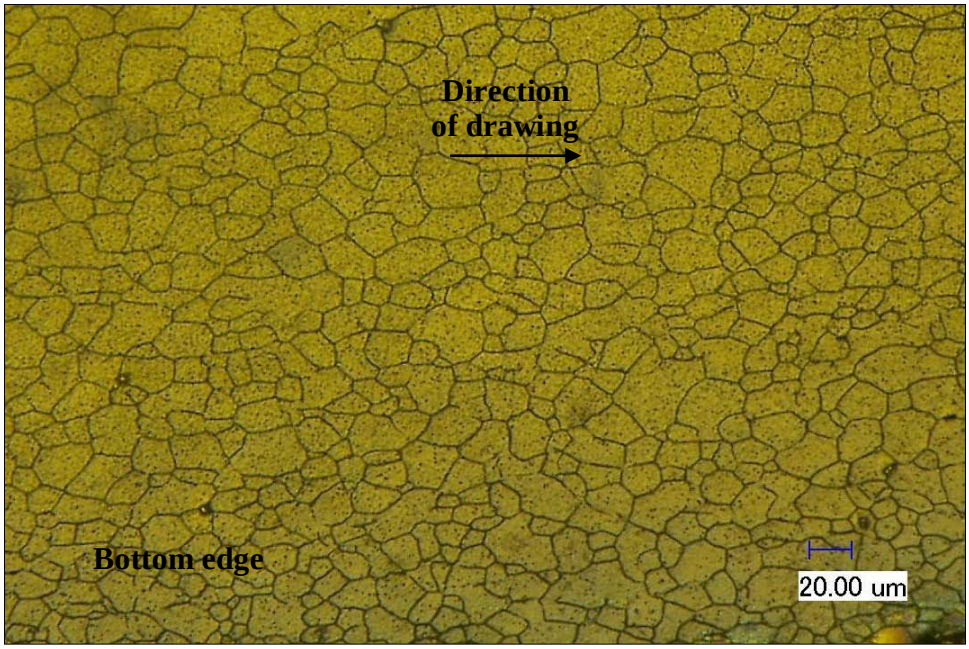

Fig. 76. Optical micrograph of ECAD: IF steel sheet (route 4C) flow plane view.

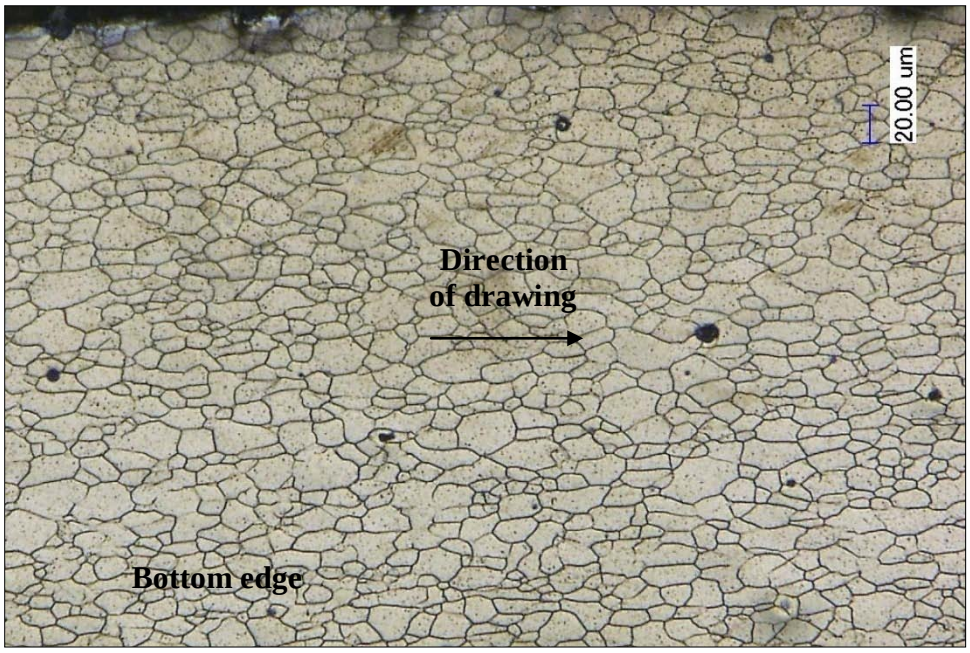

Fig. 77. Optical micrograph of ECAD: IF steel sheet (route 8A) flow plane view.

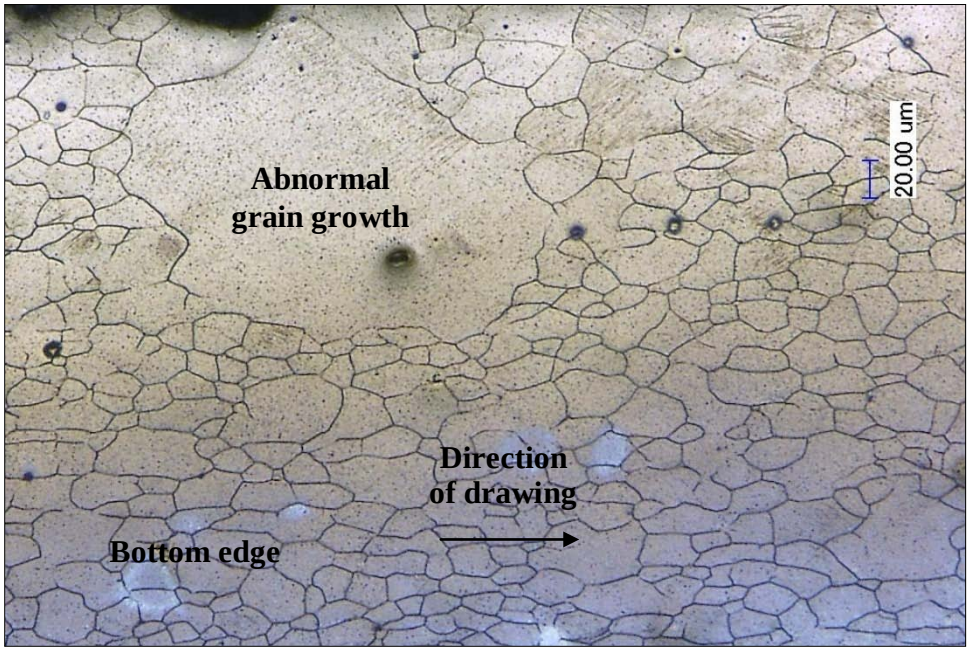

Fig. 78. Optical micrograph of ECAD: IF steel sheet (route 8C) flow plane view.

As seen in Fig. 75 (route 4A) and Fig. 78, (route 8C) abnormal growth of some of the grains is observed during optical microscopy. These grains had relatively low values of hardness compared to surrounding grains. It is concluded, that annealing at higher temperatures has adverse effects on mechanical properties of IF steel and as a result, there is a possibility that as-received sheets after annealing exhibit a heterogeneous microstructure.

5.3.2. Microstructure evolution of canned IF steel sheet samples during ECAE

Optical microscopy of ECAE processed IF steel samples, in some cases (like route 2C, route 4A, and route 4A reveals that severe plastic deformation has resulted in a very fine grain structure, which is difficult to observe under a light microscope. Figs. 79 to 85 present optical micrographs along flow plane and longitudinal plane of IF steel sheet samples subjected to ECAE.

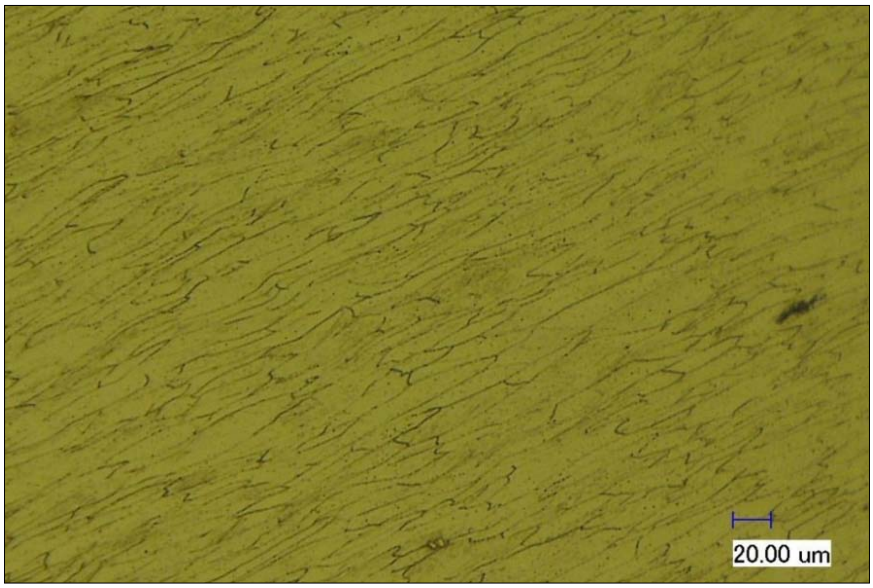

Fig. 79. Optical micrograph of ECAE: IF steel sheet (route 1A) on the flow plane.

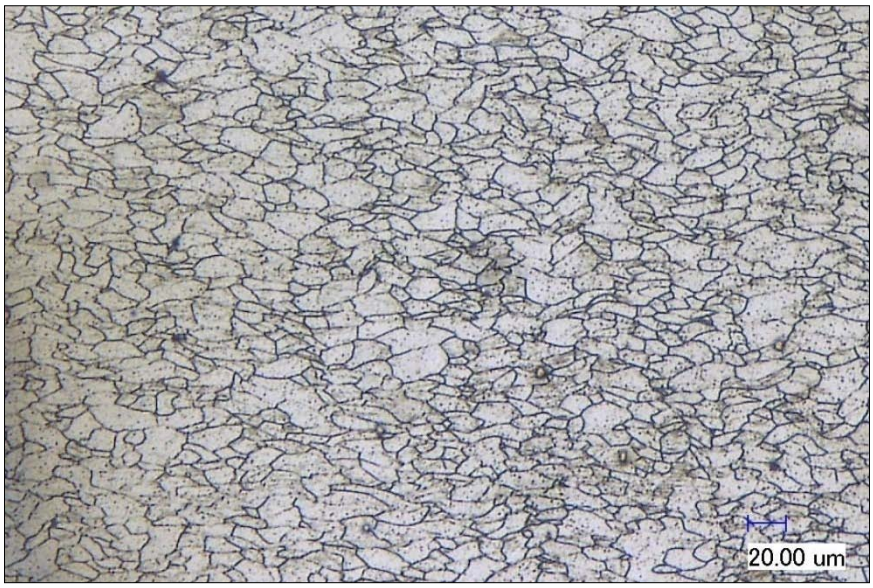

Fig. 80. Optical micrograph of ECAE: IF steel sheet (route 1A) on the longitudinal plane.

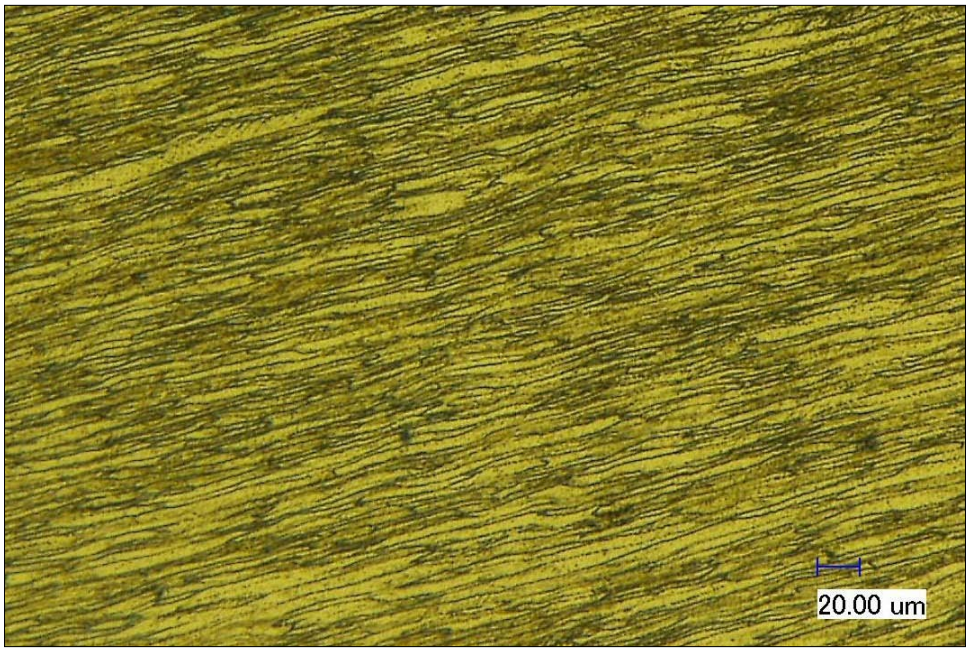

Fig. 81. Optical micrograph of ECAE: IF steel sheet (route 2A) on the flow plane.

Fig. 82. Optical micrograph of ECAE: IF steel sheet (route 2A) on the longitudinal plane.

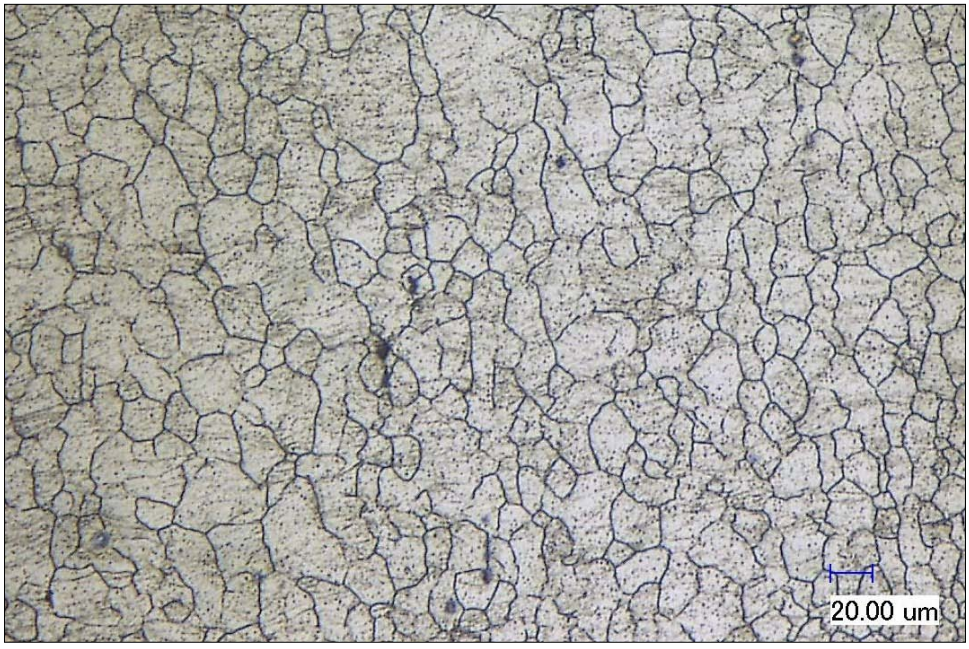

Fig. 83. Optical micrograph of ECAE: IF steel sheet (route 2C) on the longitudinal plane.

Fig. 84. Optical micrograph of ECAE: IF steel sheet (route 4A) on the longitudinal plane.

Fig. 85. Optical micrograph of ECAE: IF steel sheet (route 4C) on the longitudinal plane.

As expected, even after one pass of ECAE, the grains are elongated significantly. After route 4A, the microstructure is heavily deformed and it is difficult to observe grain boundaries under a light microscope. On the other hand, for the sample processed through route C, (rotation of 180° between each subsequent pass) elongated subgrains are quickly eliminated and evolution of low angle grain boundaries into high angle grain boundaries is improved.

5.4. Discussion of results

5.4.1. Force vs. time curve for ECAD

As presented in Fig. 86, in the force-time curve for the ECAD process, up to the peak force, the unbending of the sheet (as it is pulled over sharp corner) is the primary deformation mechanism, during which the force requirement increases gradually. It is believed that this force is directly dependent on material properties, drawing angle, friction coefficient, strain rate and specimen thickness to die radius, *t/r*.

After the peak, the curve shows a negative force gradient and over time it appears to reach a constant value. This is mainly due to static to dynamic frictional transition. In addition, it is assumed that during this stage, the typical stretching mechanism (as in case of conventional rolling operation) consisting of two different affects acting simultaneously. The first is thinning i.e. reduction in thickness; the second is strain/ work hardening. Thinning tends to reduce the required pulling force, while strain hardening raises the drawing force. At higher *t/r* ratios wearing of sheet metal over a period may have some additional influence [28]. After some stroke length, an

equilibrium between thinning and strain hardening is achieved thereby resulting in a steady drawing force.

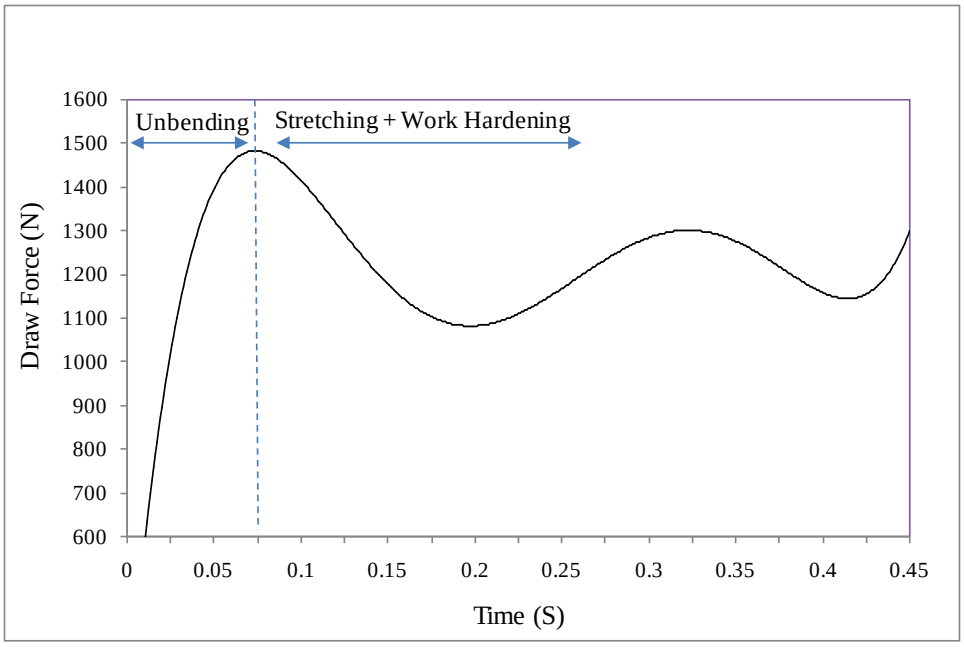

Fig. 86. Force vs. time curve: showing stages of deformation.

It is believed that beyond some threshold value of negative force gradient after the peak, thinning (or necking) effects will be very severe resulting in failure of material, Hence, it will be interesting to study the parameters influencing the negative force gradient after the peak in detail as this can be interpreted as an indirect measure of the safe zone limit. Further investigations in this area are proposed.

5.4.2. Inhomogeneity in the microstructure

Deformation mechanics during ECAD consist of two concurrent effects: stretching (thinning) and transition between static and dynamic friction. The individual

contribution of each effect is not very clear. Hence, it is expected that the resulting microstructure may not be uniform. In numerical simulations this can be demonstrated by plotting the distribution of strain across the thickness (Fig. 87).

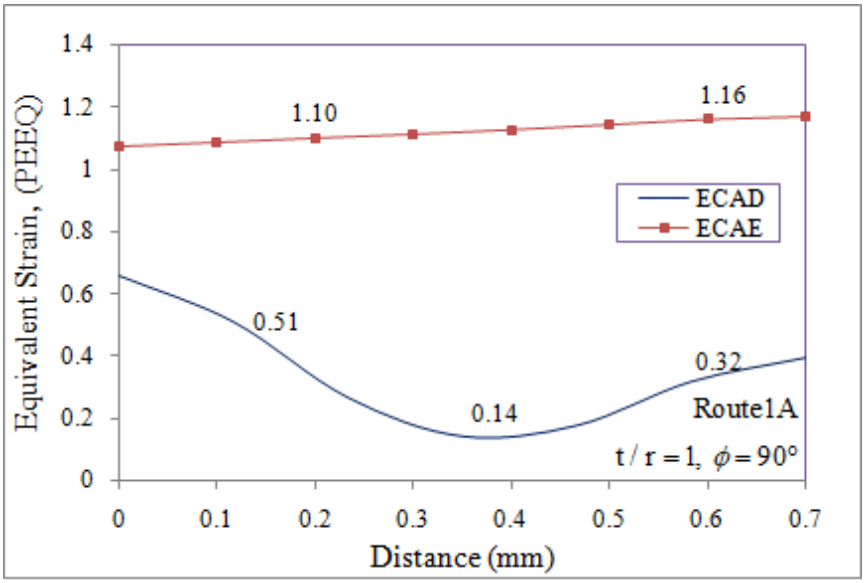

Fig. 87. Distribution of equivalent strain across the thickness after one pass.

In order to study the uniformity of ECAD by experiments, hardness measurements were taken across the thickness. Fig. 88 presents a schematic showing the approximate location of these measurements.

Numerical results indicate development of higher strain regions near the edges as compared to the center of the sheet thickness, after a single pass. Fig. 89, which presents the variation of hardness across the thickness, confirms this result and is in agreement with the numerical results. As observed, hardness is higher at the bottom edge (inner edge which is in contact with the die), and gradually decreases toward the center and

again increases towards the opposite edge. With the increase in the number of passes, the hardness gradient decreases. The hardness values through thickness for an as-received material appear to be fairly constant, indicating a uniform microstructure.

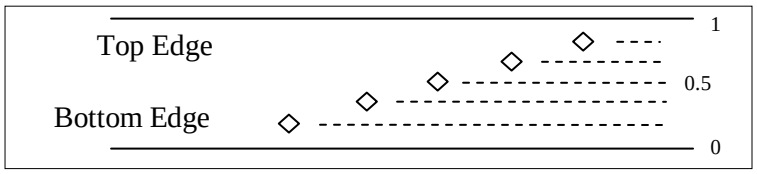

Fig. 88. Schematic showing locations of hardness measurement across the sheet thickness.

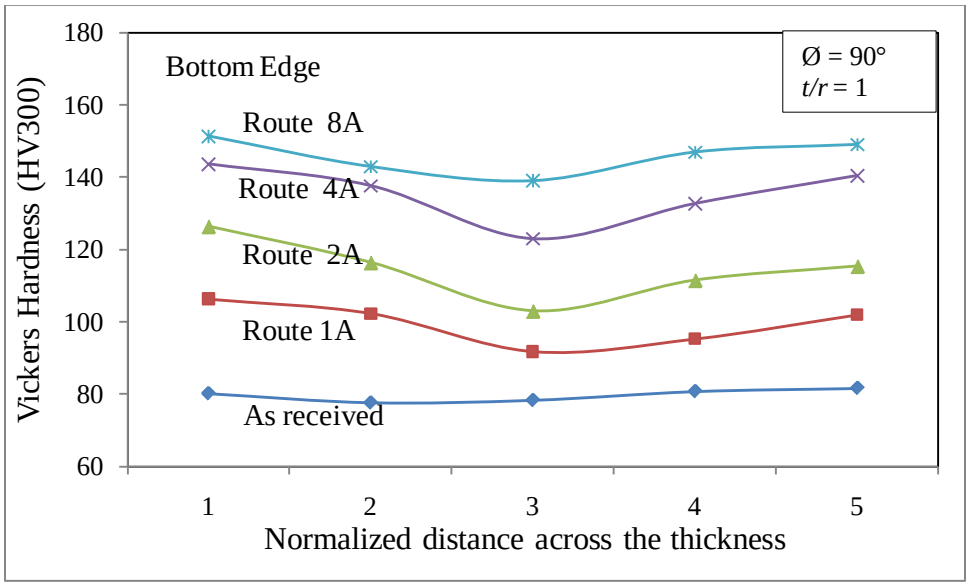

Fig. 89. ECAD: variation of Vickers hardness across the thickness.

Thus, it can be confirmed that pure ECAD, results in a non-uniform microstructure. However, with an increase in the number of passes, this non-uniformity in microstructure is reduced.

5.4.3. Validity of numerical results

In order to validate and confirm the legitimacy of the numerical results, two dependent variables i.e. the drawing force requirement and the reduction in thickness along the length are compared with the experimental study, for the same process variables i.e. number of pass (N=1), drawing angle, ($\phi = 90°$) and thickness to die radius ratio,(t/r =1).

5.4.3.1. Comparison of drawing force requirement

Fig. 90 presents the comparison of drawing force requirement for the above mentioned configuration. Numerical results are a little higher compared to the experimental observations. The average deviation in force at the peak value is 5.4% while the steady state difference is 14.2%, with the simulation giving the higher force.

The nature of the force-displacement curve after the peak in experimental study is slightly different (i.e. the drawing force does not remain steady, but reduces with stroke length). It is believed that this may be due to the assumption in the numerical analysis that the friction coefficient remains constant, which is not the real case. In reality due to continuous change in frictional contact area, and heating during sliding motion, the dynamic coefficient of friction must vary. In addition, the force measurement is not perfect. Using a simple assembly, a fish scale measures one fourth of the actual drawing force, and thus any small error in reading the gauge is amplified.

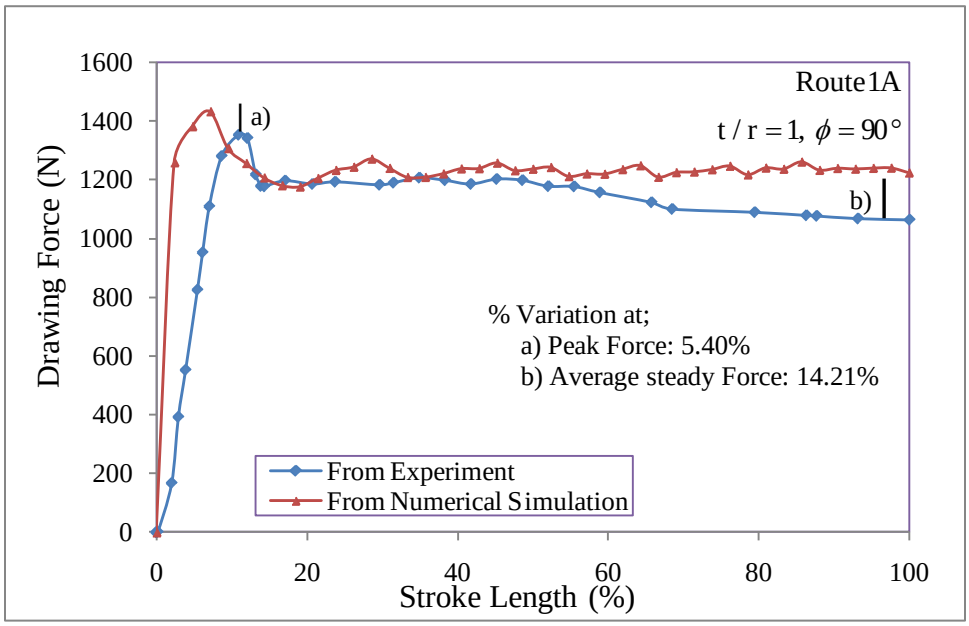

Fig. 90. ECAD: comparison of drawing force measurement.

In summary, it can be stated that the drawing forces determined measured from numerical analysis are in good agreement with the experimental measurements.

5.4.3.2. Comparison of reduction in thickness

The deformed shape of the IF steel sheet specimens for $\phi = 90°$ and *t/r* =1, for route 1A from the experiment and numerical simulation, are presented in Fig. 91 (a) and (b) respectively. The nature of the deformed shape of the drawn specimens from both analyses present similar nature (bumps) at the front (A) and rear (B) ends, validating the simulation results.

Table 18 presents the profile of reduction in the thickness for the experimental and numerical results after a single pass. The same has been plotted in Fig. 92. It is evident that from the numerical analysis, the reduction in thickness varies from 8.9% to 7.6%,

while experiments demonstrate this variation to be from 8.7% to 7.4%; with an average error of 1%. Thus, the numerical results are nicely reflected by the experimental study.

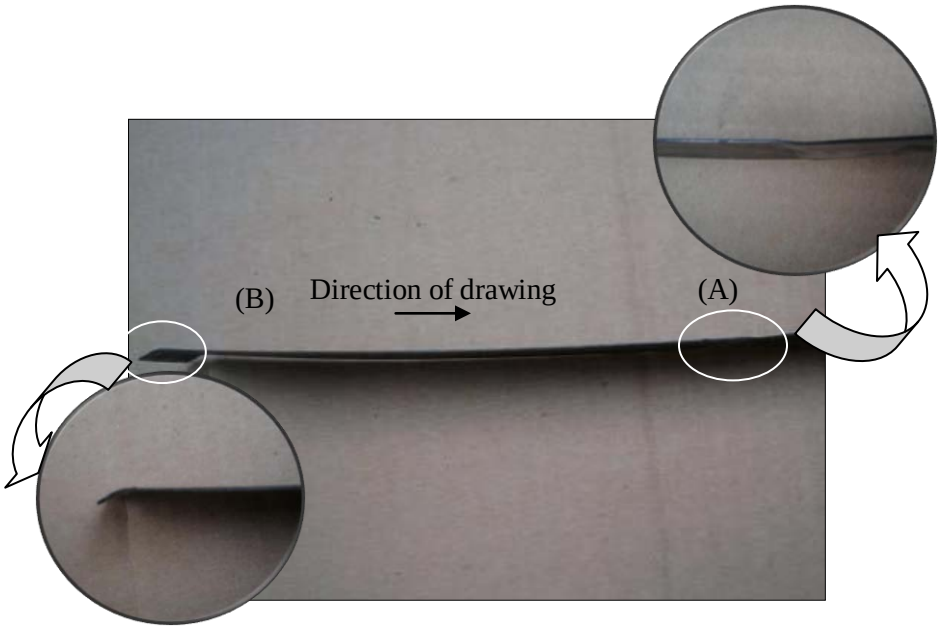

(a)

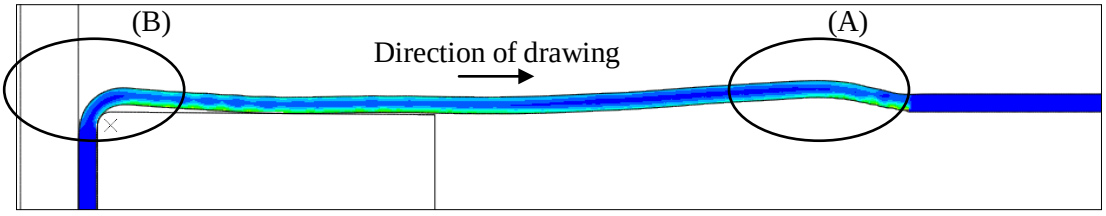

(b)

Fig. 91. (a) Experimental results for ECAD: deformed shape after one pass.

(b) Model results for ECAD: deformed shape after one pass.

Table 18
Comparison of reduction in thickness along the length for one pass

Normalized Distance along length	0.20	0.40	0.60	0.80	1.00	Average
From Experiment	8.66	8.10	8.49	8.31	7.44	8.20
From Simulation	8.86	7.71	8.43	8.00	7.60	8.12
% Variation	2.33%	4.77%	0.70%	3.75%	2.19%	0.96%

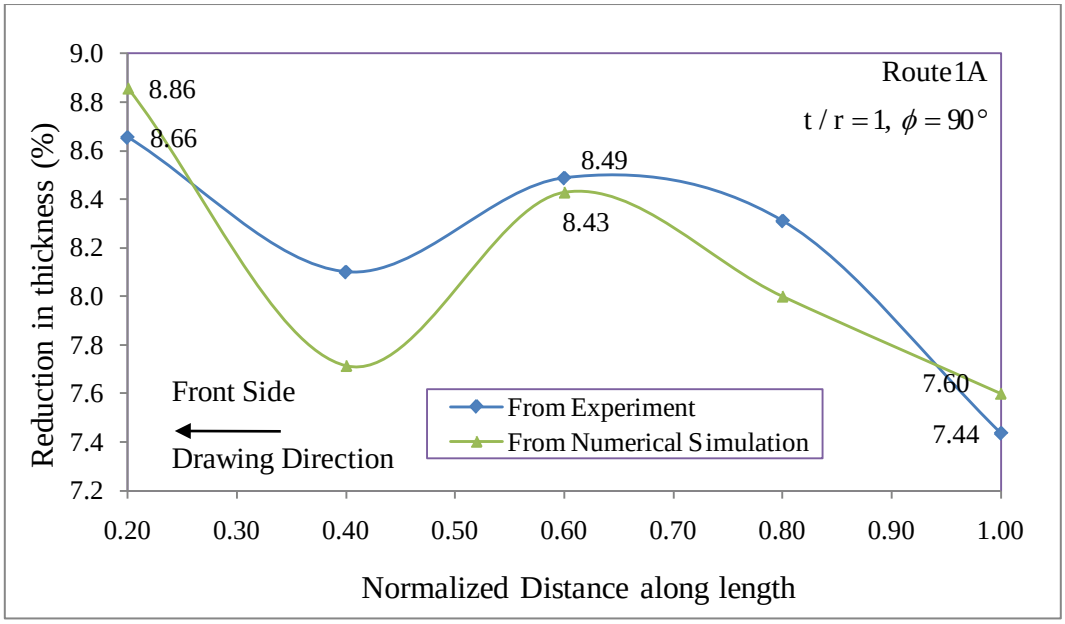

Fig. 92. Comparison of reduction in thickness after one pass.

Table 19 presents a summary of comparison of experimental and numerical results.

Table 19
Comparison of experimental and numerical results

Sr. No.	Process Variable	Experimental	Numerical Simulation
1)	ECAD: Drawing Force (Ø=90°, *t/r* =1)		
	At peak	1354 N	1430 N
	Steady value	1064 N	1240 N
2)	ECAD: Reduction in thickness (Ø=90°, t/r =1)		
	Average	8.2 %	8.12 %
3)	ECAE: Equivalent strain values (n=1) at the sheet centerline		
	Route 1A	1.155	1.156
	Route 2A	2.311	2.304
	Route 2C	2.311	2.262
4)	ECAE: Shear Angle comparison		
	Ø=90°	26.56°	26.83°
	Ø=115°	38.13°	39.71°
	Ø=135°	50.36°	54.03°

The reasonableness of the numerical results is confirmed by comparison of thickness profiles and drawing force, with experimental results.

CHAPTER VI

SUMMARY AND CONCLUSIONS

In the present study numerical simulations were performed to evaluate two SPD techniques: ECAE and ECAD, and validate the hypothesis that by combining these two processes, classic ECAE can be extended for the continuous processing of sheet metals. Experiments were conducted to analyze the mechanical response of IF steel sheet material subjected to ECAE and ECAD techniques and to validate the results obtained from the numerical study.

6.1. Summary of analytical and experimental results

Initially, conventional open channel drawing was modeled and compared with the numerical results of the closed channel configuration. The equivalent strain contours appear to be similar without considerable variations in requirements of drawing force. A significant advantage is observed with regards to controlling the reduction in thickness. For the open channel configuration, the reduction in the thickness varies from 9% to 11%, while for the same processing parameters in the closed channel configuration; it is 7.6% to 8.9%. For higher *t/r* ratios, the results are encouraging, suggesting the possibility of multi-pass drawing. Numerical results indicate development of higher strain regions near the surfaces as compared to the center of the sheet thickness, after a single pass. This indicates that resulting sheet microstructure may not be uniform.

From the numerical results of equivalent strain history illustrating the influence of the drawing angle in ECAD, it is concluded that with an increase in drawing angle,

though the equivalent strains are significantly reduced, this situation results in improvements with regards to strain uniformity and minimization in thickness reduction.

Numerical modeling of the response of canned IF steel sheet samples subjected to classical ECAE, after routes 1A, 2A and 2C were performed. The resulting equivalent strains are in conformity with the analytical models presented by Segal et al. This confirms the validity of the numerical results.

Then, the performance of a proposed continuous process was analyzed by assuming a simplified geometrical model. It consist of set of rollers as a feeder mechanism to push the strip/ billet into ECAE dies and another set of rollers as a drawing mechanism to pull the strip out from the die. A comparison of numerical results with classic ECAE and ECAD after single pass suggests that the proposed shear deform process provides an advantage over ECAD technique by imparting higher plastic strains, better strain uniformity and little variation in original dimensions. Thus it offers potential for multi-pass processing which may have commercial potential.

Experimental analyses of the mechanical response of IF steel sheet specimens subjected to ECAD and ECAE were carried out to validate the deformation process using numerical analysis. Material characterization tests included, Vickers micro-hardness, and optical microscopy. Experimental results were presented which show the influence of process variables including route and no. of passes, drawing angle (ϕ), and ratio of initial thickness of specimen to drawing die radius (t/r) on thickness reduction, hardness and microstructure.

The validity of the numerical results was confirmed by comparing the drawing force measurement and reduction in thickness along the length, with experimental results during single pass ECAD. For most cases, the numerical results are in good agreement with experiment.

In ECAD, with an increase in the number of passes, the thinning effect is more significant, resulting in a higher reduction in thickness. Moreover, in route C as thinning effects are observed at both the top and bottom surfaces, the percent reduction is slightly higher as compared to route A. It is seen that the thickness reduction is minimized (though with slight increase in deviation) with an increase in drawing angle.

When hardness results of ECAD-processed IF-steel sheet samples are compared to ECAE, after each pass, it is noticed that the average hardness values of the ECAE-processes samples are almost twice the ones corresponding to the ECAD-processed samples. Thus, confirms the superiority of ECAE in refining the grain structure over pure ECAD.

6.2. Conclusions

From the above mentioned summary of results, the following conclusions can be made:

1) The closed channel drawing configuration provides the upper hand on conventional (open channel) drawing by providing a significant improvement in minimizing the percent reduction in thickness, even at higher *t/r* ratios, and gives a slight improvement in resulting plastic strains.

2) Despite being a continuous process, ECAD alone cannot provide a satisfactory solution to development of higher shear strains and improved mechanical properties by grain refinement.
3) The proposed continuous process (shear deformation: obtained by combining ECAE and ECAD) appears to be effective in retaining continuity of the drawing operation, minimizing the percent reduction in thickness, and imparting higher plastic strains, which can approach those of classic ECAE.
4) Annealing of IF steel is very temperature and time sensitive and needs to be carried out with care. From the optical microscopy, it is observed that annealing at slightly higher temperatures or for longer times, may result in abnormal grain growth and may provide a starting material with an inconsistent microstructure. It is believed that this may significantly affect the mechanical properties of as-received material.
5) Being soft, IF steel is fairly easy to grind and polish. It is seen that for an IF steel Marshall's reagent delineates all ferrite boundaries and it is more effective than 2% nital alone. Still for better results specimens may be pre-etched in 2% nital solution. Addition of few drops of Hydrofluoric acid in Marshall's reagent provides a deeper etching response.
6) During ECAD process, homogeneity among flow and transverse planes increases with the increase in the number of passes. This reduces the hardness gradient which is observed during initial few passes.
7) In the ECAD experiments, the provision of a small gap between the sheet metal and the support plates leads to significant improvement in minimizing the reduction in

thickness. In addition, the reduction in thickness can be effectively minimized by either lowering the *t/r* ratio or increasing the drawing angle. However, these changes result in lowering the equivalent strain. Hence, further investigation is recommended to find a drawing angle that shall yield an optimum balance between reduction in thickness and equivalent strain.

8) Optical microscopy results confirm that the initial few passes of ECAD result in a non-uniform microstructure. With an increase in the number of passes, the non-uniformity is reduced resulting in a lamellar microstructure. ECAE produces a homogenous and ultra-fine microstructure, and at higher number of passes the microstructure is difficult to characterize under optical microscope.

CHAPTER VII

RECOMMENDATIONS FOR FURTHER STUDY

Though the hardness measurements present information regarding the improvement in mechanical properties, for a better understanding of the variation in yield strength, ultimate tensile strength and ductility, further investigation of the stress-strain behavior of ECAD-processed IF steel sheet samples is needed.

Back scattered electron imaging of ECAD-processed IF steel samples may be performed to understand the resulting surface topology and texture evaluation.

A prototype tool needs to be designed and manufactured, based on the proposed continuous process, using sets of driven rollers. The prototype should be tested and analyzed to confirm numerical results and explore further improvements needed for commercialization.

Simulation of multipass shear deformation process may be carried out to investigate the influence of the process variables in detail and to better identify optimum conditions for better results.

The present study involves numerical analyses of processes on a macroscopic level. It would be interesting to model the deformation mechanism, dislocation movement and grain refinement at the microscopic level.

REFERENCES

[1] D. T. Llewellyn, R. C. Hudd, Steels: Metallurgy and Applications, Butterworth-Heinemann Publication, Oxford, 3rd ed. 1998.

[2] R. Z. Valiev, J. of the Minerals, Metals and Mater. Soc. 58 (2006) 33-39.

[3] T. Lowe and R. Z. Valiev, J. of the Minerals, Metals and Mater. Soc. 56 (2004) 64-67.

[4] L. Olejnik and A. Rosochowski, Bulletin of the Polish Academy of Sc. 53 (2005) 413-423.

[5] H. Utsunomiya, K. Hatsuda, T. Sakai, Y. Saito, Mater. Sci. and Eng. A 372 (2004) 199-206.

[6] V. M. Segal, Mater. Sci. and Eng. A 17 (1995) 157-164.

[7] R. Z. Valiev, R. K. Islamgaliev, I. V. Alexandrov, Prog. in Mater. Sci. 45 (2000) 103-189.

[8] D. Bryan, Master's Thesis, Texas A&M University, College Station, TX (2005).

[9] K. Nakashima, Z. Horita, M. Nemoto, T. G. Langdon, Mater. Sci. and Eng. A 281 (2000) 82-87.

[10] Y. Iwahashi, Z. Horita, M. Nemoto, T. G. Langdon, Acta Mater. 46 (1997) 3317.

[11] U. Chakkingal, A. Suriadi, P. Thomson, Mater. Sci. and Eng. A 266 (1999) 241.

[12] L. Perez, C. Berlanga, J. Perez-Ilzarbe, J. of Mater. Proc. Tech. 143 (2003) 105.

[13] A. Zisman, V. Rybin, S. Van Boxel, M, Seefeldelt, B.. Verlinden, Mater. Sci. and Eng. A 427 (2006) 123-129.

[14] ASM Metals reference book, ASM, 3rd ed. 1993.

[15] H. Cui, Ph.D. Dissertation, Texas A&M University, College Station, TX (1996).

[16] V. M. Segal, Mater. Sci. and Eng. A 345 (2003) 36.

[17] D. Lee, Scripta Mater., 43 (2002) 115.

[18] Y. Iwahashi, J. Wang, M. Nemoto, T. Langdon, Scripta Mater. 35 (1996) 143.

[19] Jon Alkorta and Javier Gil Sevillano, J. of Mater. Proc. Tech. 141 (2003) 313.

[20] R. Goforth, K. Hartwig, L Cornwell, Severe plastic deformation of materials by equal-channel angular extrusion (ECAE), Investigations and Applications of severe plastic in: T.C. Lowe, R. Z. Valiev (Eds.), Kluwer Academic Publishers, Dordraecht, The Netherlands, (2000), p. 3.

[21] Luis Perez, Modelling and Sim. in Mater. Sci. and Eng. 12 (2004) 205.

[22] B. Altan, G. Purcek, I. Miskiglu, J. of Mater. Proc. Tech. 168 (2005) 137.

[23] B. Avitzur, Metal Forming: Processes and Analysis, McGraw-Hill Publication, New York, 1968.

[24] J. Alkorta, M. Rombouts, J. Messemaeker, L. Froyen, J. Sevillano, Scripta Mater. 47 (2002) 13-18.

[25] P. Chaudhury, R. Srinivasan, S. Viswanathan, Continuous severe plastic deformation process for metallic materials, Patent No. 6895795 (2002).

[26] H. Sandim, J. Lins, A. Pinto, A. Padilha, Mater. Sci. and Eng. A 354 (2002) 217-228.

[27] J. Alkorta, M. Rombouts, J. Messemaeker, L. Froyen and J. Sevillano, Scripta Mater. 47 (2002) 13-18.

[28] G. Ambrogio, L. Falice, and F. Micari, J. of Mater. Proc. Tech. 177 (2006) 413.

APPENDIX

Engineering Drawings of ECAD Die Assembly

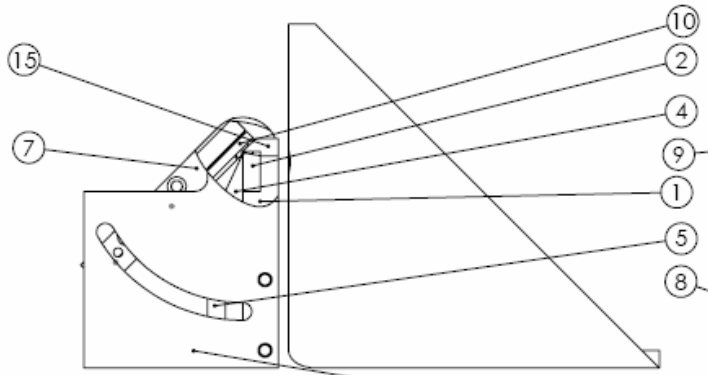

FRONT VIEW

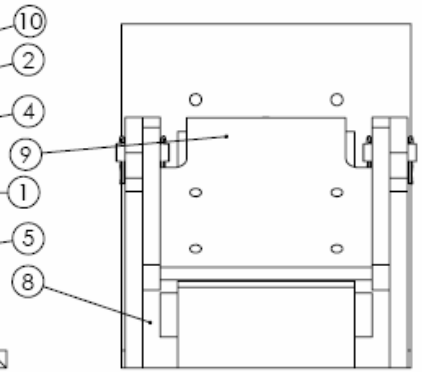

L.H. SIDE VIEW

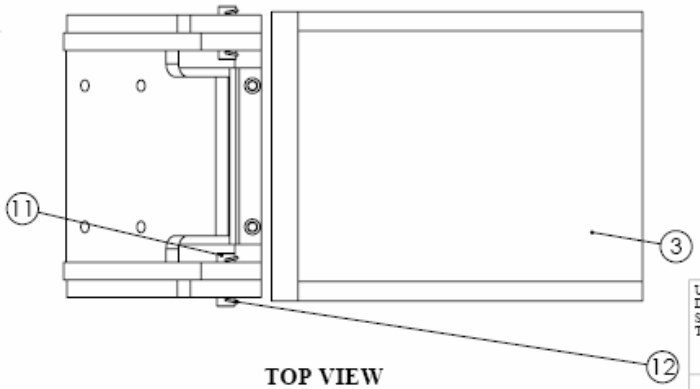

TOP VIEW

BILL OF MATERIALS

SR. NO.	PART NUMBER	DESCRIPTION	MATERIAL	QTY
1	S002	90 DEGREE ADAPTER	STEEL 4140	1
2	TS001	DIE NOSE	S7 TOOL STEEL	1
3	S001	DIE BLOCK	STINLESS STEEL	1
4	S003	115 DEGREE ADAPTER	STEEL 4140	1
5	S004	135 DEGREE ADAPTER	STEEL 4140	1
6	S005	SIDE SUPPORT PLATE	STEEL 4140	2
7	S006	ROTATING SUPPORT PLATE	STEEL 4140	2
8	A001	SIDE SPACER	ALUMINUM	2
9	S007	SUPPORT PLATE	STEEL 4140	1
10	S008	WEAR PLATE	STEEL 4140	1
11	S009	SWIVEL PINS	STEEL 4140	2
15	S010	TOP SUPPORT PLATE	STEEL 4140	1

UNLESS OTHERWISE SPECIFIED:
DIMENSIONS ARE IN INCHES
SURFACE FINISH:
TOLERANCES:
LINEAR:
ANGULAR:

		NAME	DATE
	DRAWN	RRM	
	CHECKD	RB	
	ENG APPR.		
	MFG APPR.	RB	

MATERIAL:

COMMENTS:

WEIGHT:

ECAE GROUP
TEXAS A&M UNIVERSITY

TITLE:

DIE ASSEMBLY

DWG NO. **S000**

SIZE **A4**

SCALE: 1:4

SHEET 1 OF 1

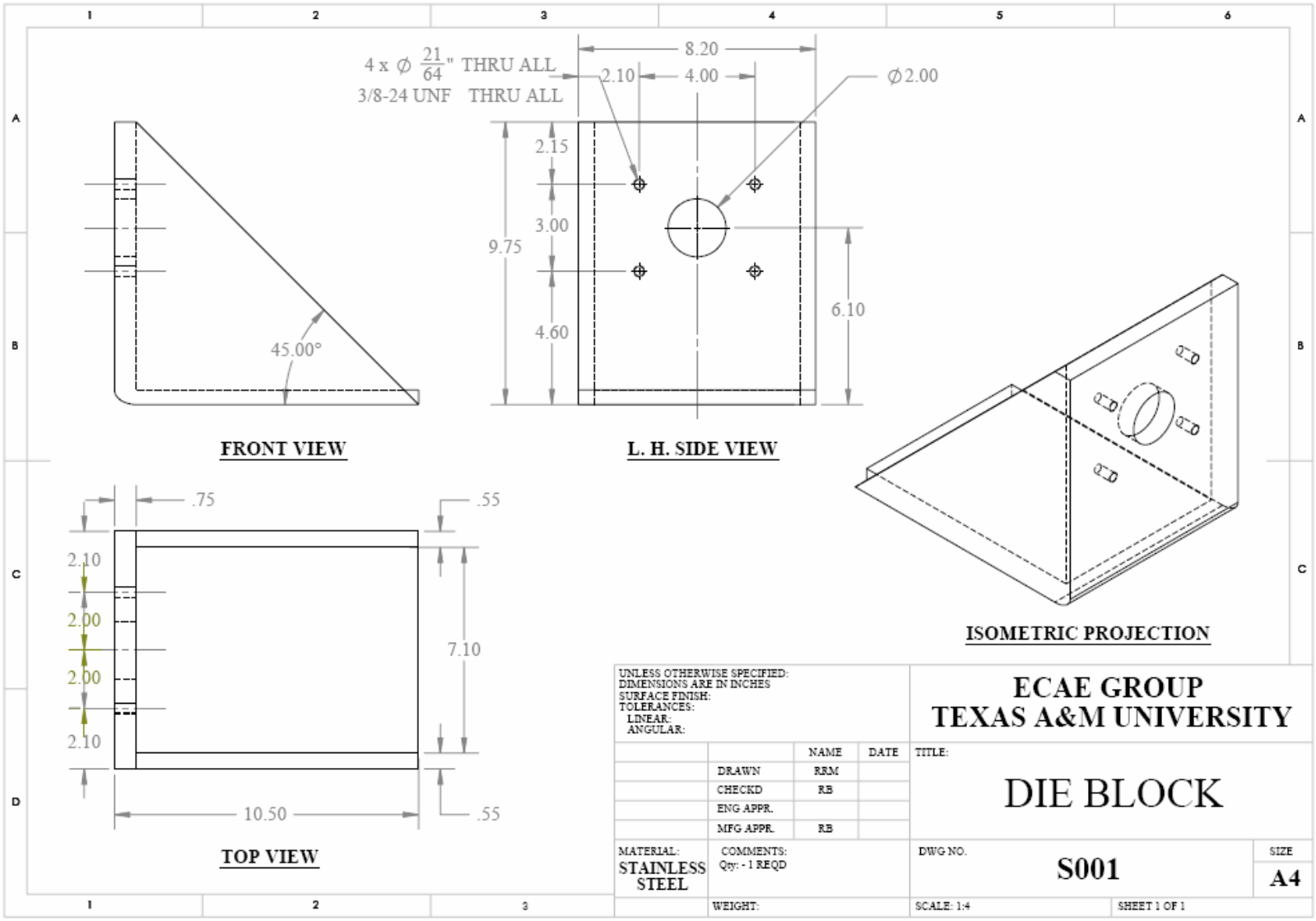
4 x ∅ 21/64" THRU ALL
3/8-24 UNF THRU ALL
8.20
2.10
4.00
∅2.00
2.15
3.00
9.75
4.60
6.10
45.00°
FRONT VIEW
L. H. SIDE VIEW
ISOMETRIC PROJECTION
.75
.55
2.10
2.00
2.00
2.10
7.10
10.50
.55
TOP VIEW
UNLESS OTHERWISE SPECIFIED:
DIMENSIONS ARE IN INCHES
SURFACE FINISH:
TOLERANCES:
LINEAR:
ANGULAR:
NAME
DATE
DRAWN
RRM
CHECKD
RB
ENG APPR.
MFG APPR.
RB
MATERIAL:
STAINLESS STEEL
COMMENTS:
Qty: - 1 REQD
WEIGHT:
ECAE GROUP
TEXAS A&M UNIVERSITY
TITLE:
DIE BLOCK
DWG NO.
S001
SIZE
A4
SCALE: 1:4
SHEET 1 OF 1

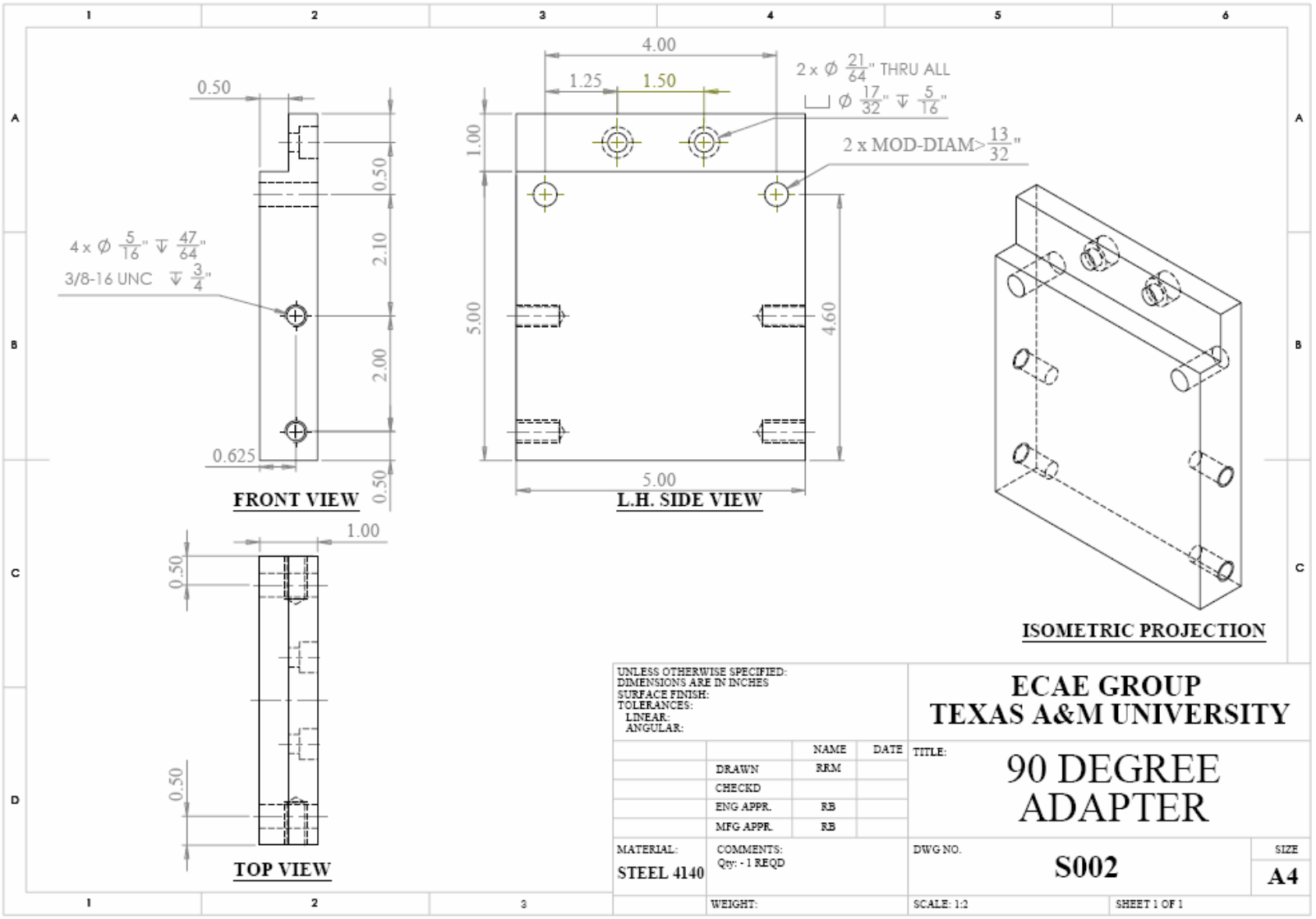
4.00
1.25
1.50
2 x Ø 21/64" THRU ALL
Ø 17/32" ↧ 5/16"
2 x MOD-DIAM> 13/32"
1.00
5.00
4.60
5.00
0.50
0.50
2.10
2.00
0.625
0.50
4 x Ø 5/16" ↧ 47/64"
3/8-16 UNC ↧ 3/4"
FRONT VIEW
L.H. SIDE VIEW
ISOMETRIC PROJECTION
1.00
0.50
0.50
TOP VIEW
UNLESS OTHERWISE SPECIFIED:
DIMENSIONS ARE IN INCHES
SURFACE FINISH:
TOLERANCES:
LINEAR:
ANGULAR:
NAME
DATE
DRAWN
RRM
CHECKD
ENG APPR.
RB
MFG APPR.
RB
MATERIAL:
STEEL 4140
COMMENTS:
Qty: - 1 REQD
WEIGHT:
ECAE GROUP
TEXAS A&M UNIVERSITY
TITLE:
90 DEGREE
ADAPTER
DWG NO.
S002
SIZE
A4
SCALE: 1:2
SHEET 1 OF 1

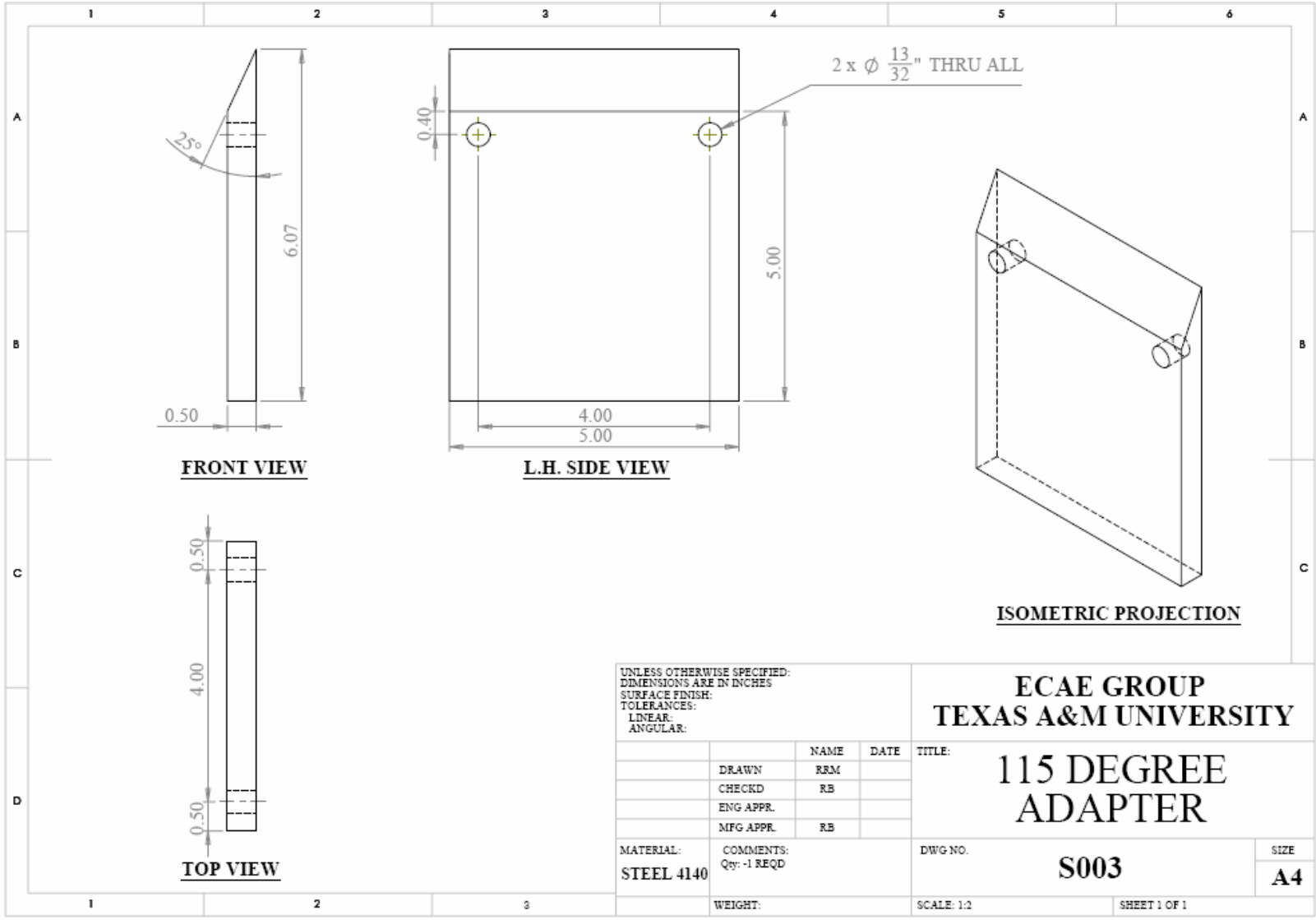
25°
6.07
0.50
FRONT VIEW
2 x Ø 13/32" THRU ALL
0.40
5.00
4.00
5.00
L.H. SIDE VIEW
ISOMETRIC PROJECTION
0.50
4.00
0.50
TOP VIEW
UNLESS OTHERWISE SPECIFIED:
DIMENSIONS ARE IN INCHES
SURFACE FINISH:
TOLERANCES:
LINEAR:
ANGULAR:
NAME
DATE
DRAWN
RRM
CHECKD
RB
ENG APPR.
MFG APPR.
RB
MATERIAL:
STEEL 4140
COMMENTS:
Qty: -1 REQD
WEIGHT:
ECAE GROUP
TEXAS A&M UNIVERSITY
TITLE:
115 DEGREE ADAPTER
DWG NO.
S003
SIZE
A4
SCALE: 1:2
SHEET 1 OF 1

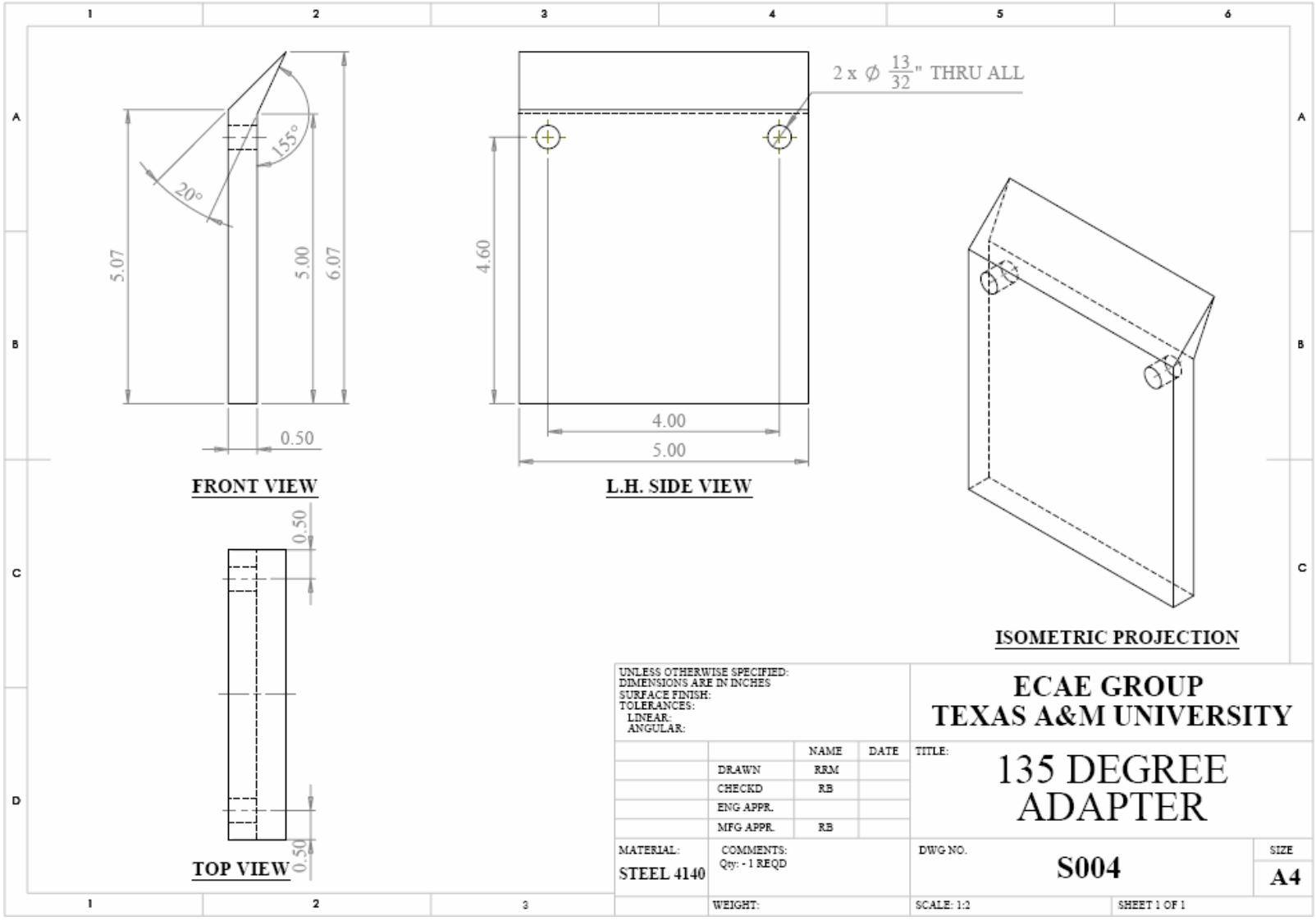
1
2
3
4
5
6
A
B
C
D
155°
20°
5.07
5.00
6.07
0.50
FRONT VIEW
2 x ∅ 13/32" THRU ALL
4.60
4.00
5.00
L.H. SIDE VIEW
ISOMETRIC PROJECTION
0.50
0.50
TOP VIEW
UNLESS OTHERWISE SPECIFIED:
DIMENSIONS ARE IN INCHES
SURFACE FINISH:
TOLERANCES:
LINEAR:
ANGULAR:
NAME
DATE
DRAWN
RRM
CHECKD
RB
ENG APPR.
MFG APPR.
RB
MATERIAL:
STEEL 4140
COMMENTS:
Qty: - 1 REQD
WEIGHT:
ECAE GROUP
TEXAS A&M UNIVERSITY
TITLE:
135 DEGREE
ADAPTER
DWG NO.
S004
SIZE
A4
SCALE: 1:2
SHEET 1 OF 1

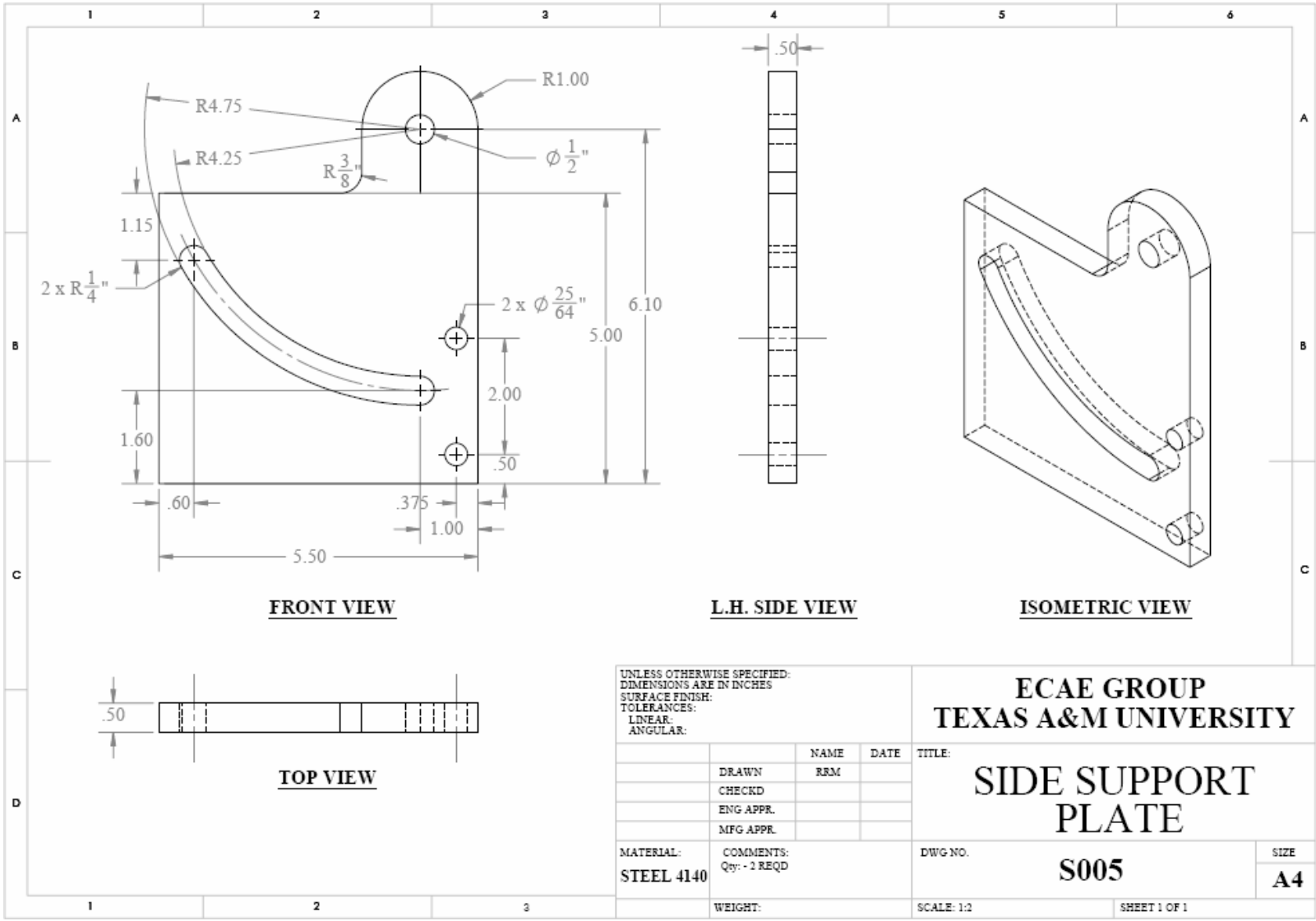
R4.75
R1.00
R4.25
R3/8"
Ø1/2"
1.15
2 x R1/4"
2 x Ø25/64"
6.10
5.00
2.00
1.60
.50
.60
.375
1.00
5.50
.50
FRONT VIEW
L.H. SIDE VIEW
ISOMETRIC VIEW
.50
TOP VIEW
UNLESS OTHERWISE SPECIFIED:
DIMENSIONS ARE IN INCHES
SURFACE FINISH:
TOLERANCES:
LINEAR:
ANGULAR:
NAME
DATE
DRAWN
RRM
CHECKD
ENG APPR.
MFG APPR.
MATERIAL:
STEEL 4140
COMMENTS:
Qty: - 2 REQD
WEIGHT:
ECAE GROUP
TEXAS A&M UNIVERSITY
TITLE:
SIDE SUPPORT PLATE
DWG NO.
S005
SIZE
A4
SCALE: 1:2
SHEET 1 OF 1

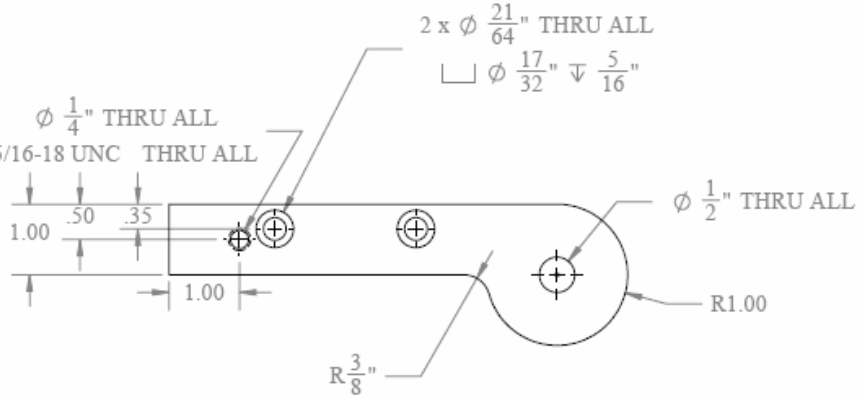

FRONT VIEW

L.H. SIDE VIEW

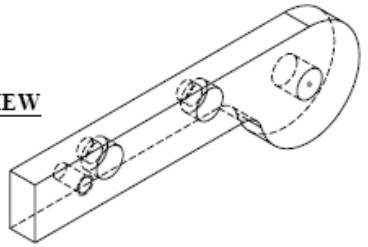

ISOMETRIC PROJECTION

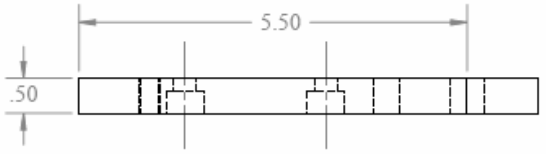

TOP VIEW

UNLESS OTHERWISE SPECIFIED: DIMENSIONS ARE IN INCHES SURFACE FINISH: TOLERANCES: LINEAR: ANGULAR:			**ECAE GROUP** **TEXAS A&M UNIVERSITY**
	NAME	DATE	TITLE:
DRAWN	RRM		**ROTATING SUPPORT PLATE**
CHECKD	RB		
ENG APPR.			
MFG APPR.	RB		
MATERIAL: **STEEL 4140**	COMMENTS: Qty: - 2 REQD		DWG NO. **S006** / SIZE **A4**
	WEIGHT:		SCALE: 1:2 / SHEET 1 OF 1

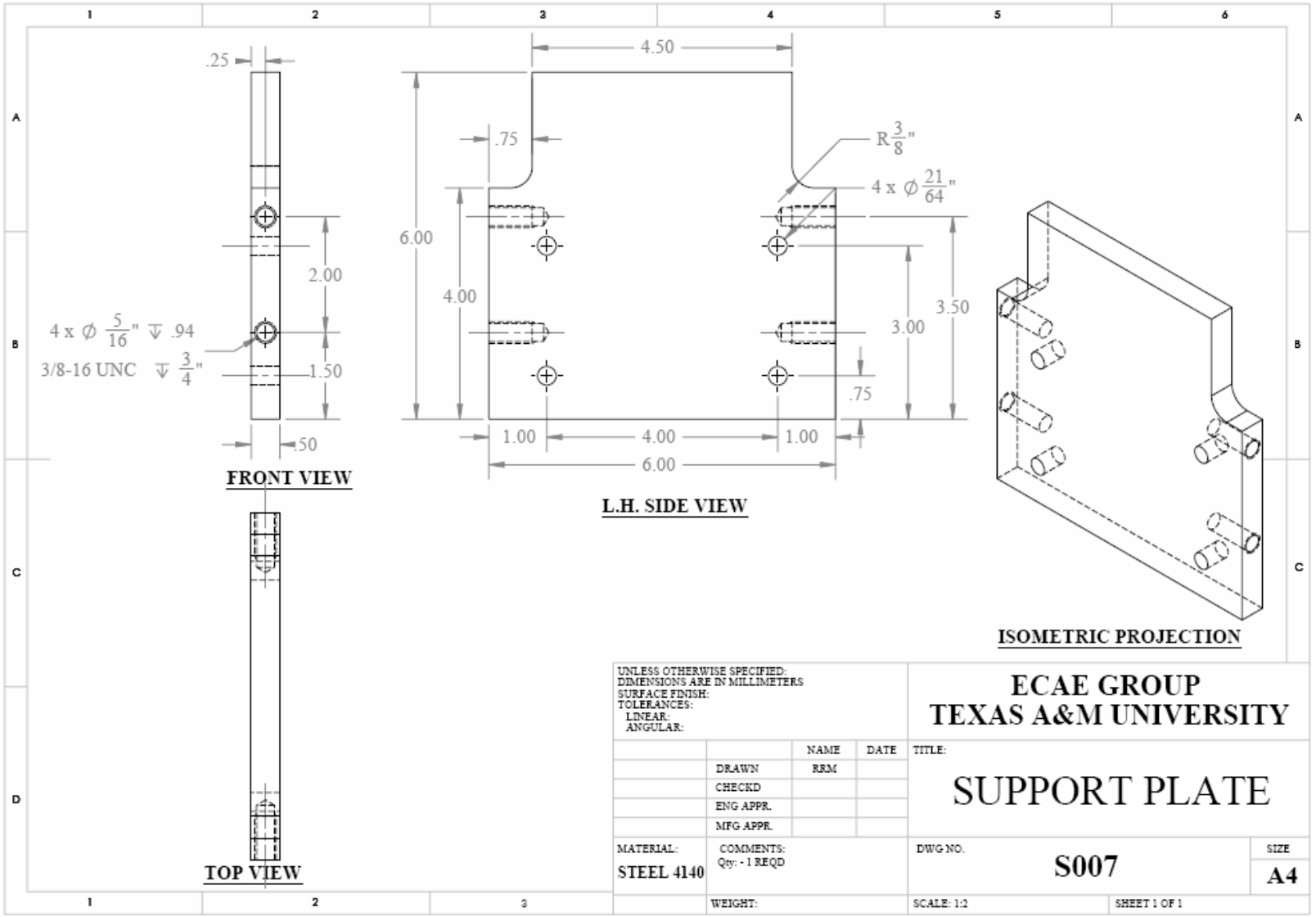
.25
2.00
4 x Ø 5/16" ↧ .94
3/8-16 UNC ↧ 3/4"
1.50
.50
FRONT VIEW
4.50
.75
R 3/8"
4 x Ø 21/64"
6.00
4.00
3.50
3.00
.75
1.00
4.00
1.00
6.00
L.H. SIDE VIEW
ISOMETRIC PROJECTION
TOP VIEW
UNLESS OTHERWISE SPECIFIED:
DIMENSIONS ARE IN MILLIMETERS
SURFACE FINISH:
TOLERANCES:
LINEAR:
ANGULAR:
NAME
DATE
DRAWN
RRM
CHECKD
ENG APPR.
MFG APPR.
MATERIAL:
STEEL 4140
COMMENTS:
Qty: - 1 REQD
WEIGHT:
ECAE GROUP
TEXAS A&M UNIVERSITY
TITLE:
SUPPORT PLATE
DWG NO.
S007
SIZE
A4
SCALE: 1:2
SHEET 1 OF 1

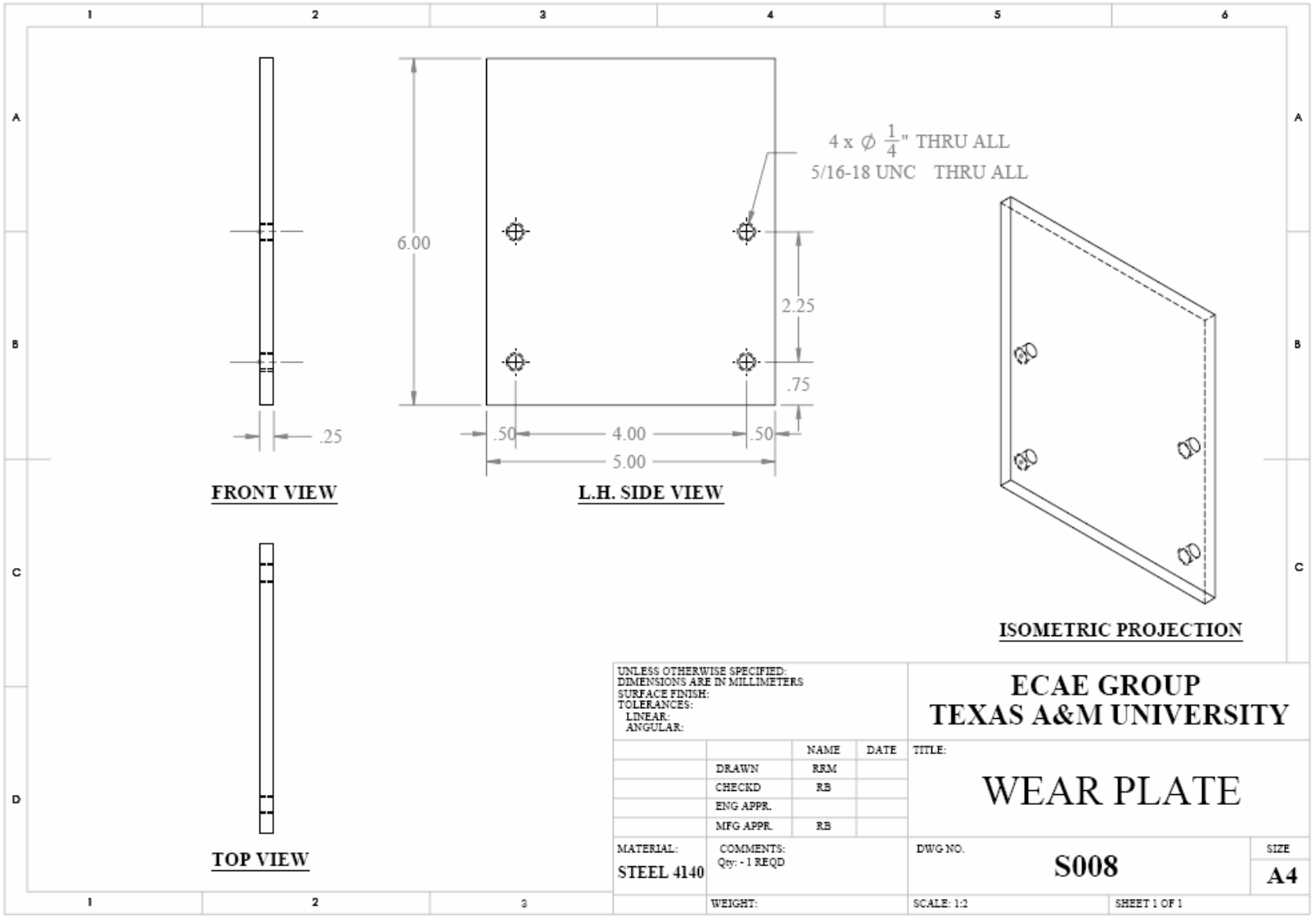
1
2
3
4
5
6
A
B
C
D
6.00
2.25
.75
.25
.50
4.00
.50
5.00
4 x Ø 1/4" THRU ALL
5/16-18 UNC THRU ALL
FRONT VIEW
L.H. SIDE VIEW
ISOMETRIC PROJECTION
TOP VIEW
UNLESS OTHERWISE SPECIFIED:
DIMENSIONS ARE IN MILLIMETERS
SURFACE FINISH:
TOLERANCES:
LINEAR:
ANGULAR:
NAME
DATE
DRAWN
RRM
CHECKD
RB
ENG APPR.
MFG APPR.
RB
MATERIAL:
STEEL 4140
COMMENTS:
Qty: - 1 REQD
WEIGHT:
ECAE GROUP
TEXAS A&M UNIVERSITY
TITLE:
WEAR PLATE
DWG NO.
S008
SIZE
A4
SCALE: 1:2
SHEET 1 OF 1

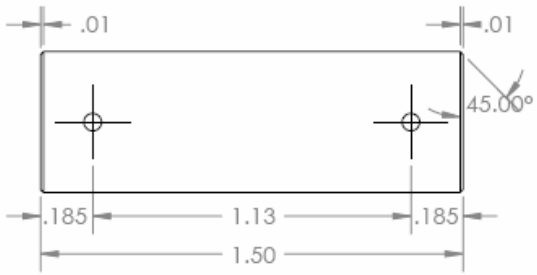

FRONT VIEW

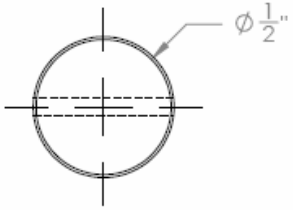

L.H. SIDE VIEW

TOP VIEW

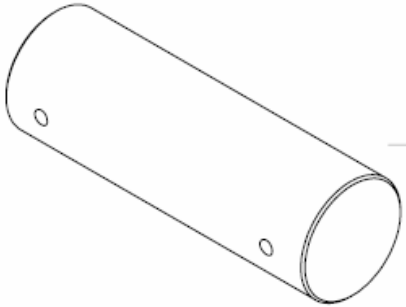

ISOMETRIC PROJECTION

UNLESS OTHERWISE SPECIFIED:
DIMENSIONS ARE IN INCHES
SURFACE FINISH:
TOLERANCES:
LINEAR:
ANGULAR:

ECAE GROUP
TEXAS A&M UNIVERSITY

		NAME	DATE
	DRAWN	RRM	
	CHECKD	RB	
	ENG APPR.		
	MFG APPR.	RB	

TITLE:

SWIVEL PINS

MATERIAL: STEEL 4140

COMMENTS: Qty: - 2 REQD

DWG NO. **S009**

SIZE **A4**

WEIGHT:

SCALE 2:1

SHEET 1 OF 1

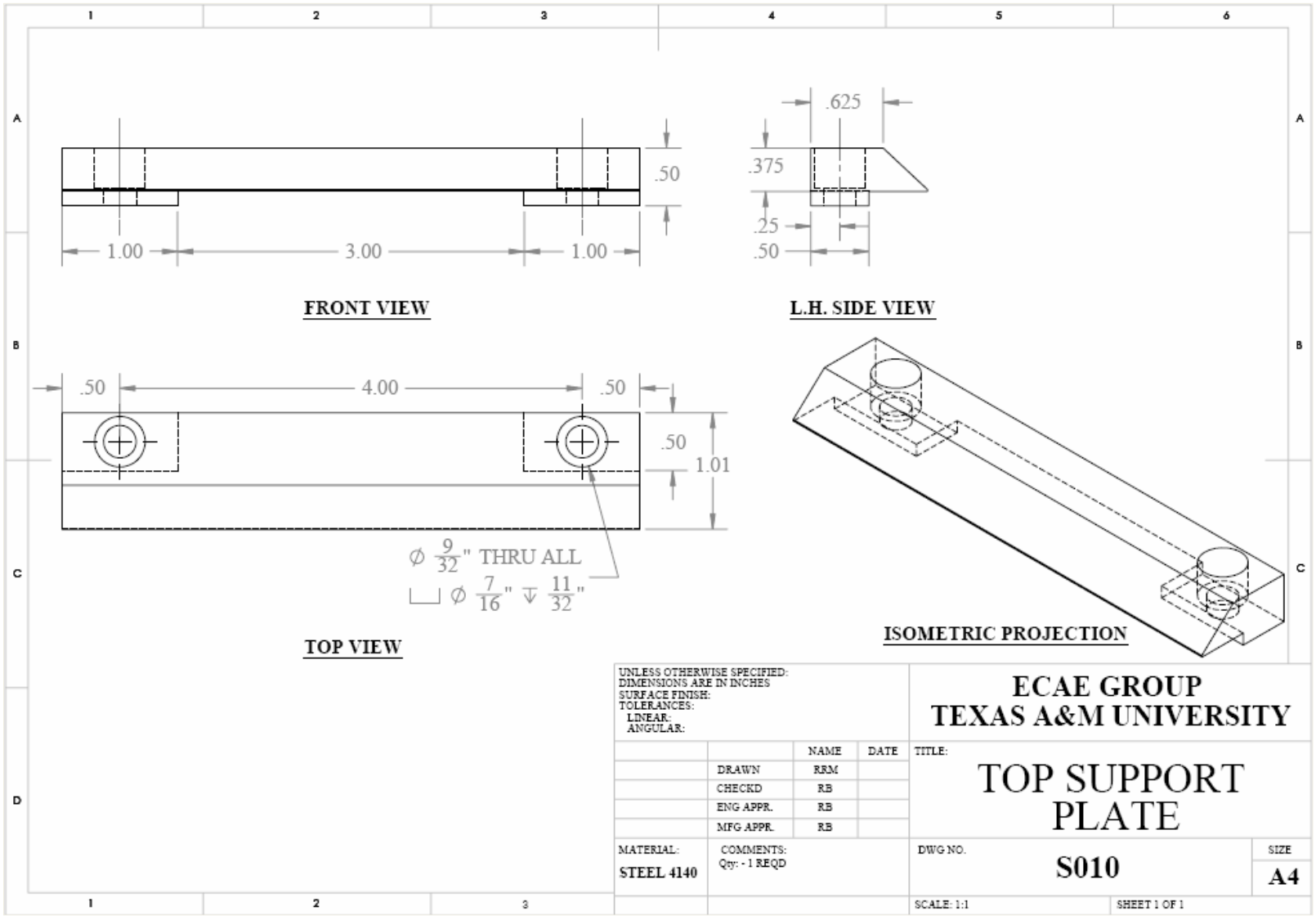
1.00
3.00
1.00
.50
.625
.375
.25
.50
FRONT VIEW
L.H. SIDE VIEW
.50
4.00
.50
.50
1.01
Ø 9/32" THRU ALL
⌴ Ø 7/16" ↧ 11/32"
TOP VIEW
ISOMETRIC PROJECTION
UNLESS OTHERWISE SPECIFIED:
DIMENSIONS ARE IN INCHES
SURFACE FINISH:
TOLERANCES:
LINEAR:
ANGULAR:
NAME
DATE
DRAWN
RRM
CHECKD
RB
ENG APPR.
RB
MFG APPR.
RB
MATERIAL:
STEEL 4140
COMMENTS:
Qty: - 1 REQD
ECAE GROUP
TEXAS A&M UNIVERSITY
TITLE:
TOP SUPPORT PLATE
DWG NO.
S010
SIZE
A4
SCALE: 1:1
SHEET 1 OF 1

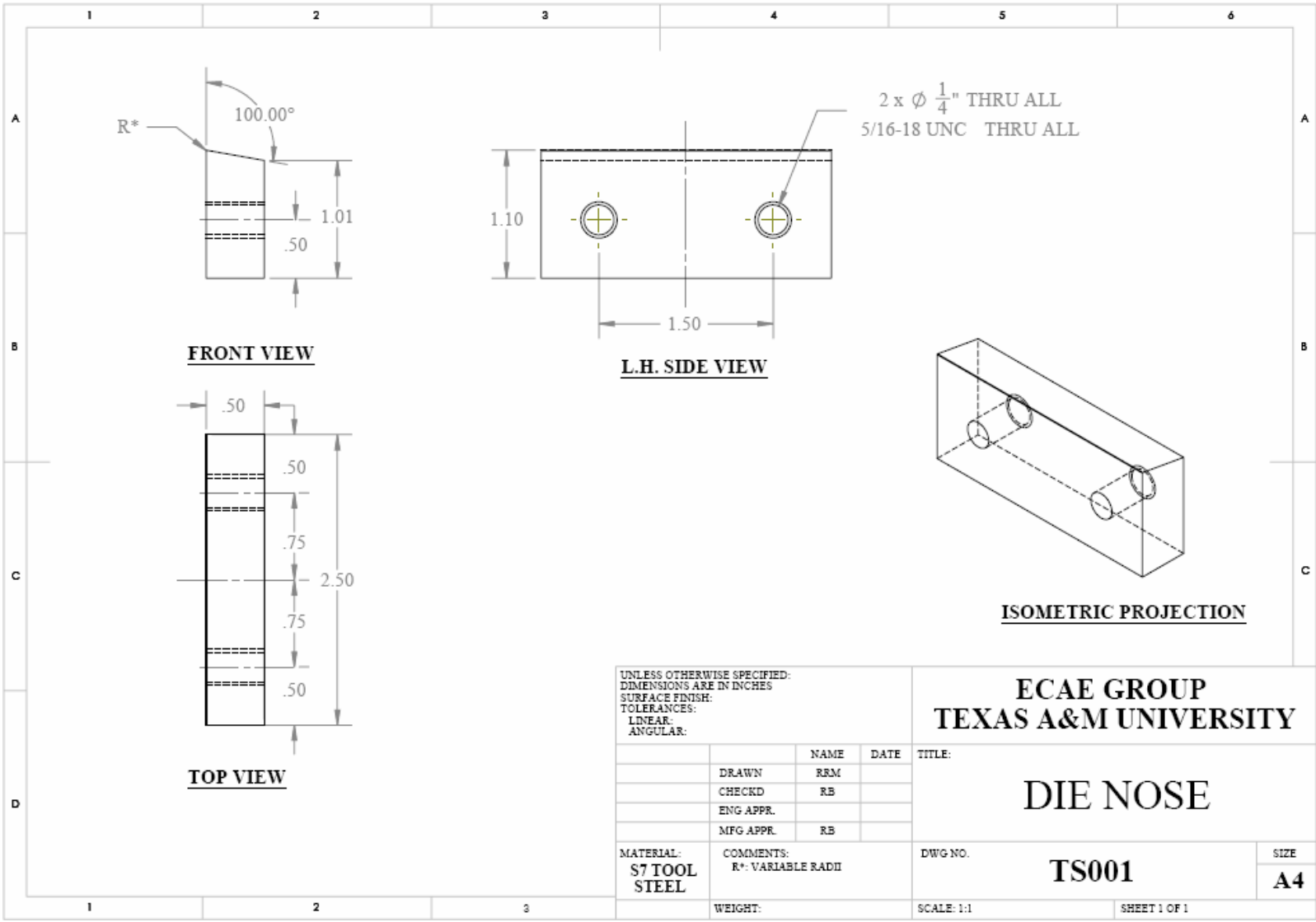
R*
100.00°
1.01
.50
FRONT VIEW
2 x ∅ 1/4" THRU ALL
5/16-18 UNC THRU ALL
1.10
1.50
L.H. SIDE VIEW
ISOMETRIC PROJECTION
.50
.50
.75
2.50
.75
.50
TOP VIEW
UNLESS OTHERWISE SPECIFIED:
DIMENSIONS ARE IN INCHES
SURFACE FINISH:
TOLERANCES:
LINEAR:
ANGULAR:
NAME
DATE
DRAWN
RRM
CHECKD
RB
ENG APPR.
MFG APPR.
RB
MATERIAL:
S7 TOOL STEEL
COMMENTS:
R*: VARIABLE RADII
WEIGHT:
ECAE GROUP
TEXAS A&M UNIVERSITY
TITLE:
DIE NOSE
DWG NO.
TS001
SIZE
A4
SCALE: 1:1
SHEET 1 OF 1

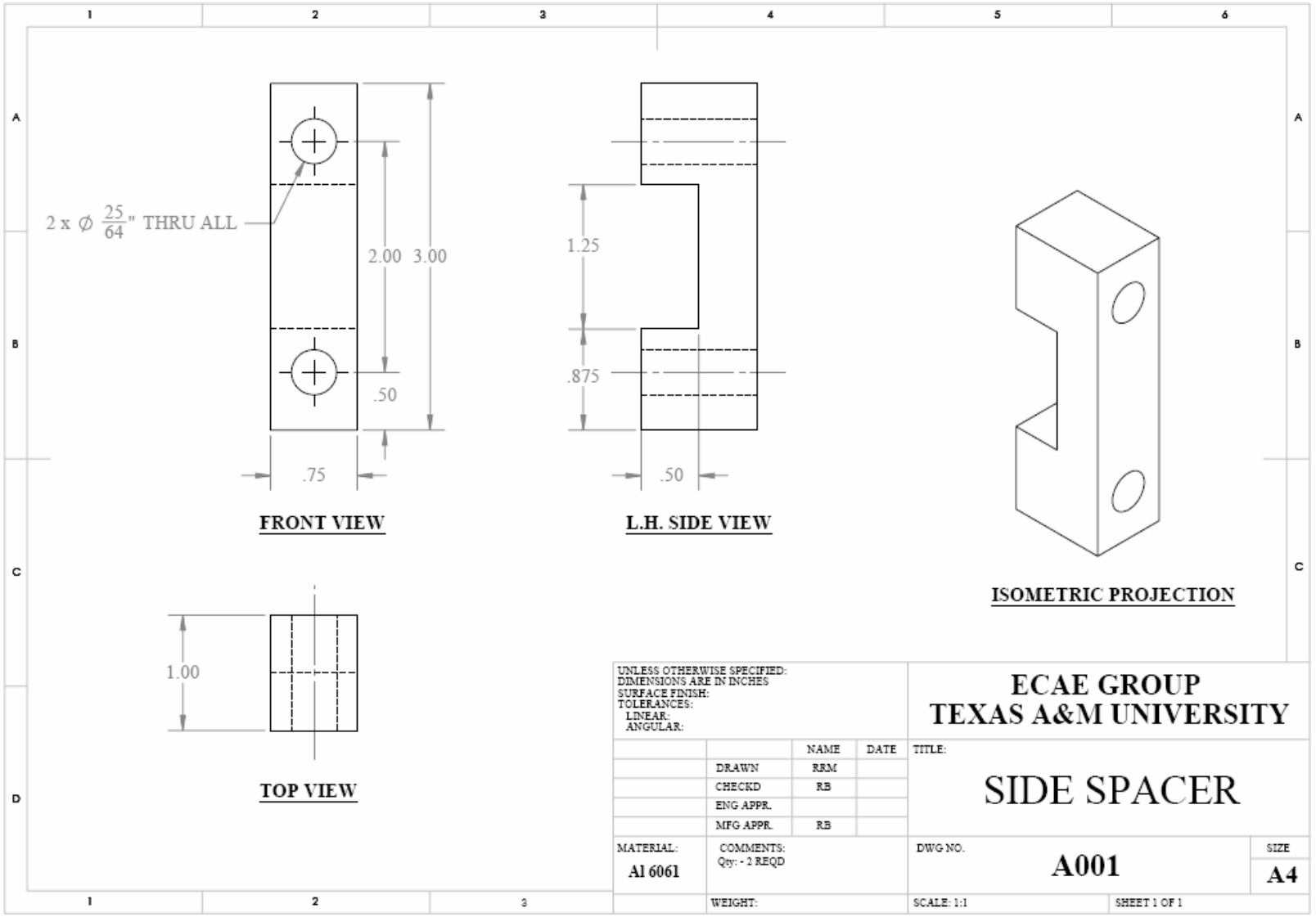
1
2
3
4
5
6
A
B
C
D
2 x ∅ 25/64" THRU ALL
2.00
3.00
.50
.75
FRONT VIEW
1.25
.875
.50
L.H. SIDE VIEW
ISOMETRIC PROJECTION
1.00
TOP VIEW
UNLESS OTHERWISE SPECIFIED:
DIMENSIONS ARE IN INCHES
SURFACE FINISH:
TOLERANCES:
LINEAR:
ANGULAR:
NAME
DATE
DRAWN
RRM
CHECKD
RB
ENG APPR.
MFG APPR.
RB
MATERIAL:
Al 6061
COMMENTS:
Qty: - 2 REQD
WEIGHT:
ECAE GROUP
TEXAS A&M UNIVERSITY
TITLE:
SIDE SPACER
DWG NO.
A001
SIZE
A4
SCALE: 1:1
SHEET 1 OF 1

VITA

Name:	Rahul Rajendra Murudkar
Address:	Department of Mechanical Engineering, Texas A&M University, College Station, Texas 77843, USA. Mail stop: 3123.
Email Address:	muru52@neo.tamu.edu
Education:	B.E., Mechanical Engineering, University of Mumbai, India, 2006 M.S, Mechanical Engineering, Texas A&M University, College Station, Texas, 2009